NUCLEAR MAGNETIC RESONANCE AND DYNAMIC NUCLEAR POLARIZATION STUDIES OF LIQUID/LIQUID AND LIQUID/SOLID INTERFACES

by

Juan Gu

Dissertation submitted to the Faculty of the

Virginia Polytechnic Institute and State University

in partial fulfillment of the requirements for the degree of

DOCTOR OF PHILOSOPHY

in

Chemistry

APPROVED:

H.C. Dorn, Chairman

J.G. Mason

J.S. Merola

J.M. Tanko

J.P. Wightman

April, 1992

Blacksburg, Virginia

NUCLEAR MAGNETIC RESONANCE AND DYNAMIC NUCLEAR POLARIZATION STUDIES OF LIQUID/LIQUID AND LIQUID/SOLID INTERFACES

by

Juan Gu

Committee Chairman: Harry C. Dorn
Chemistry

(ABSTRACT)

In the present study, interactions at the liquid/liquid and liquid/solid interfaces have been investigated by the combination of both nuclear magnetic resonance (NMR) and dynamic nuclear polarization (DNP) techniques. The ^{13}C and ^{15}N paramagnetic contact shifts, and ^{1}H, ^{13}C, and ^{15}N relaxation times in CH_3CN/2,2,6,6,-tetramethyl-1-piperidinyloxy (TEMPO) and CH_3CONH_2/TEMPO systems have been measured at high magnetic field (B_0 = 1.9-9.4 T). The ^{13}C DNP enhancements at low magnetic field (0.33 T) in the CH_3CONH_2/TEMPO system have been determined by the flow liquid-liquid intermolecular transfer (LLIT) DNP technique. The data can be understood in terms of transient hydrogen bond formation between closed shell diamagnetic molecules and the open shell free radical TEMPO. A set of static and dynamic parameters, such as hyperfine coupling constants, correlation times, and free radical-nuclear internuclear distances in the hydrogen bonding complex, have also been determined. The scalar and dipolar contributions derived from the NMR study have been subsequently employed to predict the corresponding ^{1}H, ^{13}C, and

^{15}N low magnetic field (0.33 T) DNP enhancements. Good agreement has been obtained between the NMR predicted and experimentally measured low magnetic field DNP results.

The dynamic electron-nuclear intermolecular interactions between the newly discovered fullerene, C_{60}, and the free radical TEMPO have been characterized by flow LLIT and solid liquid intermolecular transfer (SLIT) DNP techniques. A dipolar dominated ultimate DNP enhancement (-250) at 0.33 T magnetic field has been observed. The results are consistent with a model for C_{60}/TEMPO interactions involving nonspecific complex formations.

In addition to DNP studies in the liquid state, the solid/liquid surface intermolecular interactions in solid samples of various activated carbon specimens have been monitored by using flow SLIT ^{1}H and ^{13}C DNP experiments. The activated carbon samples were prepared by pyrolysis of cellulose, and commercial samples were also employed. The surface-liquid interaction in these studies were monitored with the solvent benzene (or d_6-benzene). Both time-dependent (Overhauser) and time-independent (solid-state) DNP enhancements were observed in these studies. Both chemisorption and physisorption processes of oxygen to the activated carbon were also monitored using the DNP approach.

This dissertation is dedicated to

my father, husband, and sons.

ACKNOWLEDGEMENTS

The author wishes to express her gratitude to Dr. Harry C. Dorn for his kindness, guidance, and encouragement throughout this work. Without his foresight, I would not have had the chance to get in touch with this exciting field.

I would like to thank Tom Glass who has always gladly shared his knowledge and experience throughout the course of this experimental work. I would also like to acknowledge Dr. Merola, Dr. Tanko, and Dr. Wightman's groups for being so kind to let me use facilities in their laboratories; the electronics shop for the excellent technical services; the analytical service and the glass shop of the Department of Chemistry for their help in improving and maintaining whole instrument and other assistance; IBM Research Division for providing 20% ^{13}C labelled C_{60} sample.

Thanks also go to my research colleagues, Alan Caswell, Lee Allen, David Morgan, Candy Tsaio, Rossi Gitti, and K.H. Tsai for their help. Most of all, I like to thank my father, husband, and sons for their love, support, and understanding.

Finally, I would like to thank WestVaco Company, Eastman Kodak company, Jeffress Research Foundation, and the Department of Chemistry at Virginia Polytechnic Institute and State University for their financial support through my research.

LIST OF CONTENTS

LIST OF TABLES

LIST OF FIGURES

CHAPTER 1

INTRODUCTION

The development of sensitive spectroscopic techniques has led to increasingly more sophisticated insights into the subtleties of reaction mechanisms and the dynamics of molecular interactions in solution. The short-lived solvent-solute interactions such as transient complex formation governed by weak hydrogen bonding in solutions containing paramagnetic solutes are in the 10^{-8} to 10^{-11} s time range which encompass the chemically important time scale of molecular collision in solution. Therefore, the dynamic nature of these transient associations is of great experimental and theoretical interest.

Stable nitroxide free radicals have been shown to form short-lived complexes with protic solvent molecules[1]. Several dynamic aspects of this coupling are of interest, most notably the mechanisms of the interactions and the nature of the random molecular motion that modulate these interactions. The interaction between hydrogen donor ligands and nitroxyl groups has been investigated in various solutions by several research

groups utilizing different methods[2-6]. Thus, static and dynamic interactions in the liquid state can be probed.

NMR techniques have provided particularly powerful tools for studying such phenomena. Paramagnetic contact shifts caused by the unpaired electron spin of the free radical can be derived from high-resolution spectra of the ligand molecules. While the contact interaction is not explicitly distance dependent, it does depend upon the nature of the free radical and its proximity to the compound under study. Direct overlap of a molecular orbital containing the unpaired electron or induced unpaired spin density at the magnetic nucleus via the hydrogen bond is required to induce a paramagnetic shift. Thus, the relative magnitude of these induced shifts at different nuclei within a molecule is related to the hyperfine coupling constant A and provide information on the average relative position of the free radical with respect to the molecule.

Levy and Komoroski[7] have shown that spin-lattice relaxation data can complement paramagnetic shift data. At low concentrations of the free radical the induced paramagnetic shifts are relatively small while effects upon the spin-lattice relaxation are pronounced. The observed relaxation rate is the sum of the various diamagnetic

relaxation rates R_{10}, resulting from dipole-dipolar, spin-rotation, scalar and chemical shift anisotropy mechanisms and/or from the paramagnetic relaxation rate R_{Rad}, due to the electron-nuclear relaxation mechanism. However, the magnetic interactions between substrate nuclei and the unpaired radical electron dominate the nuclear magnetic relaxation processes. When the electron-nuclear dipolar interaction dominates R_{Rad}, the usual sixth power distance dependence will control the relaxation, and the geometrical relationship between the free radical and the nuclei can be determined. Depending on the specific contact between radical and solvent molecules and on their motional behavior, the spectral density functions of the nuclei exhibit a different frequency dependence within the accessible range of frequency and temperatures and reveal details of the processes. Therefore, the interaction and its time dependence can be examined by the frequency and temperature dependence of the nuclear spin-lattice relaxation. This latter method is more effective if the accessible frequency region is large.

In addition, intermolecular dynamic nuclear polarization (DNP) is responsive to molecular encounters over precisely this range of fast interaction time and provides a valuable technique for examining intermolecular interactions in solutions and at liquid/solid interfaces[8,9,10]. Dipolar and

scalar mechanisms couple the nuclear and unpaired electron spins, and the relative coupling magnitude determines the nature of the NMR signal enhancements observed. The different sign of the DNP enhancement for dipolar and scalar coupling provides a very sensitive method for studying these interactions. Although scalar interactions often serve only to reduce the nuclear polarization, they can sometimes be used to great advantage to obtain information on molecular structure and subtle details of the molecular motion in favorable systems.

Therefore, the combination of investigations of relaxation rates with studies of dynamic polarization of solvent nuclei induced by paramagnetic solutes yields information on collision parameters such as correlation times, radical-nucleus distances of closest approach, and on the relative magnitude of the scalar and dipolar interactions between the unpaired electron and nuclear spin.

The major sections of this dissertation can be subdivided into two parts. The first five chapters are devoted to liquid-liquid intermolecular NMR chemical shift, NMR relaxation, and LLIT[11] DNP studies of weak hydrogen bonding systems (CH_3CN/TEMPO and CH_3CONH_2/TEMPO). Chapter VI of this dissertation focuses attention on the surface/liquid

interface. In this study, various activated carbon samples were prepared by pyrolysis of cellulose and examined by the ^{1}H and ^{13}C SLIT[12] DNP approach using benzene (or d_6-benzene) as the probe molecule. The results from these samples were compared with commercial activated carbon samples.

Finally, the availability in the latter stage of this study of the important new form of carbon, fullerene, provides the opportunity to study surface/liquid interaction of the fullerene, C_{60}, with silica phase immobilized nitroxide (SPIN) samples. In addition, LLIT ^{13}C DNP enhancement for the C_{60}/TEMPO system were also obtained. The results obtained in this thesis provide an excellent example of the type of information obtainable by NMR and DNP studies of liquid/liquid and surface/liquid interfaces.

CHAPTER 2

THE BASIC INTERACTION FOR A NUCLEAR-ELECTRON TWO SPIN SYSTEM

2.1 The Hamiltonian for Interaction of the Nuclear Moment with a Magnetic Field

The possession of both spin and charge confers on the nucleus a magnetic moment μ_N which is proportional to the magnitude of the spin, I, that is[13]

$$\mu_N = \gamma_I \hbar I = g_N \beta_N I \qquad (2.1)$$

where γ_I is the magnetogyric ratio of the nucleus, $\hbar$ is Planck's constant divided by 2π, g_N is a dimensionless constant called the nuclear g factor, and β_N, nuclear magneton, is equal to $e\hbar/2mc$ where e and m are, respectively, the charge and mass of the nucleus and c is the velocity of light.

If we apply a steady magnetic field B_0 on the nucleus, there is an interaction between the field and the magnetic moment, μ_N, which can be represented in terms of the

Hamiltonian

$$\hat{H} = -\hat{\mu}_N \cdot \mathbf{B}_0 \qquad (2.2)$$

If the direction of the magnetic field is defined to be the z direction, the interaction may be rewritten

$$\hat{H} = -\gamma_I \hbar B_0 \hat{I}_z = -g_N \beta_N B_0 \hat{I}_z \qquad (2.3)$$

In this expression $\hat{I}$ represents the nuclear spin operator.

2.2 The Hamiltonian for Interaction of the Electron Moment with a Magnetic Field

As for nuclei, the interaction between a magnetic field and an electron spin can be represented in terms of the Hamiltonian

$$\hat{H} = -\gamma_S \hbar B_0 \hat{S}_z = g\beta B_0 \hat{S}_z \qquad (2.4)$$

where γ_S is the magnetogyric ratio of the electron, g is again a dimensionless constant called the electron g factor which is equal to 2.002322 for a free electron, and β is the electronic Bohr magneton, equal to $e\hbar/2mc$ where e and m are the charge and mass of the electron.

2.3 The Hamiltonian of the Nuclear-Electron Interaction

2.3.1 The Zeeman Energy

For a two-spin system consisting of one spin I and one spin S in an external magnetic field, B_0, the nucleus and the electron both interact with the steady magnetic field giving an energy

$$\hat{H} = -\gamma_I \hbar B_0 \hat{I}_z - \gamma_S \hbar B_0 \hat{S}_z \qquad (2.5)$$

2.3.2 The Dipolar Interaction

In addition to interactions with the steady magnetic field, the magnetic moments of two spins are coupled by two different mechanisms. One is called the dipolar interaction which is entirely analogous to classic dipolar coupling between two bar magnets which yield the dipolar interaction Hamiltonian

$$\hat{H} = \gamma_I \gamma_S \hbar^2 \left(\frac{3(\mathbf{r}.\hat{\mathbf{S}})(\mathbf{r}.\hat{\mathbf{I}})}{r^5} - \frac{\hat{\mathbf{S}}.\hat{\mathbf{I}}}{r^3} \right) \qquad (2.6)$$

The dipolar term can be expressed in polar coordinates and written in components. One finds that it is proportional to $(3\cos^2\theta - 1)/r$, where r is the distance between the two spins, and θ is the angle between the magnetic field direction and a line joining the two dipoles. Depending on the value of θ, the local field contribution at the nucleus can be either

aid or oppose the external magnetic field. Since the angle varies rapidly because of the molecular motion in a low viscosity liquid, the dipolar part of the interaction is averaged to zero and does not contribute to the time independent interactions of the system; i.e., it does not affect the energy levels. It does, however, affect the time dependent phenomena such as relaxation and dynamic nuclear polarization. Because of the distance dependence, the dipolar interaction can provide structure information involving molecular collisions.

2.3.3 The Scalar Interaction

The other interaction mechanism is called the scalar interaction. The magnetic moments of electrons and nuclei are coupled via the so-called contact interaction. This interaction, first introduced by Fermi[14] to account for hyperfine structure in atomic spectra, has the form

$$\hat{H} = A\hat{I}\cdot\hat{S} \tag{2.7}$$

where A is called the hyperfine coupling constant and has the dimensions of energy.

$$A = \frac{8\pi}{3} g\beta g_N \beta_N |\varphi(0)|^2 \tag{2.8}$$

where $|\psi(0)|$ is the amplitude of the electronic wave function at the nucleus. For $|\psi(0)|$ to be nonvanishing, the electron must have some probability of being at the nucleus. Therefore this interaction only occurs if unpaired electron spin density on the free radical is transferred to nuclei of the substrate molecule during collision. Since there is no directional aspect (e.g., not dependent on B_0) to the contact of the nuclear and electron spin, this interaction is isotropic.

Chemically, two mechanisms for scalar coupling are plausible: exchange polarization and complex formation. Exchange polarization can be understood as follows. For intermolecular coupling, the unpaired electron and the magnetic nucleus are on different compounds. During the collision, the odd electron may slightly unpair the electrons at the nucleus of the solvent on which some spin density is transferred. The degree of polarization depends on the relative orientation and time of contact of the colliding species. On the other hand, complex formation occurs when the electrons of both molecules become delocalized or redistributed upon association. Therefore, the unpaired electrons perturb the substrate molecules, causing a change of electron density and a consequent change of the hyperfine constant.

In comparison with the dipolar interaction, the scalar interaction contribution to the energy levels is somewhat more complicated. It does contribute to the time-independent interaction of the system and produce the isotropic component of the hyperfine structure in the EPR measurement since the effective times, nuclear relaxation and nuclear exchange times, are so long that the scalar coupling between electron and nuclei is effectively time-independent. However, the energy part of the scalar coupling for a nucleus is averaged to zero since the effective time dependence is now given by the much faster electronic relaxation times τ_1 , τ_2 and the electronic exchange time τ_e which are in general fulfilled by either one or both conditions[8]

$$\tau_1,\ \tau_2 << 1/A; \qquad \tau_e << 1/A \tag{2.9}$$

In this case, instead of a splitting of the nuclear energy levels one observes a paramagnetic shift. The detailed study of the paramagnetic shift is given in Chapter III. Similar to the dipole term, the scalar coupling does effect time-dependent phenomena such as nuclear-electron relaxation and the DNP effect.

2.3.4 The Basic Interaction for a Nuclear-Electron Two Spin System

Under these conditions, the magnetic interaction of the coupled spin system I and S in an external magnetic field is

represented by the spin Hamiltonian[8]

$$\hat{H} = -\gamma_S \hbar H_0 \hat{S}_z - \gamma_I \hbar H_0 \hat{I}_z + \hat{H}_{IS}(t) + \hat{H}_{II}(t) + \hat{H}_{SS}(t) \qquad (2.10)$$

where the first two terms are the electron and nuclear Zeeman terms. The third term $\hat{H}_{IS}$ (t) is composed of the classical dipolar interaction term and of the scalar Fermi contact term, and represents the time dependent electron nuclear interaction which gives rise to the electron induced nuclear relaxation and the phenomenon of DNP. The last two terms, $\hat{H}_{II}$ (t) and $\hat{H}_{SS}$ (t), express the remaining nuclear-nuclear and electron-electron interactions, respectively, which are largely unimportant for understanding DNP phenomenon.

2.4 The Energy Level Diagram

The energy level diagram for combined spin states of a nuclear spin (I = 1/2) coupled to an electron spin (S = 1/2) is represented in Fig. 2.1. The possible states are denoted by $|+->$, $|++>$, $|-->$, and $|-+>$. The plus or minus sign by convention represents the aligning of the spin with or against the magnetic field while the first sign refers to the electron spin S and the second sign to the nuclear spin I.

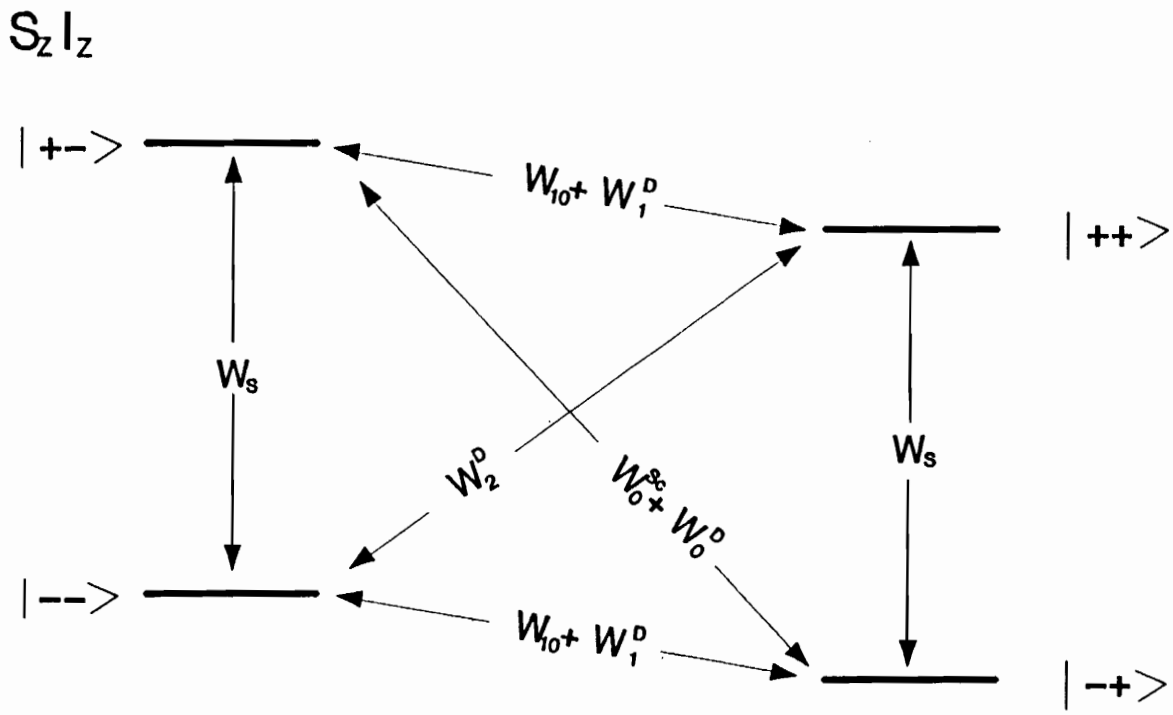

Figure 2.1: Energy Levels for the Electron-Nucleus Two-Spin System (S=1/2 and I=1/2) with the Dipolar and Scalar Radical-Induced Nuclear Relaxation Transition Probabilities(W_i).

2.5 The Time-Dependent Phenomena

2.5.1 Nuclear-Electron Relaxation

At equilibrium, nuclear spins are distributed among the energy levels according to a Boltzmann distribution. When perturbed from its equilibrium state, the spin system returns to thermal equilibrium with its surroundings (the "lattice") by a first-order relaxation process characterized by a time T_1, the spin-lattice relaxation time. The transition probabilities between these levels are denoted as W_i. The transitions W_0^D, W_1^D, and W_2^D correspond to the relaxation transitions for the coupled spin system arising from a dipolar interaction; the transition W_0^{SC} corresponds to the relaxation transition arising from a scalar interaction between electron and nucleus; the transition W_{10} corresponds to the relaxation transition arising from the nuclear-nuclear interaction. The subscript numbers donate the total change in spin quantum number of S and I corresponding to the transition, and the superscripts D, SC denote dipolar and scalar interaction respectively.

The observed nuclear spin-lattice relaxation rate $1/T_1$ is given by the sum of the radical-induced dipolar and scalar contributions as well as the nuclear-nuclear interaction contributions[8].

$$\left(\frac{1}{T_1}\right)_{obs} = W_0^D + 2W_1^D + W_2^D + W_0^{SC} + 2W_{10} \qquad (2.11)$$

The theory of the relaxation rate and experimental results are discussed in chapter four.

2.5.2 Dynamic Nuclear Polarization

Dynamic nuclear polarization (DNP) is an Overhauser technique that provides direct information about the details of the relaxation mechanisms. The DNP phenomenon is critically dependent on the coupled relaxation transitions W_0 and W_2 for which the electron spin and nuclear spin change sign simultaneously. The dipolar and scalar contributions to the electron nuclear spin coupling are related to the DNP ultimate enhancement A_∞ as[8,9,10]

$$A_\infty = \frac{W_2^D - W_0^D - W_0^{SC}}{W_0^D + W_0^{SC} + 2W_1^D + W_2^D} \frac{\gamma_S}{\gamma_I} \qquad (2.12)$$

The theory of DNP in liquid and flow LLIT DNP experimental data for both CH_3CN/TEMPO and CH_3CONH_2/TEMPO system are given in Chapter V. The application of flow LLIT and solid/liquid intermolecular transfer (SLIT) experiments in various carbon samples is summarized in Chapter VI.

CHAPTER 3

Paramagnetic ^{13}C and ^{15}N Shifts Induced by Free Radicals

3.1 Introduction

Metal chelated lanthanide compounds have been widely used as shift reagents in NMR since they were discovered by Hinckley in 1969[15]. By using lanthanide metal chelated shift reagents, not only can spectral resolution be improved where overlapping peaks occur in a spectrum, but structural information can also be obtained[16]. In a similar fashion, paramagnetic shift and nuclear relaxation results for a variety of compounds utilizing di-tert-butyl nitroxide (DTBN) and other nitroxide free radicals were reported by Morishima et al[17]., and by Sysoeva et al[2].. The radical induced upfield ^{1}H contact shift and downfield ^{13}C contact shift observed in proton donor molecules were interpreted in terms of the hydrogen bond formation. The formation constants, enthalpies, limiting contact shifts, and spin density on the proton and carbon atoms were also determined from ^{1}H and ^{13}C contact shift measurements at various temperatures. Although many of the mechanistic features of free radical induced paramagnetic

shifts are not completely understood, there is general agreement that the existence of only a collision or otherwise very weak transient complex between the radical and other compounds in solution is sufficient to give rise to a paramagnetic shift from which the electron-nuclear hyperfine coupling constant (A) can be determined. Therefore, NMR contact shifts can be used as a sensitive probe to study the electron spin distribution on the diamagnetic solvent molecule perturbed by the interaction with an open shell free radical molecule.

The electron paramagnetic resonance (EPR) method has also been used to study the intermolecular interaction of the nitroxide radical and the change in the hyperfine coupling constant A or the electron g factor value of a free radical itself[18]. However, only limited information on the electronic structure of the solvent molecule perturbed by the interaction with the free radical can be obtained. Although EPR has the advantage of greater inherent sensitivity than NMR, the EPR spectra of some radicals, (e.g., organic radicals,) are very complex and an analysis of these spectra is difficult. In contrast to EPR spectra, NMR spectra are relatively simple, since for every group of equivalent nuclei only a single line is obtained. On the other hand, the resolution of NMR spectra is better than that of EPR spectra. Thus, NMR is particularly

useful in the determination of small coupling constants which can not be resolved by EPR and is a sensitive probe for elucidation of the nature of molecular interactions in solutions.

Instead of using DTBN, a similar nitroxide radical, TEMPO (2,2,6,6,-tetramethylpiperidinyl-1-oxy), has been used to induce paramagnetic ^{13}C shifts in both aromatic and paraffinic hydrocarbons and the results for 22 compounds were reported[19]. The results demonstrated that the TEMPO radical is more effective as a shift reagent than other free radicals.

In this study, the weak hydrogen bond formation between the open-shell free radical TEMPO and closed-shell molecules (e.g., CH_3CN and CH_3CONH_2) was investigated using ^{13}C and ^{15}N NMR contact shift measurements. The reasons for selecting TEMPO for this study are as follows: 1) the unpaired electron is localized in the N-O group and has been shown to undergo transient complex formation with hydrogen bond forming solvents; 2) TEMPO has a relatively high solubility in many organic solvents and is rather chemically inert; 3) it is readily available commercially, relatively stable, and has been used as a spin-probe or spin-labeling reagent in EPR. Both acetonitrile and acetamide molecules were selected because they have several different nuclei accessible in NMR

studies that can be used to probe the nature of the interaction with various parts of the substrate molecules. The two chemically different carbons may provide a direct and sensitive probe of such behavior. In addition to providing a third accessible site, ^{15}N nucleus is of great interest as it is sensitive to a scalar mechanism coupling the unpaired electron with the nuclei on the substrate molecule.

3.2 Basic Theory of Fermi Contact Shift

The paramagnetic induced shift results from two terms: a contact interaction and a dipolar or pseudocontact interaction between an electron and a nucleus[20]. The dipolar term acts through space in which the unpaired electron exerts a magnetic field on the nucleus by the dipolar-dipolar interaction and is inversely proportional to r_{IS}, the distance between the free electron and the magnetic nucleus. This shift is only observed if the magnetic field produced by the unpaired electron does not average to zero, i.e. it is anisotropic. The theoretical treatment of the pseudocontact term depends, among other things, on the anisotropy of the electron spin **g** tensor[21]. Hirayama and Honyu have assumed an axially symmetric **g** tensor in their treatment of Eu and Pr complexes in arriving at relative geometric factors for quinoline, isoquinoline, and acridine[22]. On the other hand, contact interaction arises from

a finite unpaired electron spin density on the nucleus caused by a partially covalent bond or weak transient complex formation. Since there is no directional aspect to the contact of the nucleus and the electron, this interaction is generally isotropic.

In liquids, if the molecules tumble randomly many times during a time shorter than the reciprocal of the hyperfine frequency, the field at the electron due to the dipolar interaction with the nucleus will average to zero. Therefore, the hyperfine interaction between the electron and the nucleus is due to the Fermi contact interaction only. The hyperfine interaction in solutions of organic radicals is generally isotropic and the shift of the NMR lines can usually be understood in terms of the Fermi contact interaction[20].

3.2.1 Basic Equations for Fermi Contact Shift

The equation relating the contact shift to the coupling constant can be derived from a Hamiltonian containing terms for the electronic Zeeman interaction, the nuclear Zeeman interaction, and the Fermi contact interaction.

$$\hat{H}=g\beta B_0\hat{S}_z-g_N\beta_N B_0\hat{I}_z+A\hat{I}_z\hat{S}_z \qquad (3.1)$$

The portion of the Hamiltonian containing the nuclear spin can be rewritten as

$$\hat{H}_N = -g_N\beta_N\hat{I}_Z(B_0 - A\hat{S}_z/g_N\beta_N) \tag{3.2}$$

The second term in this expression can be thought of as an effective local field at the nucleus produced by the nuclear-electron hyperfine interaction resulting in the shift of the spectral line from the position of a normal diamagnetic molecule. In cases in which the electron spin energy levels are rapidly averaged, the nucleus sees only a time averaged local field proportional to the mean value $\langle S_z \rangle$ of the electron spin component. Therefore, the effective field is equal to $-A \langle S_z \rangle / g_N\beta_N$ and the nuclear resonance signal shifts to high field by the amount

$$\Delta H = A\langle S_z \rangle / g_N\beta_N \tag{3.3}$$

Now the average of $\langle S_z \rangle$ is easily calculated from the bulk magnetic susceptibility χ of the electrons, for the quantity $M_0 = -Ng\beta\langle S_z \rangle$ is simply the equilibrium magnetic moment of the electrons in the external field, being equal to χB_0.

$$\langle S_z \rangle = \frac{-\chi B_0}{Ng\beta} \tag{3.4}$$

where N is the total number of the unpaired electrons. The shift of the NMR line is therefore given by

$$\Delta B = -\frac{A\chi B_0}{Ng\beta g_N\beta_N} \tag{3.5}$$

and is proportional to the applied field B_0. Substituting the standard expression for the spin susceptibility of a free electron

$$\chi = \frac{Ng^2\beta^2 S(S+1)}{3kT} \tag{3.6}$$

where k is Boltzmann's constant and T is absolute temperature. For organic free radicals with S = 1/2 , the relative shift is given by

$$\frac{\Delta B}{B_0} = -\frac{g\beta}{g_N\beta_N}\frac{A}{4kT} = \frac{\gamma_S}{\gamma_I}\frac{A}{4kT} \tag{3.7}$$

$$\frac{\Delta\nu}{\nu_0} = -\frac{\gamma_S}{\gamma_I}\frac{A}{4kT} \tag{3.8}$$

where $\Delta\nu$ is the relative change in chemical shift represented in units of frequency, and ν_0 is the observed frequency. The paramagnetic induced shift would be similar to the conventional chemical shift in ordinary NMR experiment, if down field shifts were reported as negative when expressed as $\Delta B/B_0$ and positive when expressed as $\Delta\nu/\nu_0$. Therefore, equation 3.7 or 3.8 can be used to determine the coupling

constant A from the corresponding NMR contact shift.

Not only the magnitude of the hyperfine coupling but also its sign can be determined by this NMR technique. The electron spin density at the nucleus may arise from excess electrons S = -1/2 or S = 1/2. Spin density arising from an excess of electron S = -1/2 is taken as positive since its magnetic moment has same direction as the applied magnetic field. It will augment the effective magnetic field of the nucleus and cause a downfield contact shift. The coupling constant is positive in this case and the reverse holds for the excess electron with spin, S= 1/2. Therefore, from the direction of the contact shift, the sign of the coupling constant can be easily determined. Lines shifted to low field have positive electron spin density and coupling constant while those shifted to a higher magnetic field have a negative density and coupling constant.

3.2.2 Equations for the System of Solvent-Solute Interaction

In the system where the radicals interact with the diamagnetic solvent molecules, the contact shifts of the diamagnetic solvent molecules induced by the free radicals depend on the radical concentration, solvent concentration, and equilibrium constant. In this case, the coupling constant can not be obtained by direct application of equation (3.7 or

3.8). The methodology for determining the coupling constant in these systems is discussed below[5].

Assume the interaction of a radical R and a substrate S can be expressed as the following equation

$$R\bullet + S \rightleftharpoons [R\bullet \cdots S] \qquad (3.9)$$

where $[R\bullet \cdots S]$ is the short-lived solvent-solute transient complex.

For the case of fast exchange, the observed chemical shift δ is given by

$$\delta_{obs} = \chi \cdot \delta_{R\cdot\cdot S} + (1-\chi) \cdot \delta_S \qquad (3.10)$$

where χ is the mole fraction of $[R\bullet \cdots S]$, $\delta_{R\cdot\cdot S}$ and δ_S are the chemical shifts of the complex $[R\bullet \cdots S]$ and the substrate S, respectively. If C_χ is the concentration of the complex $[R\cdot\cdot S]$, C_0 and C_R are initial concentrations of the substrate molecule and radical, respectively, and $C_0 >> C_R$, χ can be expressed as

$$\chi \approx \frac{[R\cdot\cdot S]}{[S]_0} = \frac{C_x}{C_0} \qquad (3.11)$$

and we can define the relative chemical shift as follow:

$$\Delta = \delta_{obs} - \delta_S \tag{3.12}$$

$$\Delta_0 = \delta_{R\cdots S} - \delta_S \tag{3.13}$$

Substitute Δ, Δ_0 into eq.(3.10), we have

$$\chi = \Delta / \Delta_0 \tag{3.14}$$

Thus, Δ is the observed shift change from the diamagnetic solution (C_R = 0) to the paramagnetic solution (C_R) and it is equal to the limited contact shift Δ_0, if the mole fraction of solvent-solute complex χ is one.

The formation constant of complexes K_c can be expressed as

$$K_c = \frac{[R\cdots S]}{([S]_0 - [R\cdots S])([R]_0 - [R\cdots S])} = \frac{C_\chi}{(C_0 - C_\chi)(C_R - C_\chi)} \tag{3.15}$$

If $C_0 >> C_R$ eq.(3.15) can be simplified as

$$K_c = \frac{C_X}{C_0 (C_R - C_X)} \tag{3.16}$$

Combining eq.(3.11), (3.14), (3.16), we have

$$\frac{C_R}{\Delta} = \frac{1}{K_c \Delta_0} + \frac{C_0}{\Delta_0} \tag{3.17}$$

Using this equation, K_c and Δ_0 can be determined from the measurement of contact shifts with varying initial concentrations of substrate molecule C_0. If the experimental C_R/Δ values plotted versus the concentration C_0, then Δ_0 is obtained from the slope, and the equilibrium constant K_c is obtained from the intercept.

3.3 Experimental Section

3.3.1 Chemicals

The substrate molecules and free radicals were commercial samples purchased from Aldrich Chemical co. and used directly without further purification. The preparation of $CH_3C^{15}N$ and $CH_3CO^{15}NH_2$ have been presently described[23].

3.3.2 Preparation of the Samples

A concentrate $CH_3C^{15}N$ solution was prepared in a solvent mixture of 5% C_6H_{12}/5% C_6D_{12}/90% CCl_4. A weighed amount of TEMPO was added to this solution. The acetonitrile concentrations in a series of samples were made by successive dilution with the solvent mixture described in the range 0.4 M to 2.0 M for the chemical shift measurement study. A series of ^{15}N-acetamide solutions were made in a similar manner but dissolved in d_8-dioxane because of inherent low solubility in CCl_4. The samples were purged of dissolved oxygen by the

freeze-thaw method.

3.3.3 NMR Measurements

All of the spectra were recorded on a Varian Unity 400 FT-NMR Spectrometer at ambient temperatures. C_6D_{12} was used as an internal lock standard.

3.4 Results and Discussions

3.4.1 Paramagnetic Induced Chemical Shift

3.4.1.1 $CH_3C^{15}N$/TEMPO System

In samples containing different concentrations of $CH_3C^{15}N$ ranging from 0.4 M to 2.0 M, the ^{13}C chemical shifts were measured relative to an internal cyclohexane reference[17] and listed in Table 3.1. ^{15}N chemical shifts were not referenced to an internal ^{15}N NMR standard, but rather were referenced by direct frequency comparison with the ^{13}C NMR shift standard, C_6H_{12}. The data for ^{15}N paramagnetic shifts are listed in Table 3.2. The $-^{13}CH_3$ signal appears to shift from 3.9 to 7.9 ppm (downfield) in the presence of a given amount of the free radical, whereas the signal of $-^{13}CN$ is shifted to a higher field and the shift is less than 1 ppm for the concentrations employed. It is noteworthy that the methyl group has greater paramagnetic shifts than does the cyano group in the same molecule. This indicated that there is a stronger interaction

Table 3.1: ^{13}C Contact shifts[a] of CH_3CN/TEMPO System

Concentration (M)[b]		0.4	0.8	1.2	1.6	2.0
Paramagnetic Shift δ(ppm)[c]	$-^{13}CH_3$	7.90	6.19	5.51	4.71	3.94
	$-^{13}CN$	- 1.01	- 0.90	- 0.45	- 0.27	-0.42

a. All measurements were made at room temperature(25 ^{0}C).
b. Molarity of CH_3CN in CCl_4.
c. Chemical shifts were measured relative to internal cyclohexane[19].

Table 3.2: ^{15}N Contact shifts[a] of $CH_3C^{15}N$/TEMPO System

Concentration (M)[b]	0.2	0.4	0.6	0.8	1.0	1.2
Paramagnetic Shift δ(ppm)[c] of $-C^{15}N$	2.19	1.87	1.88	1.62	1.68	1.38

a. All measurements were made at room temperature(25 ^{0}C).
b. Molarity of CH_3CN in CCl_4.
c. ^{15}N chemical shifts were not referenced to an internal ^{15}N NMR standard, but rather were referenced by direct frequency comparison with the ^{13}C NMR shift standard, C_6H_{12}.

between the methyl group and the free radical TEMPO. The N-O linkage containing the free electron in TEMPO would be expected to be closer to the methyl group, providing correspondingly a larger contact shift. As pointed out by Draney and Kingsbury[24], the interaction of certain substrates with free radicals yields concentration-dependent chemical shifts, which can be interpreted in terms of transient complex formation. Morishima[17] suggested that hydrogen bonding would seem to be involved in the $CHCl_3$/DTBN system, and the C-H bond appeared to be the site of interaction. On the other hand, if the intermolecular interactions between a substrate and a free radical involve only weak van der Waal forces, then to a good approximation, ideal solution behavior will be obtained and the chemical shift appears to be functionally independent of the substrate concentration. In this case, it is possible that equilibrium relationships are not appropriate and a momentary contact interaction is merely governed by diffusional constraints, as pointed out by Poindexter some years ago[25]. Therefore, the concentration dependent chemical shift results of the methyl carbon suggest that there is an association equilibrium governed by transient hydrogen bonding formation for CH_3CN/TEMPO system, and that the C-H bond appears to be the site of complexation. The observed downfield ^{13}C contact shift of the methyl carbon in CH_3CN results from the hydrogen bonding and electron spin transfer

from TEMPO to the C-H bond by the spin polarization mechanism[24]. The pattern of the data that carbons attached to hydrogens undergo downfield shifts and carbons lacking an attached hydrogen provide upfield shifts is consistent with Morishima's observation[17]. In contrast with the $-^{13}CH_3$ contact shift, radical-induced ^{15}N shifts within the same molecule (acetonitrile) are small. The result can be understood in terms of the nitrogen atoms in TEMPO and CH_3CN tend to orient in opposite directions from one another in the collision complex. Presumably, electrostatic repulsion between the lone-pair electrons of the nitrogen atom and the unpaired electron of the TEMPO could account for this effect[26]. The preferential collision of CH_3CN molecule with the free radical TEMPO is showed in Fig. 3.1.

3.4.1.2 ^{15}N-Acetamide/TEMPO System

In samples containing different concentrations of acetamide ranging from 0.05 M to 0.5 M, the ^{13}C and ^{15}N contact shifts observed are listed in Table 3.3. It is noteworthy that larger ^{15}N paramagnetic shifts are observed in comparison with the methyl group for the acetamide molecule. This suggests that there is a greater affinity for complexation between the amino group and the free radical TEMPO. The results suggest that the N-O linkage containing the free electron in TEMPO would be closer to the amino group,

a)

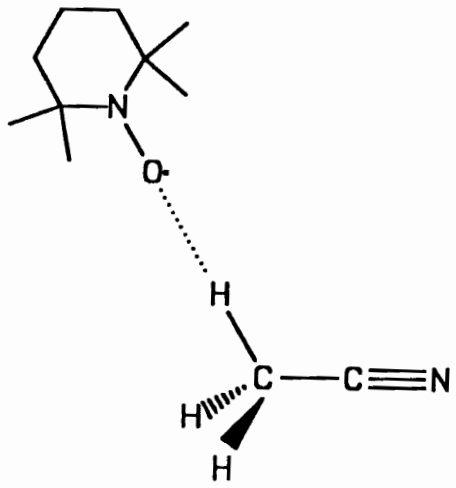

b)

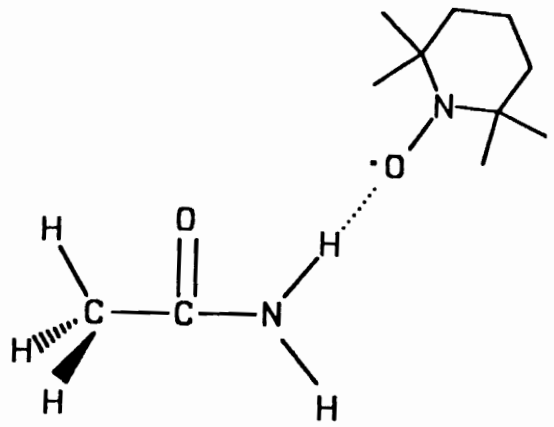

Figure 3.1 Preferential Collision in a) CH_3CN/TEMPO, and b) CH_3CONH_2/TEMPO Systems.

Table 3.3: ^{13}C and ^{15}N Contact shifts[a] for ^{15}N-Acetamide/TEMPO System

Concentration (M)[b]		0.1	0.2	0.3	0.4	0.5
Paramagnetic Shift δ(ppm)	$-^{13}CH_3$[c]	0.60	0.59	0.56	0.53	0.51
	$-^{13}CONH_2$[c]	- 0.34	- 0.26	- 0.30	- 0.24	-0.26
	$-CO^{15}NH_2$[d]	5.99	5.93	5.59	5.38	5.10

a. All measurements were made at room temperature(25 ^{0}C).
b. Molarity of CH_3CONH_2 in Dioxane.
c. ^{13}C chemical shifts were measured relative to internal cyclohexane[19].
d. See Table 3.2.

providing a larger contact shifts (see Fig. 3.1). This may be understood since acetamide, unlike the acetonitrile, has hydrogens attached to the nitrogen atom, and the protons may hydrogen bond with the nitroxyl group of TEMPO thereby increasing the interaction with the nitrogen nucleus. These results are consistent with that observed in nitrogen heterocycles[26].

3.4.2 The Formation Constant K and Hyperfine Coupling Constant A

As described earlier, the hyperfine coupling constant A can be easily obtained from the NMR contact shift using equation (3.7 or 3.8). However, in systems where the radicals and the diamagnetic solvent molecules form a transient hydrogen bonding complex, a plot of C_R/Δ versus C_0 is needed to analyze the data, where C_R and C_0 are the concentration of TEMPO and $CH_3C^{15}N$ (or $CH_3CO^{15}NH_2$) respectively. Fig. 3.2 and Fig. 3.3 illustrate these plots for solutions of ^{15}N-acetonitrile and ^{15}N-acetamide with TEMPO, respectively. The formation constant K and the limiting contact shift Δ_0 were obtained from the intercept and the slope of these plots, respectively. After resolving the limiting contact shift, the hyperfine coupling constant A for both systems were calculated using equation (3.8). The limiting contact shifts Δ_0, hyperfine coupling constants A, and equilibrium constants K

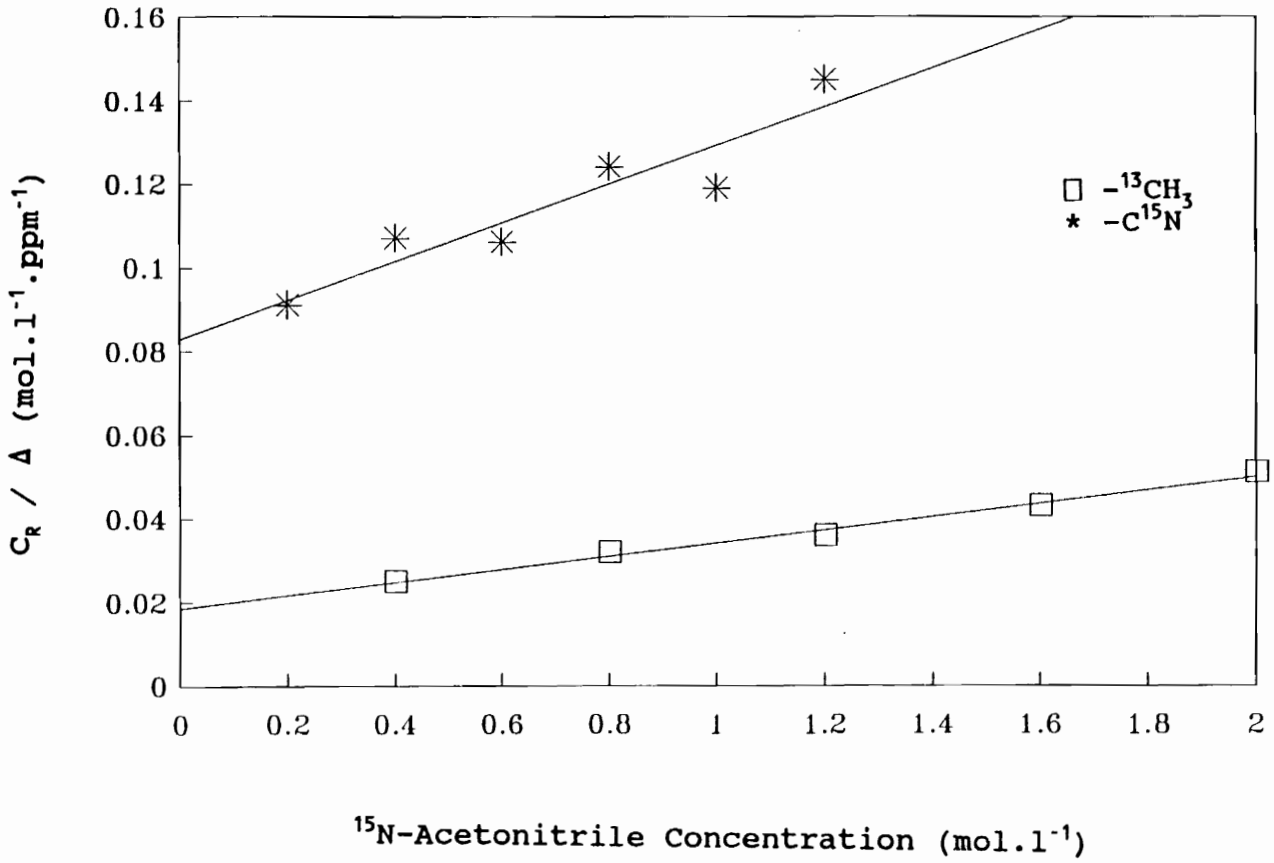

Figure 3.2: Experimental C_R/Δ Values (9.4T) Plotted Versus the Concentration of ^{15}N-Acetonitrile C_0 for the System ^{15}N-Acetonitrile/TEMPO Diluted with Carbon Tetrachloride. □: $-^{13}CH_3$; Slope: 0.015 ± 0.001 (ppm^{-1}); Intercept: 0.019 ± 0.001(mol.L^{-1}.ppm^{-1}). *: $-C^{15}N$; Slope: 0.046 ± 0.009 (ppm^{-1}); Intercept: 0.083 ± 0.007 (mol.L^{-1}.ppm^{-1}).

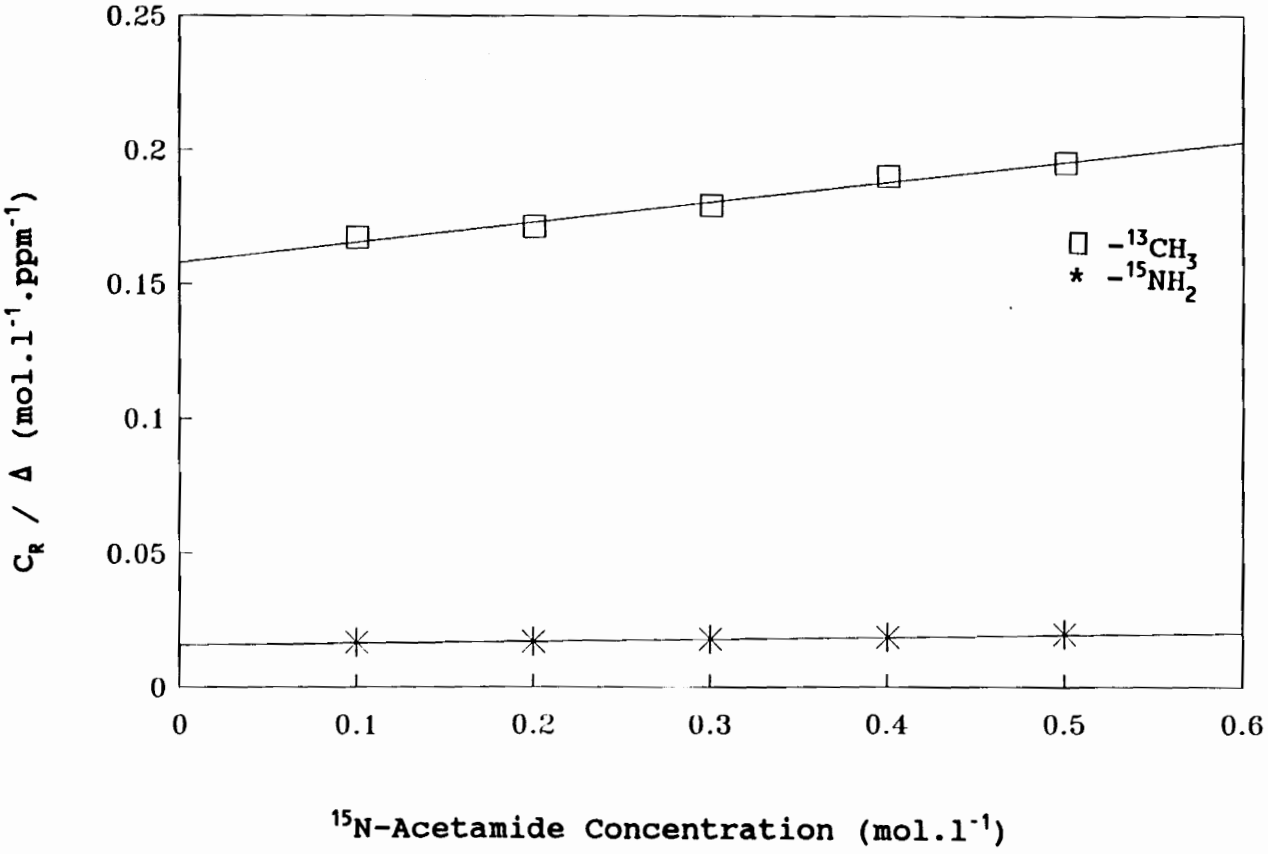

Figure 3.3: Experimental C_R/Δ Values (9.4T) Plotted Versus the Concentration of ^{15}N-Acetamide C_0 for the System ^{15}N-Acetamide/TEMPO Diluted with Dioxane. □: $-^{13}CH_3$; Slope: 0.075 ± 0.007(ppm^{-1}); Intercept: 0.158 ± 0.002 (mol.L^{-1}.ppm^{-1}). *:$-^{15}NH_2$; Slope: 0.0075 ± 0.0008 (ppm^{-1}); Intercept: 0.0157 ± 0.0003 (mol.L^{-1}ppm^{-1}).

derived from the paramagnetic shift measurements for both systems are listed in Table 3.4 & 3.5.

3.5 Summary

With the use of the free radical TEMPO as a shift reagent, the ^{13}C and ^{15}N Fermi contact shifts induced by hydrogen bond formation in CH_3CN/TEMPO and CH_3CONH_2/TEMPO system have been studied. The downfield ^{13}C and ^{15}N contact shifts can be interpreted in terms of the spin polarization mechanisms of electron spin transfer from N-O group of TEMPO radical to the X-H bond (X = C, or N). The formation constants, the limiting contact shifts, and the hyperfine constant have been determined for the X-H$\cdots$TEMPO hydrogen bond interaction from ^{13}C and ^{15}N contact shifts measurements. In the CH_3CN/TEMPO system, the data show that the stronger interaction is at the methyl group. It would appear that the nitrogen atom in CH_3CN molecule tends to orient away from the N-O linkage in the TEMPO radical. In contrast, the amino linkage in CH_3CONH_2 molecule exhibits a much stronger interaction with TEMPO via hydrogen bond formation.

The hyperfine coupling constant A observed in the present study range from 0.1-0.6 MHz and are somewhat lower than alcohol/nitroxide systems previously reported[5]. However,

Table 3.4: Limiting ^{13}C and ^{15}N Contact Shifts Δ_0, Hyperfine Constant A and Equilibrium Constant K_c for the ^{15}N-Acetonitrile/TEMPO System

Group	K_c[a]	Δ_0 (ppm)	A/h (MH_z)
$-^{13}CH_3$	0.8 ± 0.08[b]	70[c] ± 4	0.66 ± 0.04
$-^{13}CN$		0[c] ± 2	0
$-C^{15}N$	0.6 ± 0.1	22 ± 4	-0.08 ± 0.02

a. The values are calculated from the slope of the chemical shifts versus concentration plot.
b. Standard deviations are estimated from regression analysis.
c. The values are calculated from the slope of the chemical shifts versus concentration plot and corrected with the internal reference Δ_0 = 4.0 ppm[19].

Table 3.5: Limiting ^{13}C and ^{15}N Contact Shifts Δ_0, Hyperfine Constant A and Equilibrium Constant K_c for the ^{15}N-Acetamide/TEMPO System

Group	K_c[a]	Δ_0 (ppm)	A/h (MH_z)
$-^{13}CH_3$	0.48 ± 0.04[b]	17[c] ± 1	0.16 ± 0.01
$-^{13}CONH_2$		-1[c] ± 2	-0.01 ± 0.02
$-^{15}NH_2$	0.48 ± 0.05	130 ± 10	-0.5 ± 0.04

a. The values are calculated from the slope of the chemical shifts versus concentration plot.
b. Standard deviations are estimated from regression analysis.
c. The values are calculated from the slope of the chemical shifts versus concentration plot and corrected with the internal reference Δ_0 = 4.0 ppm[19].

they are consistent with that found in other comparable systems where weaker hydrogen bond formation is possible (e.g. aniline/nitroxide solutions)[27]. The differences appear reasonable since the N-H bond in CH_3CONH_2 and C-H bond in CH_3CN are less positively polarized than O-H bonds in alcohols and C-H bonds in halogen-methanes[5].

In the next two chapters of this dissertation, this weak hydrogen bond interaction was further examined using electron-nuclear relaxation and DNP studies.

CHAPTER 4

FREE RADICAL INDUCED NUCLEAR RELAXATION RATES

4.1 Introduction

Magnetic resonance techniques have been used for a long time to obtain detailed information on chemical systems at the molecular level. In addition, the measurement of nuclear relaxation times provides dynamic information about molecular motion and intermolecular interactions. The nuclear relaxation times in a diamagnetic liquid are considerably reduced when small concentrations of paramagnetic solutes are added. The relaxation is then dominated by pairwise interactions between an unpaired electron spin of the solute and the nuclear spin being studied. Therefore, a detailed analysis of the nuclear relaxation time induced by stable free radicals will provide further insight into the dynamic behavior of these intermolecular interactions.

Gutowsky and Tai[28] studied the solvent-radical interaction from measurement of proton and fluorine relaxation times and demonstrated that the ^{1}H relaxation mechanism for the

solvent/radical bimolecular system could be explained by a nuclear-electron dipole-dipole interaction characterized by a combination of translational and rotational motions. Poindexter et al.[29] have shown from DNP studies that the fluorine nuclei of fluorobenzenes are relaxed by collision with free radicals with a characteristic translational correlation time. These studies, however, dealt with very weak molecular interactions with nonspecific complexation.

Solutions of nitroxide radicals in protic solvents have been of particular experimental and theoretical interest for studying molecular interactions in liquids by NMR relaxation techniques. Hydrogen-bonded complexes of nitroxide radicals with various alcohols have been extensively studied by proton spin-lattice relaxation[1,2,6,30]. Bundfuss et al.[6] have measured the ^{1}H spin-lattice relaxation rates of methanol, 2-propanol, and acetic acid over a wide range of magnetic field strengths and a range of temperatures. The results demonstrate hydrogen bond formation between the solvent proton and the N-O linkage of the free radical. The relaxation of the acidic protons were dominated by dipole-dipole interactions modulated by anisotropic motion of the complexes. The scalar interaction contributed only at low frequency and was modulated by the lifetime of the complex of the radicals with the organic ligands. However, for small molecules such as

chlorofluoromethanes[1] the radical induced relaxation processes of both ^{1}H and ^{19}F nuclei were governed by isotropic rotational diffusion of the complex.

Müller-Warmuth et al.[7] have measured ^{1}H NMR relaxation rates of solutions of aniline with nitroxide free radicals over a large frequency range between 100 kHz and 300 MHz. The relaxation of the protons was dominated by a dipolar interaction modulated by rotational diffusion during the lifetime of complex.

Morishima and co-workers[30], have used pulsed NMR methods to measure associations on the order of 10^{-11} s between typical weak hydrogen bond-forming solvent molecules such as CH_3OH and $CHCl_3$ and paramagnetic solutes such as di-tert-butyl nitroxide (DTBN) free radical. The intermolecular bond lengths and the lifetimes of the complexes were also determined.

Overall, the relaxation rates of solvent molecules induced by free radicals contain important parameters of molecular collision in liquids such as the radical-solvent distances, correlation times associated with radical-solvent interaction, and the intermolecular hyperfine constant. Therefore, a set of static and dynamic parameters of solvent-solute interaction can be obtained by studying the radical

induced relaxation times.

In this investigation, the ^{1}H NMR relaxation times in both CH_3CN/TEMPO and CH_3CONH_2/TEMPO systems were measured as a function of frequency in order to obtain more detailed information regarding the molecular motions involved in TEMPO/substrate system. The observed relaxation rates were analyzed on the basis of the general Solomon-Bloembergen[31,32] approach. The dipolar correlation times, and the intermolecular distances between the proton and the unpaired electron were obtained for both systems. The ^{13}C and ^{15}N relaxation rates were measured at high magnetic field and the scalar correlation times were also determined.

4.2 Models for Nuclear-Electron Intermolecular Interactions

The relevant theory for these studies has been summarized recently[10,31-36]. The general requirement for relaxation is a magnetic field which fluctuates at the appropriate frequency, inducing a transition between two energy levels. The nuclear magnetic moments, μ_I , provide local magnetic fields that fluctuate according to the molecular motion. In a nonviscous liquid a molecule remains in one state of motion for about 10^{-10} ~ 10^{-12} sec. After this time it suffers a collision which changes its spatial position. If the molecule persists in one state of motion for a time of 10^{-12} sec., we expect that its motion will have frequency components from 0 to 10^{12} Hz. Therefore, the frequency of the molecular motions in a liquid covers a wide range; at any given time some of the molecules are moving quite slowly while others are moving very rapidly. However, only molecular motions at the resonance frequencies will induce relaxation transitions.

A constant τ_c defined as the correlation time can be viewed as a time scale for these random fluctuations. For rapid random motions, the nuclei lose memory of previous orientations very rapidly, producing a small τ_c value. The τ_c values for liquids are in range of 10^{-10} - 10^{-12} s.

A more quantitative fashion to express τ_c is the correlation function $G(\tau)$ and its Fourier transform partner $J(\omega)$ referred to as the spectral density which will provide the intensities or probabilities of the molecular motions at the resonance frequency[21].

$$J(\omega) = \int_{-\infty}^{\infty} G(\tau) \exp(i\omega t) d\tau \qquad (4.1)$$

The correlation function $G(\tau)$ decays with τ_c , as "memory" is lost, and this decay is often assumed to be exponential:

$$G(\tau) = \exp(-|\tau|/\tau_c) \qquad (4.2)$$

Substitution of eq. 4.2 followed by explicit integration gives

$$J(\omega) = \frac{2\tau_c}{1+\omega^2\tau_c^2} \qquad (4.3)$$

For any random motion there is a whole spectrum of frequencies, and the variation of the intensity of the fluctuations with frequency $J(\omega)$ must depend on the type of motion concerned. In most cases, the variation of $J(\omega)$ with ω is of the general form shown in Fig.4.1[35]. $J(\omega)$ is independent of ω until $\omega\tau$ approaches unity, and then approaches zero as ω increases. When τ is small, $J(\omega)$ is low and extends to high values of ω; when τ is large, $J(\omega)$ is greater, but falls to zero at lower frequencies. The relaxation times are thus dependent on the values of $J(\omega)$ at the particular value of ω. When the value of $J(\omega)$ at the

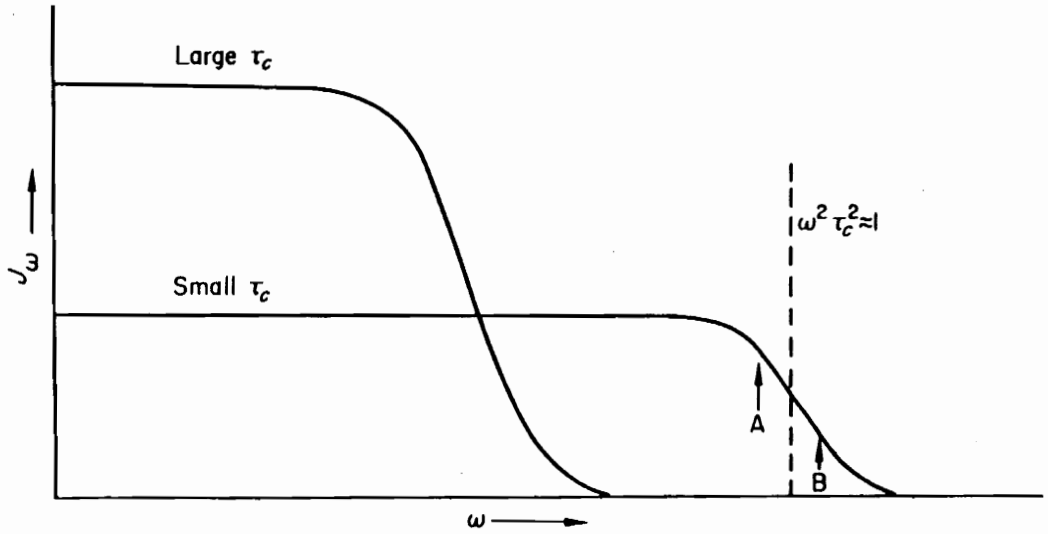

Figure 4.1 Spectrum of Frequencies of Molecular Motion in a Liquid. ω_I usually is in the flat part of the curve, ω_S can be near A or B for magnetic field strengths in the range 1-10 Kgauss.

resonance frequency is small, T_1 will be long. The fact that the area under these curves is constant is important, which means the amount of molecular power available for molecular motions is fixed and changing τ_c changes only the way that the power is distributed.

For most liquids, τ_c is on the order 10^{-10} ~ 10^{-12} sec and $\omega_I\tau$ is usually much less than unity. The corresponding value of $J(\omega)$ is more or less independent of ω and hence the applied magnetic field strength. This region is known as the extreme narrowing condition[31], $\omega_I\tau << 1$.

The spin-lattice relaxation times depend not only on the value of $J(\omega)$, but also on the strength of the coupling between the spin system and the lattice. In the coupled electron-nuclear system, the local magnetic field generated by the unpaired electron spin is much greater than the nuclear spin because the electron magnetic moment, μ_s, is ~ 10^3 times greater than the nuclear magnetic moment μ_I. Therefore, nuclear relaxation is dominated by nuclear-electron interactions in solutions containing free radicals[32]. Since simultaneous nuclear-electron spin transitions can occur, the nuclear relaxation processes will not only depend on the spectral density function $J(\omega_I)$, but also on the spectral density function $J(\omega_I \pm \omega_S)$ which characterize the double-spin

transitions. Since $\omega_s >> \omega_I$, the spectral density functions $J(\omega_I \pm \omega_S)$ can be approximated by those at $J(\omega_S)$. Although in most liquids $\omega_I \tau$ is generally less than unity, this is not so for $\omega_S \tau$. In this case, the extreme narrowing condition is not valid, and $J(\omega)$ is then dependent on the applied field, B_0. Thus measurement of relaxation phenomena at high magnetic fields provides a sensitive test of the shape of the correlation function and the model postulated for the molecular motion. In general, any mechanism which gives rise to a fluctuating magnetic field at a nucleus is a possible relaxation mechanism. The strong local fields produced by the electron can be coupled to the nuclei by two different mechanisms. One is dipolar coupling and the other is scalar coupling (see previous Chapter).

The different time dependencies which modulate the scalar and dipolar interactions are described in terms of models. The exact form for the transition probability will depend on the model chosen.

4.2.1 The Dipolar Model

The mode of interaction between a substrate molecule and a free radical can be classified into two typical cases: 1) no chemical interaction, and 2) formation of a labile molecular complex. In case 1, the nuclear-electron intermolecular

dipolar coupling is modulated by translational diffusion motion, the theory of which was developed by Hubbard[33]. The time dependence of this motion is introduced by a variation of both r_{IS}, the distance between the nuclear and electron spin, and the angle θ between r_{IS} and magnetic field B_0. In case 2, however, when a solvent molecule forms a labile complex with a free radical, the dipolar interaction can be modulated by the rotational diffusion motion of the transient complex. The time dependence of rotational motion is introduced solely by a variation of the angle θ between r_{IS} and B_0. The observed relaxation times can be analyzed on the basis of the general Solomon-Bloembergen theory[31,32].

4.2.1.1 The Rotational Model

If the receptor and radical molecules form a transient complex, the dipolar coupling can be modulated by rotational tumbling of the associated species. When the conditions $\omega_S\tau_r >> \omega_I\tau_r$ and $\omega_I\tau_r << 1$ are satisfied, the radical induced dipolar transition probabilities are given by[31]

$$2W_1^D-3W_0^D-W_2^D/2-\frac{3}{10}\left(\frac{\mu_0}{4\pi}\right)^2\frac{\gamma_I^2\gamma_S^2\hbar^2\tau_r}{r^6}J_r(\omega_i) \qquad (4.4)$$

where τ_r is the correlation time for rotation diffusion which is given by

$$\tau_r = \frac{4\pi b^3 \eta}{3kT} \tag{4.5}$$

η is the viscosity of the solution, b is the effective tumbling radius of the molecular complex, r is the average pair radius for the rotating adduct, μ_0 is the permeability constant, and $J_r(\omega_i)$ is the spectral density function for rotationally modulated diffusion which is given by

$$J_r(\omega_i) = \frac{1}{1+\omega_i^2 \tau_r^2} \tag{4.6}$$

The term ω_i is the Larmor frequency and is equal to ω_I, $(\omega_S + \omega_I)$, $(\omega_S - \omega_I)$ for W_1^D, W_0^D, and W_2^D respectively.

The radical induced dipolar spin-lattice relaxation rate R_1 is given by

$$R_1 = \frac{1}{T_1} = 2W_1^D + W_0^D + W_2^D \tag{4.7}$$

If equation (4.4) is inserted into equation (4.7) and the approximation $J(\omega_S \pm \omega_I) \approx J(\omega_S)$ is made, the radical induced dipolar spin-lattice relaxation rate for rotational diffusion is[31,32]

$$R_{1r} = \frac{1}{10}\left(\frac{\mu_0}{4\pi}\right)^2 \frac{\gamma_I^2 \gamma_S^2 \hbar^2 \tau_r}{r^6} [3J_r(\omega_I) + 7J_r(\omega_S)] \qquad (4.8)$$

Whereas a corresponding equation for spin-spin relaxation is given as

$$R_{2r} = \frac{1}{20}\left(\frac{\mu_0}{4\pi}\right)^2 \frac{\gamma_I^2 \gamma_S^2 \hbar^2 \tau_r}{r^6} [4J_r(0) + 3J_r(\omega_I) + 13J_r(\omega_S)] \qquad (4.9)$$

where $J_r(0)$ is the spectral density function for dipolar coupling at zero frequency.

4.2.1.2 The Translational Model

In the absence of complexing, the dipolar coupling can be modulated by translational diffusion. The radical induced dipolar transition probabilities are given by[33]

$$2W_1^D = 3W_0^D = W_2^D/2 = \frac{2\pi}{5} \frac{N_e \gamma_I^2 \gamma_S^2 \hbar^2 \tau_t}{r^3} J_t(\omega_i) \qquad (4.10)$$

Here, r is the distance of closest approach between the radical and the receptor, N_e is the unpaired electron concentration and τ_t is the translational correlation time which is given as

$$\tau_t = \frac{6\pi a \eta r^2}{5kT} \qquad (4.11)$$

where a is the radius of the interacting particles. The translational spectral density function $J_t(\omega_i)$ is given by[38-40]

$$J_t(\omega_i) \approx \frac{1}{[1+0.9(\omega_i\tau_t)^{1/2}+1.5(\omega_i\tau_t)^{3/2}]} \qquad (4.12)$$

Therefore for translational diffusion, the radical induced dipolar spin-lattice relaxation rate is given by

$$R_{1t} = \frac{2\pi}{15}\frac{N_e\gamma_I^2\gamma_S^2\hbar^2\tau_t}{r^3}[3J_t(\omega_I)+7J_t(\omega_S)] \qquad (4.13)$$

In addition to dipolar-dipolar interaction between the free radical and the substrate molecules, a scalar interaction is also a possible relaxation process in many cases. The models for scalar transition are discussed below.

4.2.2 Scalar Nuclear-Electron Interaction

The transition W_0^{SC} defines the relaxation arising from the spin exchange interaction or scalar coupling between electron and nucleus. A diffusion model[33] or a sticking model[31,41] can be used to account for the scalar transition probability W_0^{SC}.

4.2.2.1 The Sticking Model[31,32]

The sticking model assumes that there is a finite scalar interaction only during the time that the spins I and S are

"stuck" together. When the spins are stuck together, the scalar interaction is characterized by a coupling constant, A, which is zero under all other conditions. The time dependence of A arises because the time of sticking is assumed to be a random variable. This model leads to the following expression for the scalar transition W_0^{SC}

$$W_0^{SC} = \frac{1}{2}\left(\frac{A}{\hbar}\right)^2\left(\frac{\tau_{SC}}{1+(\omega_S+\omega_I)^2\tau_{SC}^2}\right) \qquad (4.14)$$

where $A/\hbar$ is the hyperfine coupling constant in frequency units times 2π and is a measure of the induced electron spin density, and τ_{SC} is the scalar correlation time.

The radical induced scalar spin-lattice relaxation rate for the sticking model is given as

$$\left(\frac{1}{T_1}\right)_{SC} = \frac{1}{2}\left(\frac{A}{\hbar}\right)^2 J(\omega_I+\omega_S) \qquad (4.15)$$

and the corresponding spin-spin relaxation rate $(1/T_2)$ is given as

$$\left(\frac{1}{T_2}\right)_{SC} = \frac{1}{4}\left(\frac{A}{\hbar}\right)^2\left[J(0)+J(\omega_I+\omega_S)\right] \qquad (4.16)$$

The scalar correlation time τ_{sc} is defined as the sum of two terms[39,42]

$$\frac{1}{\tau_{sc}} = \frac{1}{\tau_h} + \frac{1}{\tau_s} \qquad (4.17)$$

where τ_s is the electron spin-lattice relaxation time and τ_h is the mean lifetime of the complex. For organic free radical solutions, τ_s is usually much longer than the time scale of the interaction[43,44]. For example, the electron spin-lattice relaxation time is typically 10^{-6} - 10^{-8} for organic free radical. Therefore, τ_{sc} depends only on τ_h, and an estimate of τ_h can be made by using equation(4.14) provided that the hyperfine constant A and R_{sc} are known.

4.2.2.2 The Diffusion Model[33]

In the diffusion model, the scalar interaction is assumed to be a function of the distance between the I and S spins. As in the dipolar case, the variation of distance r with time is responsible for the time dependence of the interaction. Thus, unlike the sticking model, the unpaired electron density produced at the nucleus is not at one instant finite and then zero(i. e., switched on and then off), but it approaches its maximum value as the radical and solvent molecules collide and then decays to zero again as the molecules recoil from each other. Since the scalar interaction could arise from the electron-orbital overlap with the nucleus, it is assumed to be

of a very short range and thus a steep function of the internuclear distance. It is therefore postulated that overlap varies exponentially with the internuclear distance, and A is then assumed to have the form

$$A_{IS} = \frac{Ad}{r_{IS}} \exp\left[-\lambda(r_{IS}-d)\right] \qquad (3.18)$$

where A_{IS} is the instance value of the hyperfine coupling, A and λ are constants, r_{IS} is the distance between the I and S spins and d is their distance of closest approach.

The diffusion model leads to a more complicated expression for a scalar transition probability

$$W_0^{SC} = \frac{N_e \pi A^2 d^3}{2\lambda D(\omega\tau_S)^{1/2}}\left[1+\exp(\omega\tau_S)^{1/2}\left[\sin(\omega\tau_S)^{1/2}-\cos(\omega\tau_S)^{1/2}\right]\right] \qquad (4.19)$$

where $\omega = \omega_I + \omega_S$, D is the average diffusion constant of the radical and receptor nuclei, and N_e is the number of spins.

4.2.3 Mixed Scalar and Dipolar Interactions

In principle, dipolar interactions are always present between the electrons and nuclei; additional complication will arise when there are also scalar interactions. When both interactions are present it is necessary to combine the above model for the dipolar interaction with one of the models for the scalar interaction. Obviously, there are many

combinations which are dependent on the particular system being studied. A general review of the models has been reported[8].

4.3 Experimental

4.3.1 Chemicals

The ^{15}N labelled acetonitrile and acetamide were synthesized by Mr. David Morgan from ^{15}N labelled ammonia[23]. All other solvents and the radical used were commercial samples from Aldrich. They were used without further purification. A series of TEMPO radical solutions in the concentration range of 0.026 to 0.103 M were prepared using a solvent mixture of 7% CH_3CN/ 5% C_6H_{12}/ 88% CCl_4 for the CH_3CN/TEMPO system.

4.3.2 Relaxation Rates Measurements

The ^{13}C and ^{15}N spin-lattice relaxation experiments were performed utilizing a Varian Unity 400 pulsed FT-NMR spectrometer and measured using the inversion-recovery method ($180^0 - \tau - 90^0$ pulse sequence). The ^1H NMR spin lattice relaxation rates for both the CH_3CN/TEMPO and CH_3CONH_2/TEMPO solutions were measured in the frequency range of 80-400 MHz. The ^{13}C and ^{15}N spin-spin relaxation times T_2 were derived from the broadening of the NMR signals in the presence of the free radical TEMPO.

4.4 NMR Relaxation Data Analysis and Discussions

4.4.1 Determination of Radical-Induced Relaxation Rates from the Observed Experimental Relaxation Rates

In the absence of chemical exchange, one would expect to observe separate relaxation rates for molecules that exist in different chemical environments (i.e., in the paramagnetic or diamagnetic environment). The NMR signals from these two molecules may exhibit individual resonances and in this case the measurement of the relaxation rates for the nuclei in the two environments would be straightforward. However, if the molecule undergoes chemical exchange between the two environments, the relaxation rates may be dramatically affected. In fact, the exchange process itself becomes a relaxation mechanism. The practical use of spin-induced relaxation to determine structural parameters will be limited to those cases in which the nuclei of interest are in the fast-exchange limit, and the observed relaxation rates will be[45]

$$\left(\frac{1}{T_1}\right)_{obs} = \frac{f_A}{T_{1A}} + \frac{f_M}{T_{1M}} \qquad (4.20)$$

where f_A is the fraction of the time the nuclear spin is in the diamagnetic environment, f_M is the fraction of the time the nuclear spin is in the paramagnetic environment, T_{1A} is the relaxation time of the nucleus in the diamagnetic environment, and T_{1M} is the relaxation time of the nucleus in the paramagnetic environment. In the dilute free radical solution, $f_A >> f_M$, and $f_A \approx 1$, the observed relaxation rate is dominated by the term f_M/T_{1M}, and f_M is considered as the mole fraction of associated transient radical-receptor complex χ. Under this condition, the observed relaxation rate is given by

$$\left(\frac{1}{T_1}\right)_{obs} = \left(\frac{1}{T_{10}}\right) + \left(\frac{1}{T_{1M}}\right) \cdot \chi \qquad (4.21)$$

where T_{10} is the relaxation time of bulk solution in the absence of the free radical. Therefore, the contribution of free radicals to the observed relaxation rate is given by

$$\left(\frac{1}{T_1}\right)_{Rad} = \left(\frac{1}{T_1}\right)_{obs} - \left(\frac{1}{T_{10}}\right) = \left(\frac{1}{T_{1M}}\right) \cdot \chi \qquad (4.22)$$

The difference between the observed relaxation rate and the radical induced relaxation rate is generally less than 10% with an experimental error of 5-10% for most T_1 data.

4.4.2 Preliminary Observations

Figure 4.2 demonstrates that ^{13}C NMR spin-lattice relaxation times T_1 are a function of radical concentration

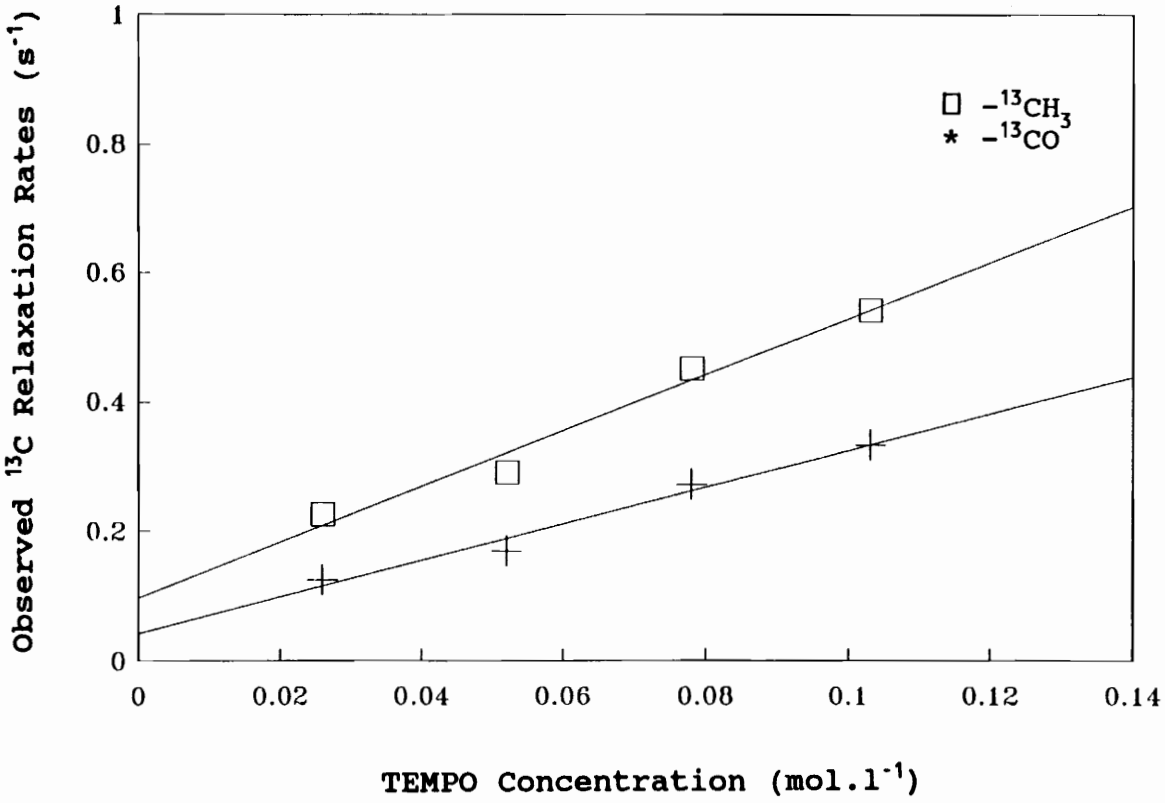

Figure 4.2 Observed ^{13}C NMR Relaxation Rates for the Two Nonequivalent ^{13}C Nuclei for CH_3CN as a Function of the radical (TEMPO) concentration (9.4 T).

and the paramagnetic species-induced relaxation rate for the -$^{13}CH_3$ group is greater than that for the -^{13}CN group in the CH_3CN/TEMPO system.

As Solomon[31] has clearly shown, equation 4.22 can be rewritten as

$$\left(\frac{1}{T_1}\right)_{obs} = \frac{1}{T_{10}} + \Gamma_R C \qquad (4.23)$$

where C is concentration of unpaired electron in solution, Γ_R is a proportional constant which is a measure of the strength of the electron-nuclear interaction and contains both dipolar and scalar terms. For systems which exhibit specific interactions (e.g. transient hydrogen bonding), the nucleus closer to the bonding site often exhibits a significantly larger coupling strength parameter (Γ_R) in comparison with other nuclei. This can arise from either a shorter interaction distance between the radical and nucleus or a longer correlation time, (or a combination of the two). Therefore, a direct comparison of Γ_R permits direct observation of the radical-nuclear coupling strength for different nuclei in a same molecule and reflects the stereospecificity of the hydrogen bonding interaction between the nucleus and the nitroxide. The results suggest that the C-H bond is the site of interaction in the CH_3CN/TEMPO system.

The site of hydrogen bonding in both CH_3CN/TEMPO and CH_3CONH_2/TEMPO systems may also be seen from the NMR line-broadening data presented in Table 4.1. The linewidth of the $^{13}CH_3$ group is dramatically changed while that of the $-C^{15}N$ group remains unchanged, suggesting that the C-H bond is the site of interaction. However, the ^{15}N linewidth for the amino group in CH_3CONH_2 is much broader than the $-^{13}CH_3$ group, indicating that the N-H bond is the principle site for complexation in this case. In both cases, the linewidth for the carbons not having a directly bonded hydrogen atom remains essentially unchanged.

4.4.3 Determination of the Dynamic Parameters

By subtracting the relaxation rate in the absence of unpaired electron ($1/T_{10}$) from the observed nuclear-electron relaxation rate $(1/T_1)_{obs}$ at a given magnetic field, $(1/T_1)_{Rad}$ can be obtained from eq. 4.20. In principle, three terms may contribute to the radical-induced relaxation rates

$$\left(\frac{1}{T}\right)_{Rad} = \left(\frac{1}{T}\right)^{D}_{r} + \left(\frac{1}{T}\right)^{D}_{t} + \left(\frac{1}{T}\right)^{SC} \qquad (4.24)$$

Table 4.1: Experimental Radical-Induced ^{13}C and ^{15}N NMR Linewidth Data[a] for the ^{15}N-Acetonitrile/TEMPO[b] and ^{15}N-Acetamide/TEMPO[c] System

Sample	^{15}N-Acetonitrile			^{15}N-Acetamide		
Group	$-^{13}CH_3$	$-^{13}CN$	$-C^{15}N$	$-^{13}CH_3$	$-^{13}CONH_2$	$-CO^{15}NH_2$
^{13}C and ^{15}N NMR Linewidths $\Delta\nu_{1/2}$ Without TEMPO	2.3	5.4	1.1	0.8	2.3	0.6
^{13}C and ^{15}N NMR Linewidths $\Delta\nu_{1/2(TEMPO)}$ in the Presence of TEMPO	19.4	5.4	1.1	1.9	2.3	5.3
$\Delta\nu_{1/2(TEMPO)} - \Delta\nu_{1/2}$	17.1	0	0	1.1	0	4.7

a. Linewidths were measured at 9.4T in Hz.
b. 0.4 M $CH_3C^{15}N/CCl_4$ solution with 0.2 M TEMPO.
c. 0.5 M $CH_3CO^{15}NH_2/C_4H_8O_2$ solution with 0.1 M TEMPO.

The dipole-dipole interaction consists of an intramolecular contribution modulated by rotational motion of the transient complex and an intermolecular term whose time dependence results from the translational motion of the individual molecules. Finally the $(1/T_1)^{SC}$ term describes the scalar contact interaction via the hydrogen bond which becomes time dependent by the "on-off" mechanisms of the complex formation.

For nuclei in which the interspecies coupling of the nuclear and electronic spin is dominated by dipolar coupling, the relaxation data can be analyzed by using either a translational diffusion or a rotational diffusion model. It should be noted that the spin-lattice relaxation rate for each case has different features of frequency dependence.

The behavior of $J(\omega_i)$ as a function of magnetic field indicates that as the magnetic field strength increases, and correspondingly, ω_I and ω_S increase, the spectral density function $J(\omega_i)$ decreases as molecular motions are no longer available for the relaxation transitions. For the W_0^D and W_2^D components, the spectral density functions are dominated by the electron resonance frequencies ω_S which is ~ 660 times the ^1H resonance frequency at a given magnetic field. Thus, W_0 and W_2^D will decrease more rapidly with increasing magnetic field than will W_1^D. In the case of rotational diffusion, the

dipolar spectral density function reaches a much more pronounced plateau in the region where the W_0 and W_2^D terms have been reduced to zero and the W_1^D terms have not started to decay as shown in Fig 4.3(a)[34]. For a rotational correlation time on the order of 10^{-11}s this plateau region will be evident for the range of ^1H observation frequencies used in these studies. In the case of translational diffusion, the transition from the falloff region in W_0 and W_2^D to the falloff region for W_1^D is more gradual, and no significant plateau is observed as shown in Fig 4.3(b). Thus the observation of a pronounced plateau in the data is strong evidence that the relaxation is dominated by a rotationally driven dipolar coupling mechanism between the two spins. Thus, characterizing the behavior of the relaxation rate as a function of magnetic field serves to identify τ, the correlation time for the relevant motion, and permits r to be evaluated.

4.4.3.1 ^1H NMR Relaxation

Almost all previous ^1H NMR relaxation studies have shown that the dipolar interaction dominates the proton-electron interaction independently of the free radical or the solvent employed. A notable exception is from the work of Bates[34] where a significant scalar component was detected for a strong hydrogen bonding system (e.g., CF_3CH_2OH/TEMPO). The ^1H

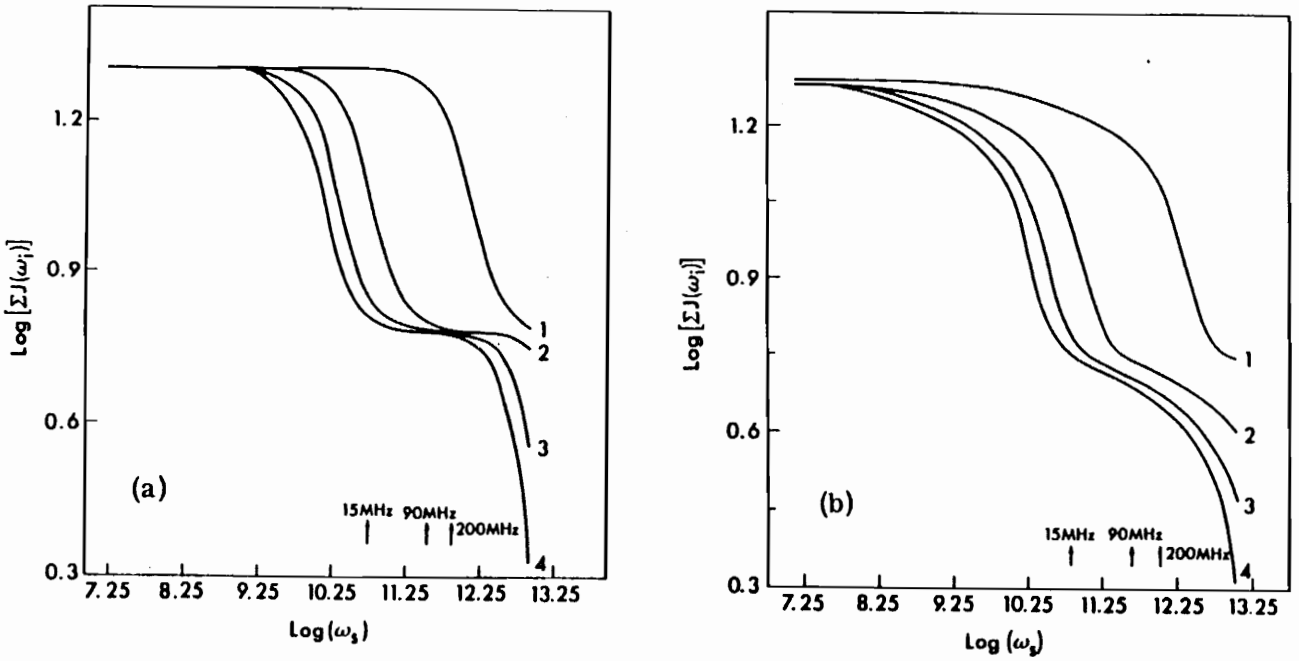

Figure 4.3 a) Composite Dipolar Spectral Density Function for the Rotational Diffusion Model for Four Different Correlation Times (1: $\tau_c = 1 \times 10^{-12}$s; 2: $\tau_c = 2 \times 10^{-11}$s; 3: $\tau_c = 6 \times 10^{-11}$s; 4: $\tau_c = 1 \times 10^{-10}$s. b) Composite dipolar spectral density function for the translational diffusion model with the same four correlation times.

relaxation results can be described in terms of a dipolar interaction modulated by translational diffusion. In cases where complex formation is possible the interaction can be considered from modulation by rotational diffusion.

The spin-lattice relaxation times for the methyl hydrogens for both systems were measured at different magnetic field strengths in the range of 1.8-9.4 T. The results in Table 4.2 show that the $-CH_3$ hydrogen relaxation times in both systems give a plateau in the range of observation of frequencies, indicating that the dipolar relaxation process is modulated primarily by rotational or tumbling motion of the bound complex. The scalar term can be neglected because $J(\omega_S)$ decays to zero in the magnetic frequency range of 0.2 to 10 MHz. It is assumed that the complex undergoes isotropic rotational diffusion and that the N-O group of the free radical TEMPO is bound in a 1:1 complex to a substrate molecule. Under this condition, $(1/T_1)_{Rad}$ is given by

$$\left(\frac{1}{T_1}\right)_{Rad} = \left(\frac{1}{T_{1M}}\right)\cdot\chi = \frac{1}{10}\left(\frac{\mu_0}{4\pi}\right)^2 \frac{\gamma_I^2\gamma_S^2\hbar^2}{r^6}\left(\frac{3\tau_r}{1+\omega_I^2\tau_r^2}+\frac{7\tau_r}{1+\omega_S^2\tau_r^2}\right)\chi \quad (4.25)$$

Table 4.2 The ^1H NMR Free Radical Induced Relaxation Times for the CH_3CN/TEMPO and CH_3CONH_2/TEMPO System

Magnetic Field(T)[a]	1.9	4.7	9.4
^1H Observation Frequency(MH_z)	80	200	400
$T_1(S)$ (C^1H_3CN)[b]	0.051 ± 0.003	0.049 ± 0.003	0.051 ± 0.000
$T_1(S)$ ($C^1H_3CONH_2$)[c]	0.06 ± 0.03	0.05 ± 0.01	0.054 ± 0.000

a. All measurements were made at room temperature (25 ^0C).
b. 1.34 M CH_3CN in CCl_4/0.1 M TEMPO solution.
c. 0.4 M CH_3CONH_2 in $C_4H_8O_2$/0.1 M TEMPO solution.

χ is again the mole fraction of the complex which can be measured from the ^{13}C and ^{15}N NMR contact shift study (see previous Chapter). The radical induced relaxation rates at different magnetic strengths were fitted to this equation using a nonlinear regression program[46,47], providing the rotational correlation time τ_r and the time averaged hydrogen bond length r between the hydrogen and nitroxyl group . The results for both systems are shown in Fig 4.4 and Fig 4.5, respectively.

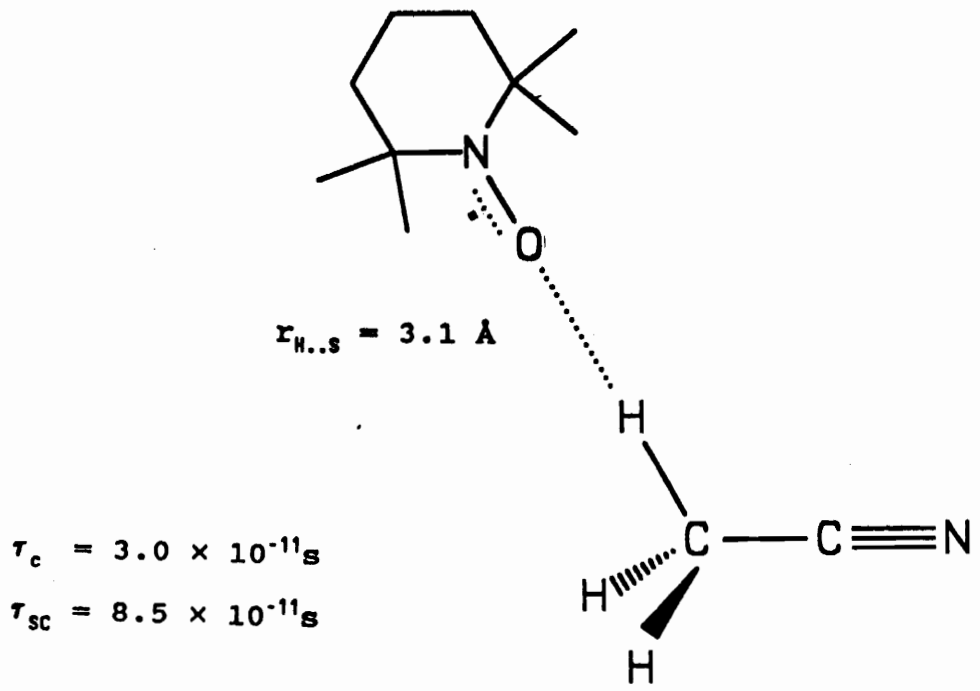

Figure 4.4: The Dynamic Nuclear-Electron Interaction in the CH_3CN/TEMPO System.

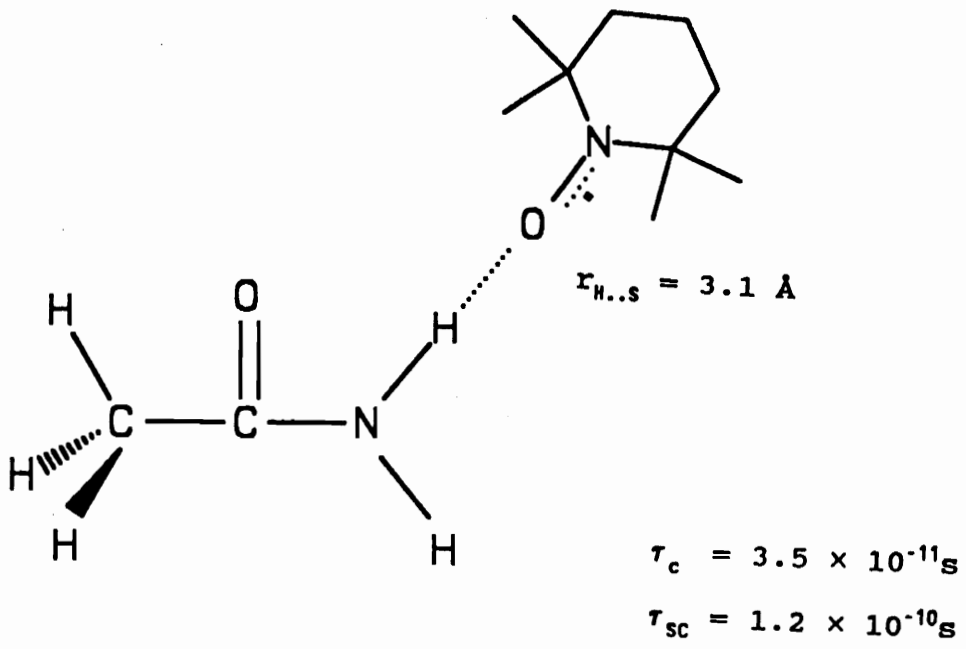

Figure 4.5: The Dynamic Nuclear-Electron Interaction in the CH_3CONH_2/TEMPO System.

4.4.3.2 The ^{13}C NMR Relaxation of the Methyl Carbon in the CH_3CN/TEMPO System

In comparison with hydrogen, carbon is more sensitive to scalar hyperfine interaction[48]. In the case of a labile complex formation, the relaxation rate can be treated by combination of the rotational model for the dipolar interaction with the sticking model for the scalar interaction. In this case, the spin-lattice and spin-spin relaxation rates are given as[31,32]

$$\left(\frac{1}{T_1}\right)_{Rad} = \frac{1}{10}\left(\frac{\mu_0}{4\pi}\right)^2 \frac{\gamma_I^2\gamma_S^2\hbar^2}{r^6}\left(\frac{3\tau_r}{1+\omega_I^2\tau_r^2} + \frac{7\tau_r}{1+\omega_S^2\tau_r^2}\right)\chi$$

$$+ \frac{1}{2}\left(\frac{A}{\hbar}\right)^2\left(\frac{\tau_{SC}}{1+\omega_S^2\tau_{SC}^2}\right)\chi \qquad (4.26)$$

$$\left(\frac{1}{T_2}\right)_{Rad} = \frac{1}{20}\left(\frac{\mu_0}{4\pi}\right)^2 \frac{\gamma_I^2\gamma_S^2\hbar^2}{r^6}\left(4\tau_r + \frac{3\tau_r}{1+\omega_I^2\tau_r^2} + \frac{13\tau_r}{1+\omega_S^2\tau_r^2}\right)\chi$$

$$+ \frac{1}{4}\left(\frac{A}{\hbar}\right)^2\left(\tau_{SC} + \frac{\tau_{SC}}{1+\omega_S^2\tau_{SC}^2}\right)\chi \qquad (4.27)$$

Under the condition that $\omega_I^2\tau^2 << 1$, and $\omega_S^2\tau^2 >> 1$, the difference between the $(1/T_1)_{Rad}$ and $(1/T_2)_{Rad}$ becomes

$$\left(\frac{1}{T_2}\right)_{Rad} - \left(\frac{1}{T_1}\right)_{rad} = \frac{1}{20}\left(\frac{\mu_0}{4\pi}\right)^2 \frac{\gamma_I^2\gamma_S^2\hbar^2\tau_r\chi}{r^6} + \frac{1}{4}\left(\frac{A}{\hbar}\right)^2\chi\tau_{SC} \qquad (4.28)$$

The scalar correlation time τ_{sc} can then be determined based on this equation if all other parameters are known. The study of paramagnetic contact shifts demonstrated that the C-H bond appeared to be the site of interaction in the CH_3CN/TEMPO system. Therefore, the $1/T_1$ and $1/T_2$ relaxation rates for methyl carbon were measured at a fixed magnetic field (9.4 T). The value of the hyperfine coupling constant A and the mole fraction χ were obtained from the ^{13}C and ^{15}N NMR contact shift measurements (Chapter III), whereas the rotation correlation time τ_c was obtained from the ^1H NMR relaxation frequency dependence measurements. The value of the closest time averaged distance between the unpaired electron and carbon were estimated from the sum of the hydrogen bond length and the bond length of C-H, providing a value of 4.1 Å. In this manner, the scalar correlation time of τ_{sc} 8.5×10^{-11} s was obtained for the CH_3CN/TEMPO system (Fig. 4.4). In the case of labile complex formation, the scalar correlation time is defined as the sum of two terms τ_h and τ_s, where τ_s, the electron spin-lattice relaxation, is usually much longer than τ_h, the mean lifetime of the complex. Therefore, this value appears to be reasonable for the lifetime of the weak hydrogen bonded complex[2].

4.4.3.3 ^{15}N NMR Relaxation of the Amino Nitrogen in the CH_3CONH_2/TEMPO System

The scalar correlation time for the CH_3CONH_2/TEMPO system was obtained using the same method as in the CH_3CN/TEMPO system. The ^{13}C and ^{15}N paramagnetic contact shift study demonstrated that the amide N-H bond appears to be the main site of interaction. Therefore, the ^{15}N relaxation rates were measured at the fixed magnetic field (9.4 T). The A and χ values were obtained from the ^{13}C and ^{15}N contact shift measurements and τ_c was obtained from the ^1H NMR relaxation measurements. Thus, a scalar correlation time of τ_{sc} of 1.2×10^{-10} s was obtained (Fig. 4.5).

4.5 Summary

An analysis of the nuclear relaxation rates affords information on the dynamic aspects of the interactions between solvent molecules and the TEMPO radical. The proton relaxation rate is dominated by the dipolar interaction modulated by rotational diffusion with a correlation time τ_c of 3.0×10^{-11} s for CH_3CN/TEMPO and 3.5×10^{-11} s for the CH_3CONH_2/TEMPO system, respectively. The observed distance of 3.1 Å can be interpreted as the length of the hydrogen bond from the hydrogen to the center of gravity of the spin density in the N-O group of the nitroxide which encompasses the range

between 2-4 Å found for other comparable systems[1,3,6,11]. However, in these studies, the primary limitation is the finite range of magnetic field strengths for which the relaxation times measurements can be determined.

Relaxation by the scalar contact interaction via the hydrogen bond is also important for the $-^{13}CH_3$ in CH_3CN and the $-^{15}NH_2$ in CH_3CONH_2, and the time dependence of the coupling can be described by an on-off mechanism with a mean lifetime for the hydrogen bonded complex. Both relaxation studies were analyzed on the basis of combination of the rotational mode for the dipolar term and the sticking mode for the scalar term, thus providing a complex lifetime of 8.5×10^{-11} s for the CH_3CN/TEMPO and 1.2×10^{-10} s for the CH_3CONH_2/TEMPO system (see Fig. 4.5).

In these systems, the lifetime of the hydrogen bonded complex is longer than the correlation time for the motion, and it is reasonable to assume that the labile complex rotates ~ three times during the lifetime of the hydrogen bonded complex. Therefore, the spin pair interaction is expected to be dominated by the rotational tumbling of the complex and the assumption of the complex undergoes isotropic rotation diffusion appears to be reasonable[5].

CHAPTER 5

Dynamic Nuclear Polarization in Liquid

5.1 Introduction

In 1953, Overhauser predicted the double resonance phenomena now known dynamic nuclear polarization by which the intensity of NMR signal could be enhanced by stimulating the conducting electron in a metal[49]. This was verified experimentally in the same year by Carver and Slichter[50] who demonstrated appreciable nuclear polarizations for lithium, sodium, and hydrogen nuclei. Since that time, a variety of enhanced NMR signals have been observed in materials such as chars, tars, metals, solutions containing transition metal ions, and solid free radicals[51-55]. However, most of these systems have been investigated from a physical chemistry viewpoint with the aim of understanding spin-spin interactions.

The first mention of chemical applications for DNP was by Richards and White[56,57]. They suggested the possibility of using DNP to increase the signal-to-noise (S/N) of inherently

weak NMR signals (e.g., ^{13}C, ^{15}N etc.). In addition, DNP enhancements are useful to determine collision parameters such as radical nuclear distance of closest approach and association times for species in solution. Simultaneously, other groups, including those of Müller-Warmuth[38] and Poindexter[52] used DNP as an experimental means for investigating molecular motions and collision dynamics in liquids. The potential of employing DNP in studying hydrogen bonding in solution of nitroxide radicals in a protic solvent has also been demonstrated. Recent work[34] has shown that the dynamic nature of short-lived solvent-solute interactions such as hydrogen bonding can be studied by the combination of investigations of substrate nuclear relaxation rates induced by the paramagnetic solutes with studies of dynamic nuclear polarization of solvent nuclei in the same system. Both techniques provide direct information about the details of the relaxation mechanisms of substrate nuclei. However, experimental DNP results have been obtained for only a small number of nuclei because of previous difficulties at low magnetic fields. The poor sensitivity of low field NMR made the studies of low magnetogyric ratio γ nuclei (e.g., ^{13}C, ^{15}N etc.) very difficult or even impossible. Therefore, only nuclei with relatively large γ_I (e.g., ^{1}H and ^{19}F) and relatively simple molecules with single line NMR spectra could be studied in low field DNP experiments[35,38].

Recently, Dorn[11,12] et al. have reported a flow DNP experiment whereby the nuclear spins are polarized at low magnetic field and monitored at a high magnetic field. Compared to classical low field DNP experiments, this method provides higher sensitivity and better resolution thereby allowing observed DNP enhancements for nuclei with low natural abundance and small magnetogyric ratios (e.g., ^{13}C, ^{15}N and ^{29}Si). For example, the first ^{15}N NMR LLIT DNP results have been reported for two nitrogen compounds: ^{15}N-acetonitrile and ^{15}N-acetamide using this approach.

In the present study, extensive high field (B_0=1.9-9.4 T) ^{1}H, ^{13}C, and ^{15}N NMR data were obtained for both the TEMPO/CH_3CN and TEMPO/CH_3CONH_2 systems. The data include: scalar contact shifts, spin-lattice, and spin-spin relaxation rates. Based on the high field NMR results, the relative scalar and dipolar relaxation contributions were calculated. The parameters for these contributions include: hyperfine coupling constants A, correlation times(τ_{sc} and τ_r), and free radical-nuclear internuclear distances r_{IS} in the hydrogen bonding complex. The scalar and dipolar contributions derived from the NMR study were subsequently employed to predict the corresponding ^{1}H, ^{13}C and ^{15}N low magnetic field (0.33 T) DNP enhancements. In all cases, good agreement was obtained between the NMR predicted and the low field measured DNP results. The scalar

contribution to the DNP enhancement is critically dependent on the site of hydrogen bonding (i.e., methyl group in CH_3CN and amino group in CH_3CONH_2) and the nucleus monitored.

5.2 Basic Theory of DNP in Liquids

In a solution containing free radicals, the rapid random diffusion of the molecules ensures that the solvent molecules are near a free radical many times during the nuclear relaxation time, and therefore any nucleus in solution can be considered to be in continuous interaction with an electron. Fig 2.1 shows the energy level diagram for the electron-nuclear two spin system with the dipolar and scalar radical-induced nuclear relaxation transition probabilities (W_i). At equilibrium, nuclear spins are distributed among the energy levels according to a Boltzmann distribution. The random magnetic field fluctuations can induce nuclear spin transitions involving changes in the I_z spin quantum number of -1/2 to +1/2 and of +1/2 to -1/2, which are conveniently denoted by I_+ and I_-, respectively. The strong pairwise interaction between the electron and nuclear magnetic dipoles can also induce coupled two spin transitions such as W_0 and W_2 in which the electron and nucleus make simultaneous flips. In the double-resonance experiment, the electron transitions W_s of the free radical is strongly irradiated, so that the

populations of the electron energy levels are more or less equalized. The spin lattice relaxation processes attempt to restore the populations of these energy levels back to their thermal equilibrium values, in which there are more electron spins in the lower level than in the upper level. For electron nuclear dipolar coupling, the dominant W_2 transition will cause the nucleus to perform an I_- transition simultaneously, with the result that nuclei originally in the lower nuclei energy level are transferred to the upper level, producing a deviation of the equilibrium population of the nuclear spins I. Thus the population of the upper nuclear level becomes greatly increased and the nuclear resonance becomes an emission signal, i.e., the signal is inverted. If there is also scalar coupling present between the electrons and the nuclei, then there is an additional relaxation mechanism W_0^{SC}. If this mechanism dominates, then saturation of the electron resonance will lead to an increase in the intensity of the nuclear resonance absorption signal. Therefore the sign and magnitude of the observed enhancement will give the information of electron-nuclear interaction.

5.2.1 Basic Equations for Liquid DNP

Following Solomon[31], a quantitative expression for the enhancement factor can be determined by considering the rate of population change for the individual energy states. When

the spins are in thermal equilibrium with their environment, the populations of the individual levels will be governed by a Boltzmann distribution, such that the ratio of spins in the upper state N_- to that in the lower N_+ is given by

$$\frac{N_-}{N_+}=\exp\left(-\frac{h\nu}{kT}\right) \tag{5.1}$$

where k is Boltzmann constant and T is the absolute temperature. The strength of the NMR signal is proportional to the difference of population of N_+ and N_-. In a coupled electron-nuclear two spin system, the rate of change of the population of the $|{+}{+}\rangle$ state, N_{++}, in Fig 2.1, for instance, can be expressed as[58]

$$\frac{dN_{++}}{dt}=-\left(W_1^D+W_{10}+W_2^D+W_S\right)\left(N_{++}-N_{++}^0\right)+W_2^D\left(N_{--}-N_{--}^0\right)+W_S\left(N_{-+}-N_{-+}^0\right)+\left(W_{10}+W_1^D\right)\left(N_{+-}-N_{+-}^0\right) \tag{5.2}$$

where the superscript zero labels populations of the Boltzmann equilibrium in the absence any r.f. magnetic field. There will be similar equations for the other populations. The experimentally observable quantities $\langle I_z\rangle$ and $\langle S_z\rangle$ in NMR and EPR are proportional to the appropriate population difference as

$$\langle I_z\rangle=K\left[(N_{++}-N_{+-})-(N_{-+}-N_{--})\right] \tag{5.3}$$

$$\langle S_z\rangle = K\left[(N_{-+}-N_{++})-(N_{--}-N_{+-})\right] \qquad (5.4)$$

Where K is a constant of proportionality.

Therefore, from equation 5.2 and its analogues, the rate of change of the observed NMR signal is given by

$$\frac{d\langle I_z\rangle}{dt} = -\left(W_0^D+W_0^{SC}+2W_1^D+W_2^D+2W_{10}\right)\left(\langle I_z\rangle-I_0\right)-\left(W_2^D-W_0^D-W_0^{SC}\right)\left(\langle S_z\rangle-S_0\right) \qquad (5.5)$$

where I_0 and S_0 are the values of $\langle I_z\rangle$ and $\langle S_z\rangle$, the observed value of the NMR and EPR signal respectively, at thermal equilibrium. In a steady state, $d\langle I_z\rangle/dt = 0$ and equation 5.5 reduces to

$$\langle I_z\rangle = I_0+\left(\frac{W_0^D-W_0^D-W_0^{SC}}{W_0^D+W_0^{SC}+2W_1^D+W_2^D+2W_{10}}\right)\left(\langle S_z\rangle-S_0\right) \qquad (5.6)$$

And the equation 5.6 can be rewritten as

$$\frac{\langle I_z\rangle-I_0}{I_0} = \left(\frac{W_2^D-W_0^D-W_0^{SC}}{W_0^D+W_0^{SC}+2W_1^D+W_2^D}\right)\left(\frac{W_0^D+W_0^{SC}+2W_1^D+W_2^D}{W_0^D+W_0^{SC}+2W_1^D+W_2^D+2W_{10}}\right)\left(\frac{S_0-\langle S_z\rangle}{S_0}\right)\left(\frac{S_0}{I_0}\right) \qquad (5.7)$$

It is convenient to define a nuclear-electron coupling parameter ρ as

$$\rho = \frac{W_2^D-W_0^D-W_0^{SC}}{W_0^D+W_0^{SC}+2W_1^D+W_2^D} \qquad (5.8)$$

a leakage factor f as

$$f = \frac{W_0^D + W_0^{SC} + 2W_1^D + W_2^D}{W_0^D + W_0^{SC} + 2W_1^D + W_2^D + 2W_{10}} \tag{5.9}$$

and a saturation factor s as

$$s = \frac{S_0 - \langle S_z \rangle}{S_0} \tag{5.10}$$

Substituting these factors into eq. 5.7 and using the relation $S_0/I_0 = \gamma_s/\gamma_I$, the DNP enhancement factor A will be given by

$$A = \frac{\langle I_z \rangle - I_0}{I_0} = \rho f s \frac{\gamma_S}{\gamma_I} \tag{5.11}$$

Under conditions of complete saturation (s=1) and total relaxation via electron-nuclear coupling (f=1), the ultimate enhancement A_∞ is only dependent on the coupling factor ρ as

$$A_\infty = \rho \frac{\gamma_S}{\gamma_I} = \left(\frac{W_2^D - W_0^D - W_0^{SC}}{W_0^D + W_0^{SC} + 2W_1^D + W_2^D} \right) \left(\frac{\gamma_S}{\gamma_I} \right) \tag{5.12}$$

In this way the coupling factor ρ can be obtained.

$$\rho = A_\infty \frac{\gamma_I}{\gamma_S} \tag{5.13}$$

The most important quantity in the DNP experiment is the coupling factor ρ which is closely related to the transition probabilities W_0^D, W_0^{SC}, W_1^D, and W_2^D. The coupling factor ρ can range from -1 for a pure scalar electron-nuclear interaction ($W_0^D = W_1^D = W_2^D = 0$) to +0.5 in the case of dipolar interaction only ($W_0^{SC}=0$). In practice, both scalar and dipolar interaction can be present and the observed enhancement will then range between $1/2(\gamma_s/\gamma_I)$ and $-\gamma_s/\gamma_I$. Since the magnetogyric ratio of the electron spin is two to three orders of magnitude larger than that of the nuclear spin, dramatic sensitivity improvements for the observed NMR signals can be predicted. Table 5.1 shows limiting DNP enhancements for some nuclei and clearly shows that nuclear spins with smaller γ give larger DNP enhancements.

At low magnetic fields, the transition probabilities W_i are nearly independent of ω_s and ω_I, and hence of the magnetic field B_0. The results for the DNP enhancement then do not depend upon the details of molecular motion, and the enhancement is given solely by the magnitude of dipolar and scalar coupling between the nucleus and the unpaired electron. Therefore, DNP enhancements measurements at low magnetic fields have been shown to be extremely sensitive to the detailed chemical environment of both receptor nuclei and free

Table 5.1: Limiting DNP Enhancement of Some Nuclei

Nucleus	Dipolar Limit	Scalar Limit
^{1}H	-330	+660
^{2}H	-2145	+4290
^{7}Li	-850	+1690
^{13}C	-1310	+2620
^{15}N	+3240	-6480
^{19}F	-350	+700
^{29}Si	+1655	-3310
^{31}P	-812	+1624
^{57}Fe	-10193	+20386
^{103}Rh	+10435	-20870

radical electrons. However, at high magnetic field nuclear relaxation becomes dependent on ω_S and ω_I, and hence on the magnetic field B_0. The results of DNP experiments then depend upon detailed molecular motion, and DNP measurements at high field can yield information regarding the type of molecular motion in the liquid (rotational, translational, etc.). Therefore, DNP studies of paramagnetic liquids provide fundamental information on the relative magnitude of scalar and dipolar interactions between unpaired electrons and nuclei, on the time constants of molecular motion, electron exchange, and electronic relaxation. In addition, DNP has a more practical application that is based on the high enhancement factors (which in favorable cases are on the order of 1000) obtainable.

5.2.2 Physical and Chemical Factors Affecting DNP Enhancement

In general, the DNP enhancement in solutions containing free radicals will depend on a variety of factors: 1) the external field strength; 2) the ratio of scalar to dipolar coupling; 3) the temperature of the system; 4) the viscosity of the solution; 5) the free radical used; 6) the chemical environment of the receptor nucleus; and the type of receptor nucleus monitored (e.g. ^{1}H, ^{19}F, ^{13}C ^{31}P, etc.). All these factors more or less affect the ultimate DNP enhancement.

At low free radical concentrations, two additional effects: the three spin effect and electron-electron exchange effect make the system even more complicated. The unpaired electron in the TEMPO radicals used in these studies is principally located in the N-O linkage. The ^{14}N nucleus produces a large hyperfine splitting in the EPR spectrum and the hyperfine coupling constant is ~ 16 G[59]. At low radical concentrations, the three signals of the triplet are well separated. If only one of the three electron transitions is saturated, the ultimate DNP enhancement will be 1/3 of the expected value. However, the actual measured enhancement may range from A_∞ at high free radical concentrations to $A_\infty/3$ due to the exchanging electron spin states between the free radicals during collisions. Therefore, a larger error in determination of the ultimate DNP enhancement A_∞ can be expected at low radical concentration (< 0.005 M) as discussed by Bates[59]. At high radical concentrations (> 0.8 M), however, the EPR spectrum for TEMPO gives an exchange narrowed single line. Therefore, the electron-electron exchange effect can be neglected by using a high concentration of free radicals.

The three spin effect is another factor affecting appreciably the DNP enhancement at low free radical concentration. In some cases, the monitored nucleus such as

^{13}C may interact with free radicals in two different ways as shown in Fig. 5.1. In one case, direct interaction with the free radical or in a second manner by indirect interaction with the electron spin via a third spin (e.g. ^{1}H). The basic idea of the three spin effect can be seen by considering the transitions among the Zeeman energy levels for the ^{1}H, ^{13}C and electron spin three spin system. Usually the direct electron-nuclear interaction is a dipolar interaction for hydrogens where the predominant coupled transition will be an S_-I_- one which leads to the usual negative enhancement for ^{1}H DNP. Because the dipolar coupling between the hydrogen and carbon nuclei is an appreciable relaxation process for the carbon nucleus, the H_+ transition in relaxing toward the thermal equilibrium distribution will allow the carbon nucleus to perform a simultaneous C_+ transition due to the term I_+I_+ in the carbon-proton dipolar interaction (see Fig. 5.1). Therefore, in addition to any enhancement due to the direct interaction between carbon nuclear and electron spin, there will be an additional positive enhancement due to the indirect three-spin effect. The three spin effect can be large at low radical concentrations and can be avoided by using high radical concentrations. An alternative approach is a triple irradiation experiment where the electron and the ^{1}H spin transition are irradiated simultaneously.

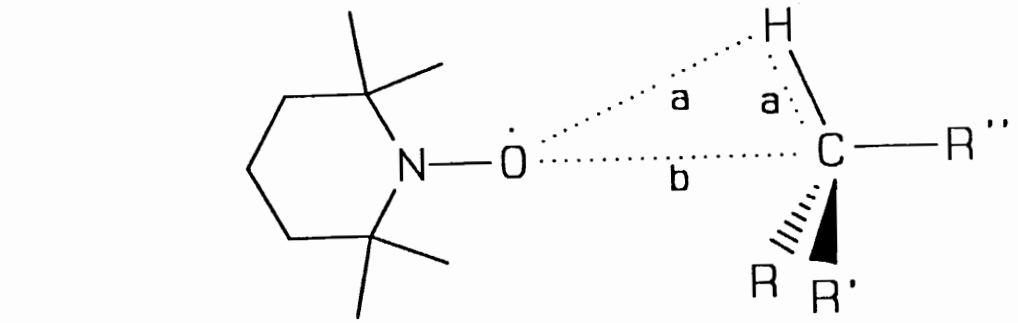

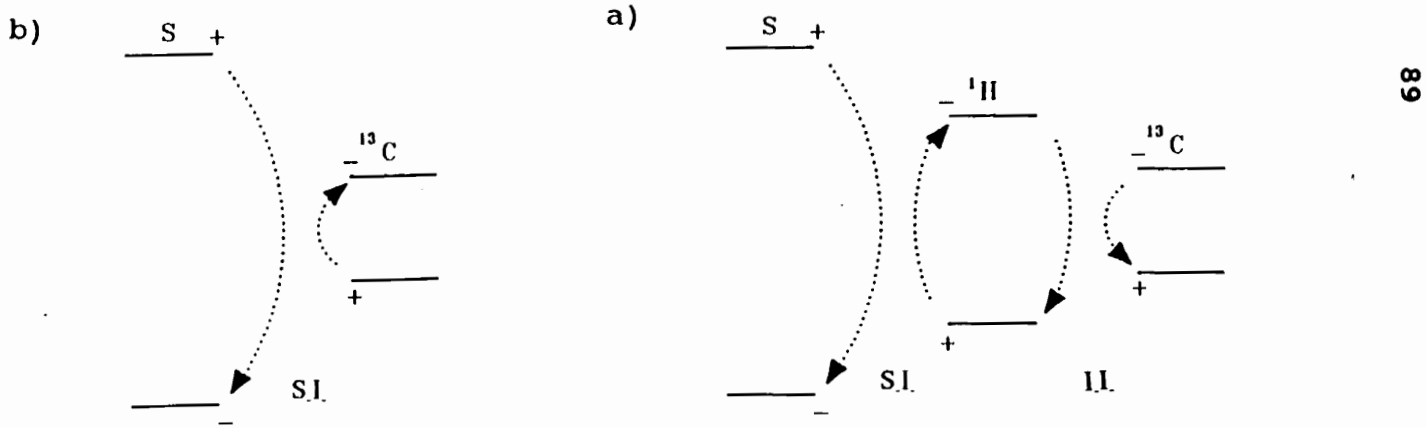

Figure 5.1: Zeeman Energy Levels for the Nuclear-Electron System: a) Three spin effect; b) Direct nuclear electron interaction.

5.2.3 Experimental Determination of the Ultimate DNP Enhancement A_∞

5.2.3.1 Correction of the DNP Enhancement for Leakage Factor (f)

The transition probability ($W_0^D + 2W_1^D + W_2^D + W_0^{SC}$) represents that part of the nuclear relaxation rate that arises from the interaction with the electron (See eq. 5.9) whereas $2W_{10}$ represents contributions to the nuclear relaxation rate from other interactions, such as those normally present in diamagnetic systems and usually written as $1/T_{10}$, the leakage factor can be written as

$$f = 1 - \frac{T_{Rad}}{T_{10}} \qquad (5.14)$$

Therefore, the leakage factor (f) can be experimentally determined very easily by measuring the nuclear relaxation time in the presence and absence of the free radicals. Thus (f) determines how effectively the nuclear spin is relaxed by the electron spin. The leakage factor (f) ranges between 0 (no relaxation via electron-nuclear coupling) and 1 (total relaxation via electron-nuclear coupling). At radical concentrations of 10^{-3} to 10^{-2} mol/l typical values of the leakage factor range usually from 0.8 to 1. Alternatively, one can use a different method to extrapolate the enhancement A to the value where f = 1. Since W_{10} is independent of the

concentration of free radical and since the other transition probabilities W_0, W_1, and W_2 are proportional to the concentration of free radical, a plot of the reciprocal DNP enhancement A^{-1} as a function of the reciprocal concentration of free radical permits extrapolation to infinite concentration, i.e., to f = 1.

5.2.3.2 Correction of the DNP Enhancement for the Saturation Factor s

The dependence of $\langle S_z \rangle$ on the strength H_{1S} of an oscillating magnetic field applied exactly at resonance is given by

$$S_z = \frac{S_0}{1+\gamma_S^2 H_{1S}^2 T_{1S} T_{2S}} \qquad (5.15)$$

where T_{1S} and T_{2S} are the electron spin-lattice and spin-spin relaxation times. With the help of equations 5.10, 5.11, 5.15, and with the fact that H^2_{1S} is proportional to the applied microwave power P, we find

$$A^{-1} = \left(f\rho\frac{\gamma_S}{\gamma_I}\right)^{-1}\left(1+\frac{1}{\alpha P T_{1S} T_{2S}}\right) \qquad (5.16)$$

where α is a constant. Consequently, a plot of reciprocal enhancement A^{-1} versus reciprocal microwave power P^{-1} should give a straight line with intercept $(f\rho\gamma_S/\gamma_I)^{-1}$, the reciprocal enhancement factor at complete saturation of electron transitions (s=1). The extrapolation method above was first applied by Carver and Slichter[50] and is frequently employed in DNP experiments. The saturation factor s under experimental conditions can be calculated from the ratio of the enhancement at microwave power employed to that at complete saturation (s=1).

5.2.3.3 Ultimate DNP Enhancement A_∞

The ultimate enhancement A_∞ for complete saturation (s=1) and complete dominance of the nuclear relaxation by the nuclear-electron interaction (f=1) can then be obtained after correcting the leakage factor f and saturation factor s as

$$A_\infty = \frac{A}{sf} = \rho\frac{\gamma_S}{\gamma_I} \qquad (5.17)$$

Therefore, the ultimate DNP enhancement A_∞ in the static system can be easily obtained using equation (5.17). However, more corrections are needed in the low to high field experiment in order to determine the ultimate DNP enhancement A_∞. The method for determination of the DNP enhancement in the flow DNP experiment is discussed in the text section.

5.2.4 Determination of the DNP Enhancement Factor A in the Flow DNP Experiment

In a classical DNP experiment, $\langle I_z \rangle$ and I_0 can be simply measured by turning the electron spin saturation source on and off respectively. In the flow transfer DNP experiment, however, the nuclear spins are polarized in a low magnetic field a and rapidly transferred via region b to a high magnetic field c where the polarization is monitored, so three separate regions as shown in Fig. 5.2[11] must be considered. The spatial separation of the detection from the buildup of the DNP enhancement makes the system more complicated. A model for the DNP enhancement factor A in the low to high magnetic field transfer DNP experiment has been established[11].

$$A_{obs} = \frac{\langle M_z^* \rangle - \langle M_z^{HL} \rangle}{M_0^H} = \frac{[A(1-E_{1a})]}{K}(E_{1b})(E_{1c}) \qquad (5.18)$$

$\langle M_z^* \rangle$ the enhanced magnetization detected at high magnetic field H_0^H,

$\langle M_z^{HL} \rangle$ the flow magnetization from both the low and high magnetic fields in the absence of the microwave field,

M_0^H the static magnetization detected in the high magnetic field H_0^H,

A the DNP enhancement factor,

K the ratio of the two magnetic fields B_0^H/B_0^L,

E_{1a} $= \exp(-t_a/T_{1a})$,

E_{1b} $= \exp(-t_b/T_{1b})$,

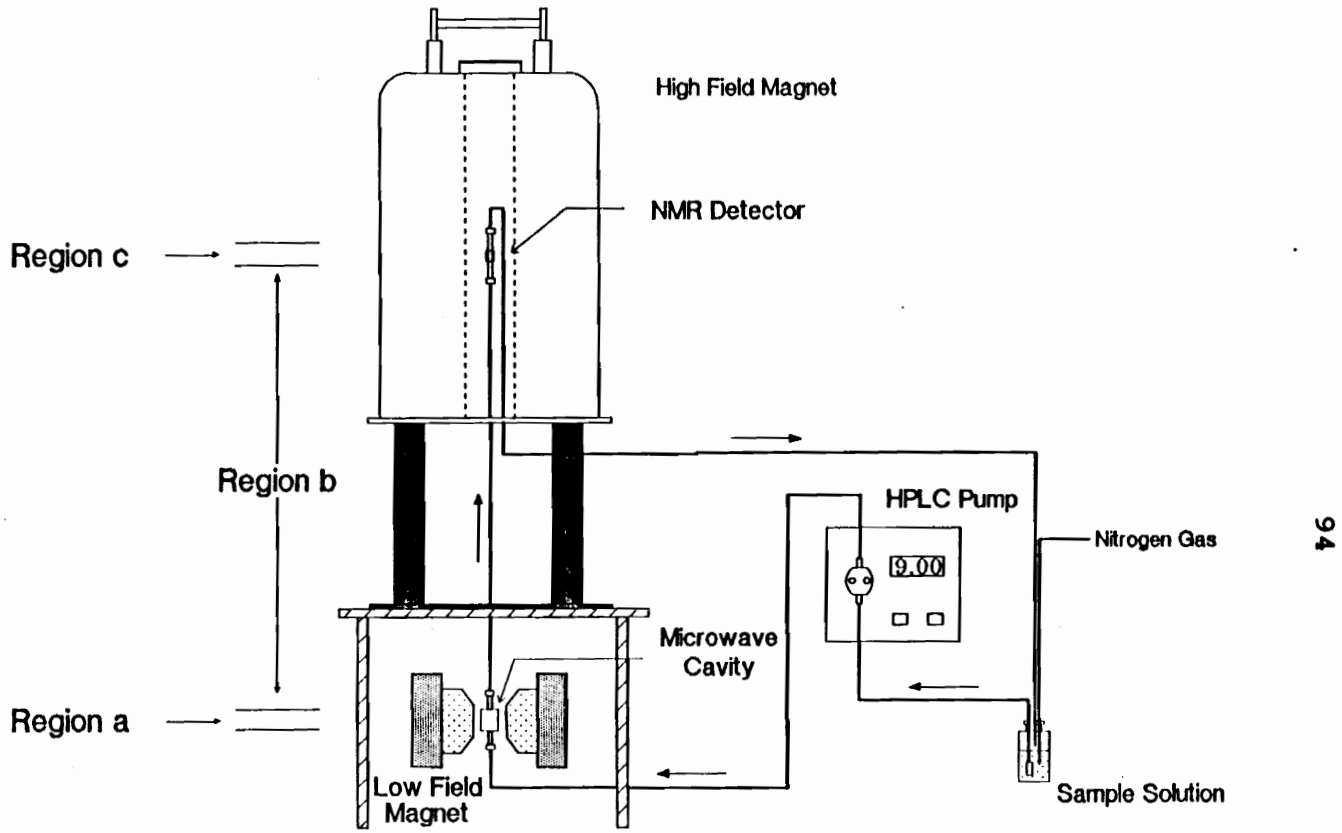

Figure 5.2: The Low to High Magnetic Field Transfer DNP Experimental Apparatus.

E_{1c} $= \exp(-t_c/T_{1c})$

t_a, t_b, t_c the residence times of a given bolus in regions a, b, and c.

T_{1a}, T_{1b}, T_{1c} the longitudinal relaxation times of a given bolus in regions a, b, and c.

The first term in equation 5.18 represents the buildup of the enhanced magnetization in the low magnetic field and the latter terms E_{1b} and E_{1c} represent transfer losses when the bolus is transferred to region b and c, respectively. When $t_a >> T_{1a}$, $t_b << T_{1b}$, and $t_c << T_c$, the maximum enhancement (A/K) can be obtained in the low to high magnetic field transfer experiment without either buildup or transfer loss.

In the above equation, $\langle M_z^* \rangle$, M_z^{HL}, and M_0^H can be experimentally measured; A_{obs} values can then be obtained at all flow rates. If a simple plug flow pattern is simply assumed, then $t_a = V_a/F$, $t_b = V_b/F$, and $t_c = V_c/F$, where F is the flow rate, and V_a, V_b, and V_c are volumes of region a, b, and c. Equation 5.18 can be rewritten as

$$A_{obs} = \left(\frac{A}{K}\right)\left(1 - e^{-\frac{V_a}{T_{1a}}\frac{1}{F}}\right) e^{-\left(\frac{V_b}{T_{1b}} + \frac{V_c}{T_{1c}}\right)\frac{1}{F}} \qquad (5.19)$$

A nonlinear regression program[46,47] can be used to fit the set of A_{obs} values versus inverse flow data and the parameters A/K, V_a/T_{1a}, and $(V_b/T_{1b} + V_c/T_{1c})$ can then be obtained from the best fit of the experimental data.

When T_{1a} is small and $V_a/F > 5T_{1a}$, E_{1a} is small and can be neglected. Under this condition, equation 5.19 reduces to

$$A_{obs} = \left(\frac{A}{K}\right) e^{-\left(\frac{V_b}{T_{1b}} + \frac{V_c}{T_{1c}}\right)\frac{1}{F}} \qquad (5.20)$$

Therefore, a plot of ln (A_{obs}) versus 1/F would give a straight line with intercept ln (A/K), and the enhancement factor can then be readily determined.

5.3 Experimental Details and Results

5.3.1 Instrumentation

The instrumental apparatus used in the flow transfer DNP experiment is shown in Fig. 5.2. A variable electromagnet (0-0.6 T) is placed directly under a 4.7 T supercoducting magnet with the centers of the magnets at a distance of 1.2 m apart. The sample in a ceramic tube is placed in a microwave TE_{102} cavity of a modified Varian E-3 EPR spectrometer. The microwave frequency is generated in a klystron source of a Bruker microwave bridge and amplified by a Varian "K" series

TWT amplifier. The microwave power at the sample can be adjusted by an attenuator in the range of 1-16 watts. In this way, the sample is polarized at low magnetic field (0.33 T) and then transferred to a high magnetic field detector where a Helmholtz detection coil is employed in the homemade probe using a standard capacitor tuning and matching circuit.

5.3.2 Chemicals

Due to the small magnetogyric ratio, γ, and low natural abundance of the ^{13}C isotope, two ^{13}C labelled compounds, $^{13}CH_3CONH_2$ and $CH_3{}^{13}CONH_2$, were synthesized using starting compounds $^{13}CH_3COCl$ and $CH_3{}^{13}COCl$ (> 90% ^{13}C isotope). A 30 ml solution of dry ethyl ether was placed in a three-necked flask with a tiny stirring bar under an atmosphere of nitrogen gas. The flask was placed in an ice water bath (~ 0^0C). Ammonia gas was bubbled through the ethyl ether solution. One gram of the ^{13}C labelled acetyl chloride sample was mixed with 10 ml of dry ethyl ether in a graduated funnel attached to the three-necked flask and added slowly to the ethyl ether solution. A large amount of white precipitate formed. The mixture was cooled. Then the solids were filtered, washed with ethyl ether, and extracted with ethyl alcohol several times. The ethyl alcohol was removed in vacuo to afford white crystals. The ^{13}C NMR spectra for the two ^{13}C labelled acetamide samples in $CDCl_3$ are shown in Fig.5.3. All other

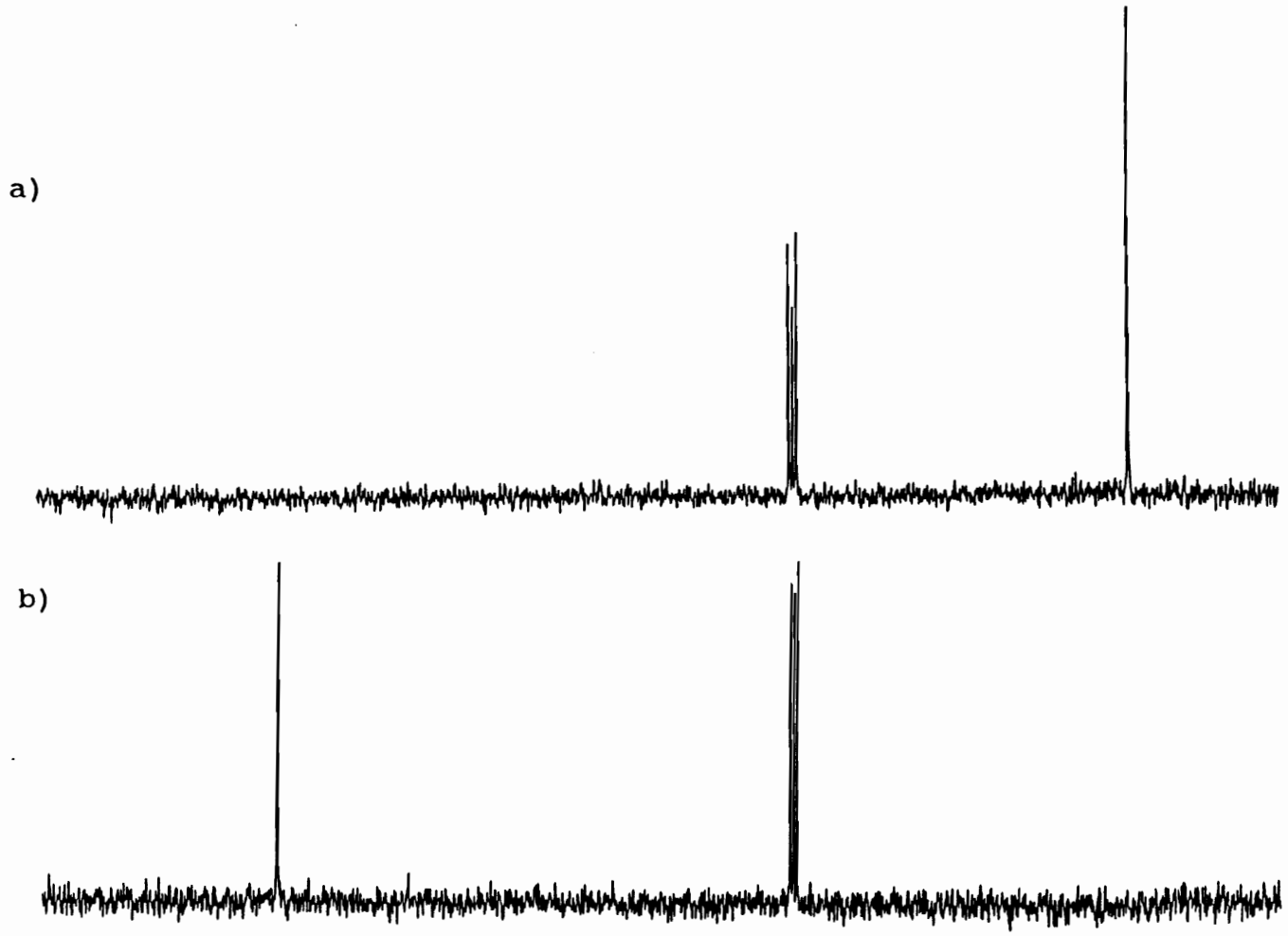

Figure 5.3: ^{13}C NMR Spectra for a) $^{13}CH_3CONH_2$ and b) $CH_3{}^{13}CONH_2$ in $CDCl_3$.

chemicals were purchased from Aldrich and used without further purification.

A high concentration of the free radical solution was employed in the flow LLIT DNP experiments to avoid both three-spin effects and electron-electron exchange effects. A 0.4 M acetamide/dioxane/0.1 M TEMPO solution was prepared. The solution was deoxygenated by bubbling nitrogen gas through the solution prior to and during the experiments. The flow LLIT ^{13}C DNP spectra for the two ^{13}C labelled samples are shown in Fig. 5.4.

5.3.3 Determination of Enhancement Factor A

At high free radical concentrations (0.1 M TEMPO), T_{1a} is short and a complete buildup of the DNP enhancement at the low magnetic field can be assumed. Therefore, the measured DNP enhancement A_{obs} is degraded by only transfer losses. Under this condition, equation 5.19 can be used to determine the enhancement factor A. A set of DNP enhancements A_{obs} were measured at different flow rates, and the low field enhancement factor A at 0.33 T was obtained from the intercept of the plot of ln A_{obs} versus reciprocal flow rate. Fig 5.5 shows the plot of ln $(-A_{obs})$ versus inverse flow rate for the ^{13}C labelled carbonyl group $(-^{13}CO)$ in the CH_3CONH_2/TEMPO system. The ln $(-A_{obs})$ is linear in this flow range with a

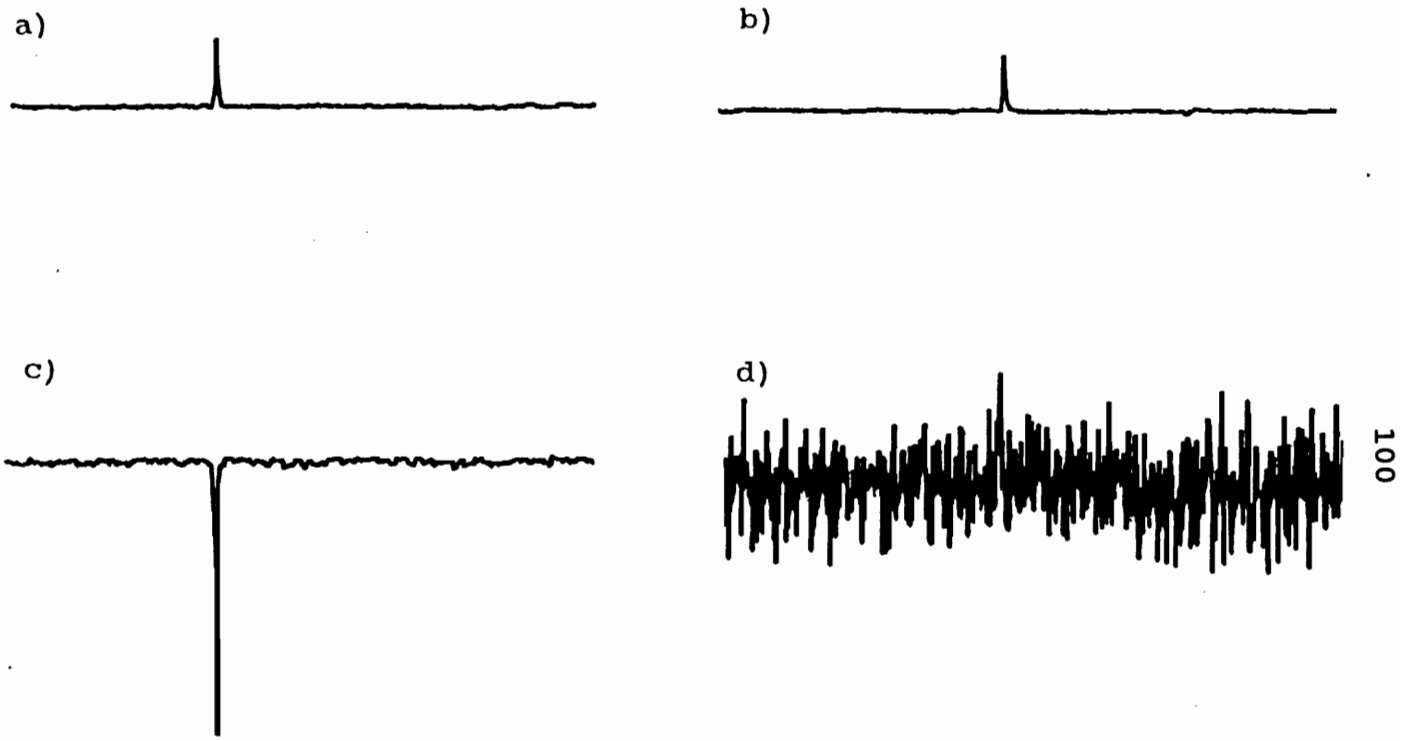

Figure 5.4: Flow LLIT ^{13}C DNP Spectra (50.1 MHz) for 0.4 M CH_3CONH_2/TEMPO System: a) Static ^{13}CO NMR signal, b) Static $^{13}CH_3$ NMR signal, c) ^{13}CO flow DNP spectrum, and d) $^{13}CH_3$ flow DNP spectrum.

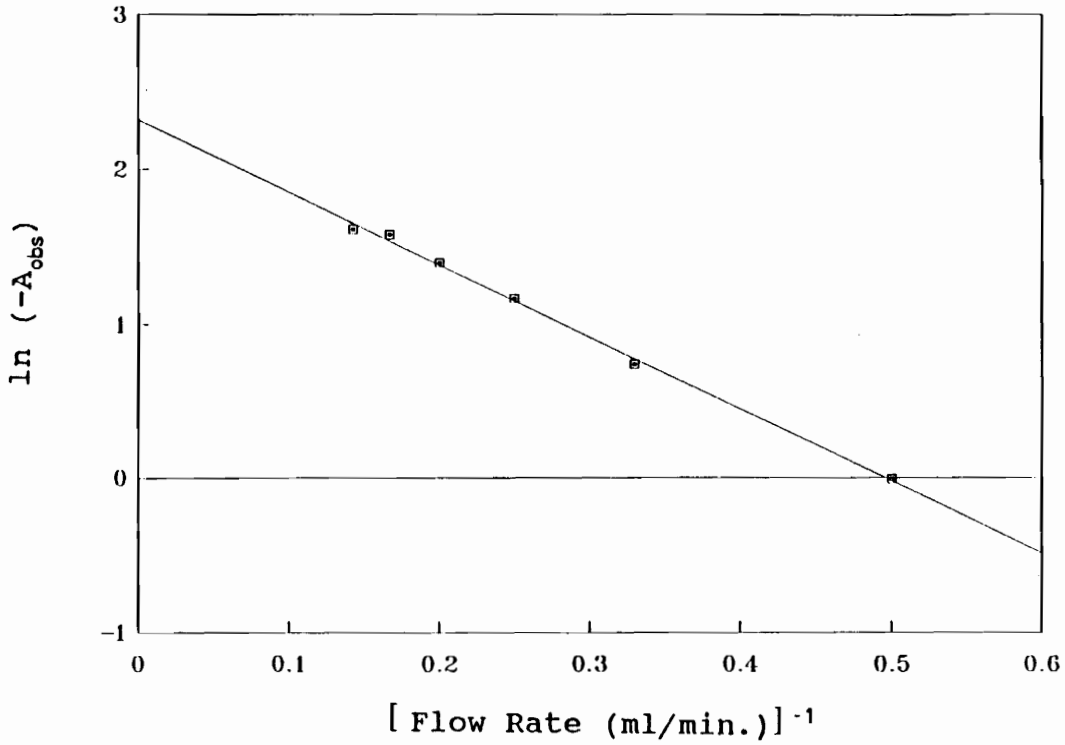

Figure 5.5: Plot of ln ($-A_{obs}$) Versus Inverse Flow Rate for ^{13}C LLIT DNP Experiment for 0.4 M CH_3CONH_2/TEMPO Solution.

projected intercept of 2.32 ± 0.08.

5.3.4 Determination of the Leakage Factor f

According to equation 5.11 the leakage factor f can be experimentally determined by measuring the nuclear relaxation time in the presence and absence of the free radicals. However, in many cases the relaxation time measurements at low field are difficult due to sensitivity limitations. Therefore, high field relaxation times were used to measure the leakage factor in this study. The ^{13}C spin-lattice relaxation times of acetamide solutions with and without TEMPO were measured using a inverse recovery pulse sequence 180^0 ~ τ ~ 90^0 ~ T on a Varian Unity 400 FT-NMR spectrometer. The leakage factor (f) was then calculated based on the high field NMR data.

5.3.5 Determination of The Saturation Factor s

^{13}C LLIT DNP enhancements A_{obs} for the acetamide/TEMPO solutions were measured using different levels of the microwave power, the reciprocal enhancement A_{obs}^{-1} at complete saturation of electron transition (s = 1) were obtained using the extrapolation method based on equation 5.16. The plot of reciprocal $-A_{obs}$ versus the reciprocal microwave power is given in Figure 5.6 with the projected intercept, 0.670 ± 0.004.

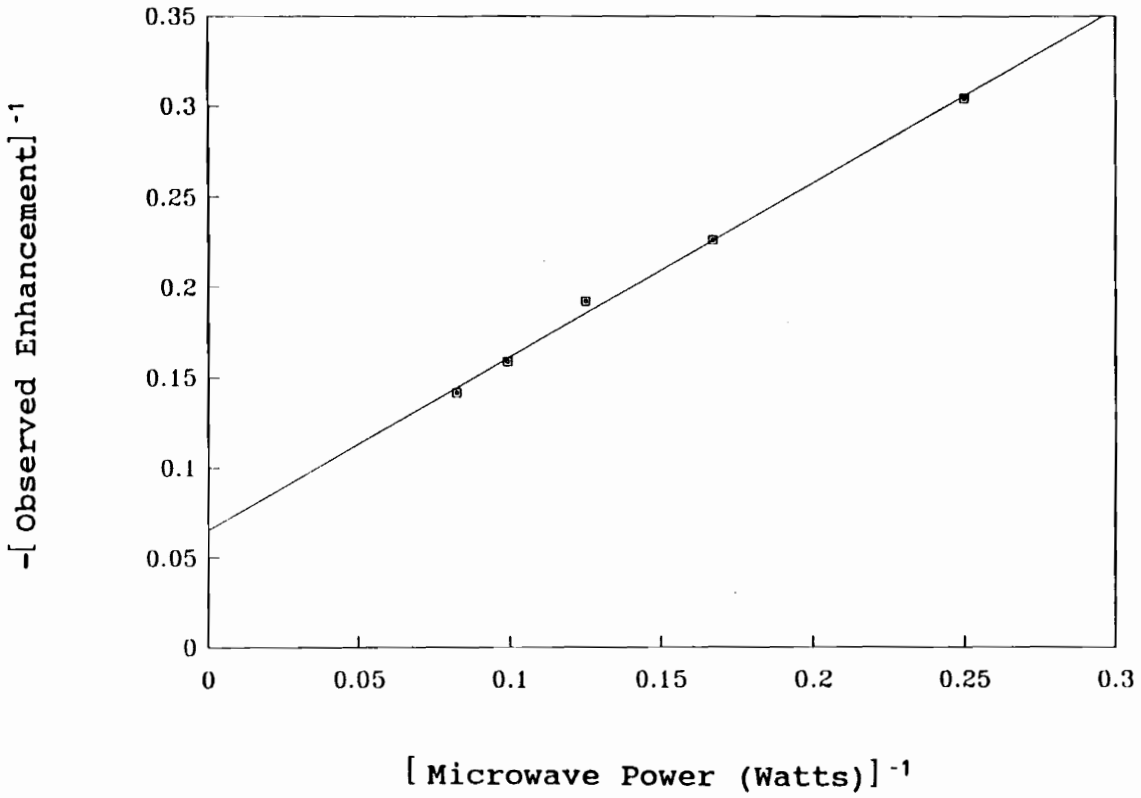

Figure 5.6: Saturation Plot for ^{13}C LLIT DNP Experiment for 0.4 M CH_3CONH_2/TEMPO System.

5.3.6 Determination of Ultimate DNP Enhancement A_∞

The ultimate enhancement A_∞ for complete saturation (s=1) and complete dominance of the nuclear relaxation by the nuclear-electron interaction (f=1) can be obtained after determining the enhancement factor A, the leakage factor f, and saturation factor s based on equation 5.17. The leakage factor f, saturation factor s, enhancement factor A, and ultimate enhancement A_∞ for CH_3CONH_2/TEMPO system are presented in Table 5.2.

The ^{13}C LLIT DNP Spectra in Fig. 5.4 clearly shows that the dominant mechanism for both nonequivalent carbons is dipolar coupling of the nuclear and electron spins. A large dipolar enhancement (A_∞ =-310) was observed for carbonyl carbon. Whereas, a small dipolar enhancement (A_∞ = -60) was observed for the methyl carbon, indicating that a significant scalar mechanism contribution is present. These results are consistent with ^{13}C contact shift and nuclear -electron relaxation times studies.

Table 5.2: ^{13}C LLIT DNP Experimental Results[a] for CH_3CONH_2/Dioxane/0.1 M TEMPO Solution.

Nucleus	f[b]	s	A_∞[c]
$-^{13}CH_3$	0.94	0.37	-60 ± 30[d]
$-^{13}CO$	0.97	0.46	-320 ± 30[d]

a. All data were obtained at room temperature and inverse gated ^1H decoupling was employed to minimize any nuclear Overhauser effects.
b. Data were obtained based on T_1 measurements at 9.4 T magnetic field.
c. DNP enhancements were measured at low magmetic field (0.33 T), but monitored at high a magnetic field (4.7T).
d. Standard deviations were obtained from regression analysis.

5.4 Data Analysis and Discussions

As discussed in early sections of this thesis, the most important parameter in the DNP experiment is the coupling factor ρ. It is related to the time-dependent part of the magnetic interaction between nuclear and electron spins in the Hamiltonian $\hat{H}_{IS}(t)$ and yields information regarding the type of molecular motions (rotational, translational etc.) in the liquid. By measuring the nuclear electron coupling factor ρ as a function of the magnetic field or the temperature in the system and fitting the results to a model, it is then possible to determine values for the electron-nuclear correlation times τ, radical-solvent distance of closest approach r, energies of activation ΔE, and average diffusion constant D. When scalar coupling is present, the intermolecular hyperfine coupling constant A and the scalar correlation time τ_{SC} may also be determined. Therefore, DNP measurements have the potential of yielding a rather detailed microscopic description of the liquid state.

On the other hand, if the exact form for the coupling factor ρ is known and other parameters are experimentally measured it is possible to calculate the coupling factor ρ and consequently to predict the ultimate DNP enhancement at a fixed magnetic field.

5.4.1 DNP Coupling Factor ρ for Mixed Dipolar and Scalar Interactions

The exact form for the coupling factor ρ will depend on the model chosen for modulation. When both dipolar and scalar interactions are present it is necessary to combine the model for the dipolar interaction with the scalar interaction. Obviously, there are many combinations dependent on the system to be studied.

In the previous sections of this dissertation, two chemical systems CH_3CN/TEMPO and CH_3CONH_2/TEMPO have been investigated utilizing contact shift measurements and relaxation time studies at high magnetic fields. Hydrogen bond formation has been shown in these two systems, and a set of parameters such as coupling constant, correlation times, and radical-nuclear distance in the hydrogen bond complex have been obtained. The results were analyzed based on the isotropic rotational diffusion model for dipolar coupling and the sticking model for scalar interaction. Under this condition the transition probabilities (W_i) will be given by[8,31]

$$W_2^D = \frac{6}{10}\left(\frac{\mu_0}{4\pi}\right)^2 \gamma_I^2 \gamma_S^2 \hbar^2 r^{-6} J_d(\omega_S - \omega_I) \qquad (5.21)$$

$$W_0^D = \frac{1}{10}\left(\frac{\mu_0}{4\pi}\right)^2 \gamma_I^2 \gamma_S^2 \hbar^2 r^{-6} J_d(\omega_S + \omega_I) \tag{5.22}$$

$$W_1^D = \frac{3}{20}\left(\frac{\mu_0}{4\pi}\right)^2 \gamma_I^2 \gamma_S^2 \hbar^2 r^{-6} J_d(\omega_I) \tag{5.23}$$

$$W_0^{SC} = \frac{1}{2}\left(\frac{A}{\hbar}\right)^2 J_{SC}(\omega_S + \omega_I) \tag{5.24}$$

where the spectral density functions are given by

$$J_d(\omega) = \frac{\tau_d}{1+\omega^2\tau_d^2} \tag{5.25}$$

$$J_{SC}(\omega) = \frac{\tau_{SC}}{1+\omega^2\tau_{SC}} \tag{5.26}$$

Substitution of equations above into equation 5.7 gives the coupling factor ρ as

$$\rho = \frac{W_2^D - W_0^D - W_0^{SC}}{W_0^D + W_0^{SC} + 2W_1^D + W_2^D}$$

$$= -\frac{6J_d(\omega_S - \omega_I) - J_d(\omega_S + \omega_I) - 5MJ_{SC}(\omega_S + \omega_I)}{6J_d(\omega_S - \omega_I) + J_d(\omega_S + \omega_I) + 3J_d(\omega_I) + 5MJ_{SC}(\omega_S + \omega_I)} \tag{5.27}$$

The mixing parameter M measures the ratio of the scalar to the dipolar coupling; it is defined by

$$M=\left(\frac{A}{\hbar}\right)^2\left(\frac{r^6}{\gamma_I^2\gamma_S^2\hbar^2(\mu_0/4\pi)^2}\right) \tag{5.28}$$

Since M becomes infinite for zero dipolar interaction, it is more convenient to introduce two mixing parameters[8]

$$M_d = 1/(1+M), \qquad M_s = M/(1+M). \tag{5.29}$$

Furthermore, it is convenient to introduce the normalized spectral density functions[8] $j(\omega) = J(\omega)/J(0)$, since they have the simple limits $j(0) = 1$ and $j(\infty) = 0$. By taking into account the relation $\omega_s >> \omega_I$ which is valid for the electron nuclear interaction, we get

$$\rho=\frac{M_d j_d(\omega_S)-M_S\frac{\tau_{SC}}{\tau_d}j_{SC}(\omega_S)}{M_d\left[\frac{7}{5}j_d(\omega_S)+\frac{3}{5}j_d(\omega_I)\right]+M_S\left[\frac{\tau_{SC}}{\tau_d}j_{SC}(\omega_S)\right]} \tag{5.30}$$

where

$$j_d(\omega)=\frac{1}{1+\omega^2\tau_d^2} \tag{5.31}$$

$$j_{sc}(\omega) = \frac{1}{1+\omega^2\tau_{sc}^2} \qquad (5.32)$$

Therefore, it is possible to calculate the coupling factor ρ based on these equations and consequently to predict the ultimate DNP enhancement at a given magnetic field strength.

5.4.2 Predicted DNP Enhancements at 0.33 T Magnetic Field for the CH_3CN-^{15}N/TEMPO System

5.4.2.1 Methyl ^1H DNP Enhancement

The ^1H relaxation studies have shown that the methyl hydrogen of the substrate molecule CH_3CN were relaxed by dipolar coupling with the unpaired electron spins and the interaction was modulated by rotational motions of the transient complex with a rotational correlation time τ_c of 3.0 $\times$ 10^{-11}s (see Fig. 4.4). For hydrogen nuclei, no scalar coupling was expected. In this case, we assume the mixing parameter M is zero, yielding a M_d value of 1 for the methyl hydrogen. The coupling factor, ρ = 0.26 at the magnetic field strength 0.33 T (ω_s = 5.8 $\times$ 10^{10} rad.s^{-1}) was obtained based on equation 5.30. Therefore, the ^1H DNP enhancement is dominated by the dipolar interaction and a negative enhancement is expected. An ultimate ^1H DNP enhancement of -170 is expected, which is in good agreement with the ^1H DNP enhancement measured at 0.33 T (A_∞ = -160)[60].

5.4.2.2 Nitrile ^{13}C DNP Enhancement

The ^{13}C paramagnetic contact shift measurements demonstrated that there is no scalar interaction between the nitrile group and the TEMPO free radical (Chapter III). Therefore, a coupling factor ρ (+0.26) was obtained for the nitrile carbon and the ^{13}C DNP enhancement is dipolar

dominated. However, this corresponds to a rather large negative enhancement (A_∞ = -690) because of the smaller magnetogyric ratio γ_c for the ^{13}C nuclide.

5.4.2.3 Methyl Carbon DNP Enhancement

Both ^{13}C NMR contact shift and relaxation times results illustrated that the C-H bond is the principle site of complexation in the CH_3CN/TEMPO system, yielding a hyperfine coupling constant of 0.66 MHz and a scalar correlation time of τ_{sc} 8.5×10^{-11}s. The mixing parameter M can be estimated based on eq. 5.28 and the distance $r_{c..s}$ (4.1 Å) between the carbon and the free radical is assumed to be the sum of the time-averaged hydrogen bond length and the bond length of the C-H bond. After resolving the mixing parameter M, the value of M_d and M_s can be easily calculated and the coupling factor ρ (-0.22) was obtained, indicating that the ^{13}C DNP enhancement for the methyl carbon is scalar dominated and a positive enhancement predicted.

5.4.2.4 ^{15}N DNP Enhancement

The ^{15}N paramagnetic contact shift results demonstrated a small limiting contact shift and a small hyperfine constant which indicates the dipolar interaction dominates the electron nuclear interaction with a small component for the scalar interaction. In order to estimate the ^{15}N ultimate DNP

enhancement at 0.33 T magnetic field it is assumed that: 1) the distance $r_{N..S}$ between the unpaired electron and the ^{15}N nucleus is longer than $r_{C..S}$, the distance between the unpaired electron and the methyl carbon nucleus, and 2) the scalar correlation time is shorter than that for the $-^{13}CH_3$ group because of the weaker scalar interaction with the free radical TEMPO than with the methyl carbon. Based on these assumptions, the predicted coupling factor is smaller than 0.11, indicating that the ^{15}N DNP enhancement is dipolar dominated. In contrast with the ^{1}H and ^{13}C DNP enhancements, however, a positive ^{15}N DNP enhancement (< 710) is predicted based on the negative magnetogyric ratio for the ^{15}N nuclide.

The predicted parameters M_d, M_s, coupling factor ρ, and the ultimate DNP enhancement A_∞ for the CH_3CN-^{15}N/TEMPO system are listed in Table 5.3. The low magnetic field measured DNP results are taken from reference (60) and listed in Table 5.3. Good agreement is obtained for the $-C^{1}H_3$, $-^{13}CH_3$, and $-^{13}CN$ groups and only a minor difference appears for the $-C^{15}N$ group resulting from the uncertainty in the distance $r_{N..S}$ and the limited knowledge of the correlation times.

The results show that the dominated dipolar mechanism dominates the DNP enhancements for the methyl hydrogen and nitrile carbon. Dramatic differences in the ^{13}C NMR relaxation

Table 5.3: The Paramaters M_d and M_{SC}, DNP Coupling Factor ρ, and the Ultimate DNP Enhancement A_∞ for the CH_3CN-^{15}N/TEMPO[a] system

Nucleus	M_d	M_{SC}	ρ		A_∞	
			cal.[b]	exp.[c]	cal.[b]	exp.[c]
$-C^1H_3$	1	0	+0.26	+0.24	-170	-160 ± 20
$-^{13}CH_3$[d]	0.16	0.84	-0.22	-0.20	+580	+520 ± 100
$-^{13}CN$	1	0	+0.26	+0.24	-690	-620 ± 120
$-C^{15}N$[e]	≤ 0.68	≥ 0.32	≤ +0.11	+0.08	≤ +710	+520 ± 100

a. 1.34 M $CH_3C^{15}N/CCl_4$/0.1 M TEMPO solution.
b. The calculated coupling constants ρ and DNP enhancements at 0.33 T magnetic field.
c. The coupling constants ρ and DNP enhancements measured at o.33 T magnetic field.
d. Assuming $r_{C..S}$ = 4.1 Å. ($r_{H..S}$ = 3.0 Å and r_{C-H} = 1.0 Å)
e. Assuming $r_{N..S} \geq$ 4.1 Å.

and DNP enhancement for the methyl and nitrile carbon have been observed for the CH_3CN/TEMPO solution. A positive DNP enhancement for the methyl carbon indicates a scalar dominated electron-nuclear interaction which results from the formation of a hydrogen bonded complex. The existence of a specific chemical intermolecular interaction between the $-^{13}CH_3$ group and the free radical TEMPO is clearly demonstrated (see Fig.4.4).

5.4.3 Predicted DNP Enhancements for the CH_3CONH_2/TEMPO System

5.4.3.1 Methyl ^1H DNP Enhancement

The ^1H NMR relaxation studies demonstrated that the methyl hydrogen relaxation was dominated by the electron-nuclear dipolar-dipolar interaction modulated by an isotropic rotational motion of the hydrogen bonded complex, $\tau_c = 3.5 \times 10^{11}$ s. The scalar component can be neglected and a coupling factor of 0.22 was calculated when M_d is assumed to be unity. A negative dipolar dominated ^1H DNP enhancement of -150 is readily predicted.

5.4.3.2 Carbonyl ^{13}C DNP Enhancement

As previously noted, no scalar coupling was suggested for the carbonyl group based on the observation of no ^{13}C paramagnetic contact shift (see chapter 3). A value $\rho = 0.22$ was calculated assuming a same correlation time for the

carbonyl carbon. Under this condition, a negative DNP enhancement was readily predicted with $A_{\infty} = -580$.

5.4.3.3 Amino ^{15}N DNP Enhancement

The large ^{15}N contact shift (130 ppm) previously described strongly suggests the presence of an appreciable amount of unpaired electron spin density transferred to the ^{15}N nucleus in the acetamide molecule. In this case, the N-H bond is clearly the site of complexation in the CH_3CONH_2/TEMPO system. Therefore, a large scalar enhancement is expected for the amino nitrogen, and the ^{15}N DNP enhancement will be negative due to the negative magnetogyric ratio for the ^{15}N nuclide.

In comparison with the methyl hydrogen, the relaxation of the amino hydrogen is more complicated and is the sum of several different relaxation processes such as electron-nuclear interactions, proton-proton exchange, etc. Therefore, it is difficult to determine the correlation time τ_c and $r_{H..S}$, distance between the amino proton and the nitroxide free radical via the usual frequency dependent relaxation studies. However, by assuming the same values for rotational correlation time τ_c and the electron-nuclear interaction distance $r_{H..S}$ for both amino and methyl protons a coupling factor $\rho < -0.5$ is calculated where the distance between the nitrogen nucleus and free radical $r_{N..S}$ is the time averaged

sum of $r_{H..S}$ and the N-H bond length (4.1 Å). Therefore, the predicted ^{15}N DNP enhancement is scalar dominated, and the enhancement is negative with $A_\infty < -3300$.

5.4.3.4 The Methyl Group ^{13}C DNP Enhancement

The ^{13}C paramagnetic contact shift results demonstrated the presence of a small limiting contact shift and a small hyperfine constant. This suggests that the dipolar interaction dominates the electron-nuclear interaction with a minor component for the scalar interaction. In order to estimate the DNP enhancement at 0.33 T magnetic field it is assumed that 1) the distance $r_{C..S}$ between the electron and methyl carbon is the sum of $r_{H..S}$ and r_{C-H}, and 2) the scalar correlation time is shorter in comparison with the amino nitrogen. Under this assumption, the predicted coupling factor is smaller than 0.20, suggesting the DNP enhancement is dipolar dominated with $A_\infty < -520$.

The parameters M_d, M_{SC}, coupling factor ρ and the ultimate DNP enhancement A_∞ derived from the mixing scalar and dipolar interaction in the CH_3CONH_2-^{15}N/TEMPO system are presented in Table 5.4 with the low magnetic field measured DNP enhancement results. The low magnetic field measured ^{15}N DNP result is taken from reference (60).

Table 5.4: The Paramaters M_d and M_{SC}, DNP Coupling Factor ρ, and the Ultimate DNP Enhancement A_∞ for the CH_3CONH_2-^{15}N/TEMPO[a] System

Nucleus	M_d	M_{SC}	ρ		A_∞	
			cal.[b]	exp.[c]	cal.[b]	exp.[c]
$-^{13}CH_3$	0.76	0.24	+0.20	+0.10	-520	-60 ± 30
$-^{13}CO$	1	0	+0.22	+0.12	-580	-320 ± 30
$-^{15}NH_2$	> 0.05	< 0.95	< -0.51	-0.36[e]	< -3300	-2300[e] ± 500

a. 0.4 M $CH_3CO^{15}NH_2$/dioxane/0.1 M TEMPO solution.
b. The calculated coupling constants ρ and DNP enhancements at 0.33 T.
c. The coupling constants ρ and the DNP enhancements exprimentally measured at 0.33 T.
d. Calculated value assuming $r_{N..S}$ = 4.1 Å. ($r_{H..S}$ = 3.1 Å, r_{N-H} = 1.0 Å)
e. These data were taken from reference (13).

The results demonstrated that dipolar DNP enhancements dominate for the methyl hydrogen, methyl carbon, and carbonyl carbon. However, a large positive ^{15}N DNP enhancement of the amino nitrogen has been observed, indicating a significant scalar dominated electron-nuclear interaction presumably resulting from the formation of a hydrogen bonded complex. The existence of a specific chemical intermolecular interaction between the $-^{15}NH_2$ group and free radical TEMPO is clearly demonstrated (see Fig.4.5).

In comparison with the CH_3CN/TEMPO system, the difference between the predicted and the measured DNP enhancements at the low magnetic field for the CH_3CONH_2/TEMPO system is much larger. The disagreement for the CH3CONH$_2$/TEMPO system can be understood in terms of the larger size, lower symmetry of the CH_3CONH_2 molecule, and inaccuracies in the measured correlation times. For example, the results were analyzed based on the isotropic rotation diffusion model for the dipolar interaction; however, anisotropy increases with the size of interacting molecule. Furthermore, the higher viscosity of the dioxane solvent could make the rotational diffusional motion of the hydrogen bonded complex even more anisotropic. In this case, it is possible that the CH_3CONH_2/TEMPO system undergoes anisotropic rotational diffusion with orientation dependent correlation times. Therefore an anisotropic

rotational diffusion model such as Woessner's[61] model could be useful to analyze the results. On the other hand, it is also possible that there are several different equilibria between CH_3CONH_2 and TEMPO free radical. Therefore, a more comprehensive analysis is needed to a obtain better match with the experimental results for the acetamide/TEMPO system.

However, in comparison with the large range of the potential DNP enhancement of the ^{13}C NMR signal (-1310 to +2620) and of the ^{15}N NMR signal(+3240 to -6480), the differences are relatively small and the predicted results are still valuable to understanding the interactions in the CH_3CONH_2/TEMPO system.

CHAPTER 6

Applications of Liquid/Liquid and Solid/Liquid Intermolecular Transfer DNP in C_{60} and Activated Carbon Samples

6.1 Introduction

DNP experiments for a number of NMR nuclides (e.g., ^{1}H, ^{13}C, ^{31}P etc.) have been demonstrated for both liquid[8,9] and solid[62-67] samples. Dynamic nuclear polarization occurs when irradiation is applied at or near the electron Larmon frequency ω_s. The magnitude of the enhancement and the circumstances under which the enhancement becomes maximal depend on the nature and the time-dependence of the electron-nuclear interaction H_{IS}. Therefore, information about the electron-nuclear interaction can be obtained from the sign, the magnitude, and the shape of the enhanced NMR signals.

In the liquid state, molecules move rapidly on a scale comparable to ω_s^{-1}; therefore, the nuclear-electron interaction H_{IS} is time-dependent and an Overhauser effect is generally observed.

In contrast with the liquid state, two limiting effects in the solid state may occur according to whether the electron nuclear coupling is static or dynamic. The nuclear-electron interaction H_{IS} is time-dependent if the electron spins in solids move rapidly or undergo rapid spin-exchange interaction on a scale comparable to ω_s^{-1}. In this case, the Overhauser effect can be observed and the enhancement can be either positive or negative dependent on the type of interaction. The enhancement can be obtained by irradiating at or near the electron frequency. An irradiation near the electron Larmor frequency ω_s provides an induced transition probability W as[10]

$$W = \pi \gamma_s^2 B_1^2 g(\omega - \omega_s) \tag{6.1}$$

where B_1 is the magnitude of the microwave field, $g(\omega)$ is the normalized EPR lineshape function. The DNP enhancement factor is given as

$$A_{Ov} = \rho \left(\frac{W}{W + W_s} \right) \left(\frac{\gamma_s}{\gamma_I} \right) \tag{6.2}$$

where W_s is the electron Zeeman relaxation rate. Other parameters in equation 6.2 have been defined before. This case is analogous to the liquid state. Therefore, the enhancement depends on the relative strength of the scalar and dipolar interaction and is a function of the microwave frequency, which gives a symmetrical curve around the electron

frequency and becomes maximal when the irradiation frequency ω equals the electron frequency ω_s (Fig 6.1).

On the other hand, a static dipole-dipole interaction between paramagnetic electrons and nuclei occurs in solids containing fixed paramagnetic centers. In this case, the electron-nuclear interactions are time-independent and the pure electron-nuclear state functions are mixed by this interaction[62]. As a result the electron-nuclear states can no longer be described by pure product functions but become mixed with these other states. Irradiation near the frequencies $\omega_s \pm \omega_I$ leads to non-zero induced transitions with a probability $W^{\pm}$ where a nucleus and an electron flip simultaneously, the so-called forbidden transitions.

$$W^{\pm} = 2|q_{ij}|^2 \pi \gamma_s^2 B_1^2 g(\omega_s - \omega \pm \omega_I) \qquad (6.3)$$

where g_{ij} is the mixed contribution and typically on the order of 10^{-7} to 10^{-8}. Though the maximum values of $W^{\pm}$ are much smaller than W, the probability of the allowed transition, it is this small probability that causes the solid state effect.

The nuclear polarization can be enhanced by irradiation at these normally forbidden transitions, and the enhancement factor (A_{ss}) near the frequencies ($\omega_s \pm \omega_I$) is due to the solid state effect and is given by

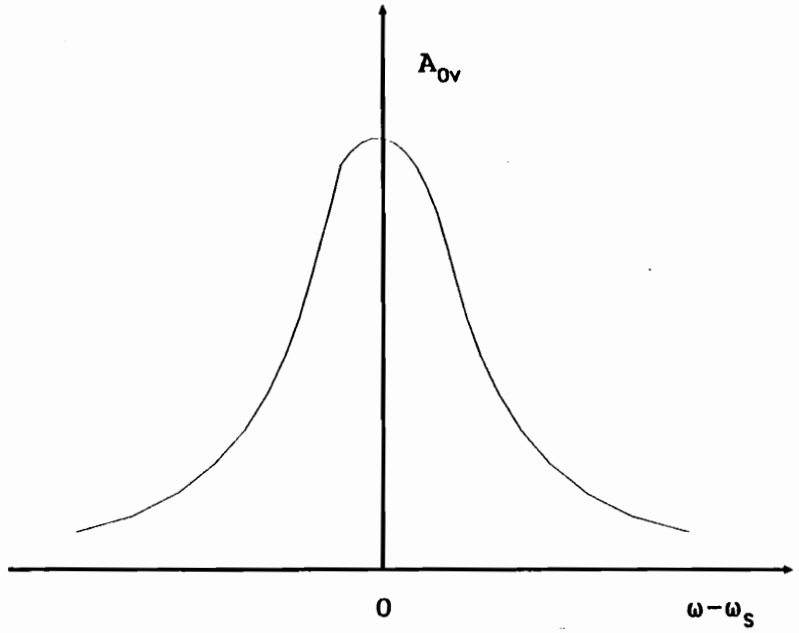

Fig. 6.1 The Overhauser Enhancement due to Scalar Electron-Nuclear Interaction as a Function of Microwave Frequency.

$$A_{SS} = \frac{W^{\pm}}{W^{\pm} + 2W_1 + 2W_{10}} \left(\pm \frac{\gamma_S}{\gamma_I} - 1 \right) \qquad (6.4)$$

where $W^{\pm}$ is the induced mixed transition probability close to the magnetic frequency $(\omega_S \pm \omega_I)$; other symbols in this equation have been defined previously. This equation shows that the enhancement is negative and becomes a maximum when the irradiation frequency $\omega = \omega_S + \omega_I$, while irradiation near $(\omega_S - \omega_I)$ leads to a positive enhancement. The result is an anti-symmetric curve and is shown in Fig 6.2.

In addition to these two limiting cases, a thermal mixing effect occurs in solids containing fixed paramagnetic centers when the broadening of the EPR signal becomes comparable to the nuclear Larmor frequency, ω_I. In this case the Zeeman system is coupled to the electron broadening system, and the nuclear polarization can be enhanced by irradiation near ω_S and becomes maximal when $\omega = \omega_S \pm \omega_{1/2}$.

In a given case it is difficult to decide which DNP effect (Overhauser or solid state) will dominate and depends on the materials being studied. Therefore, the DNP experiment can be used to increase NMR sensitivity and to study electron mobility and the chemical environment of the nuclear-unpaired electron interaction.

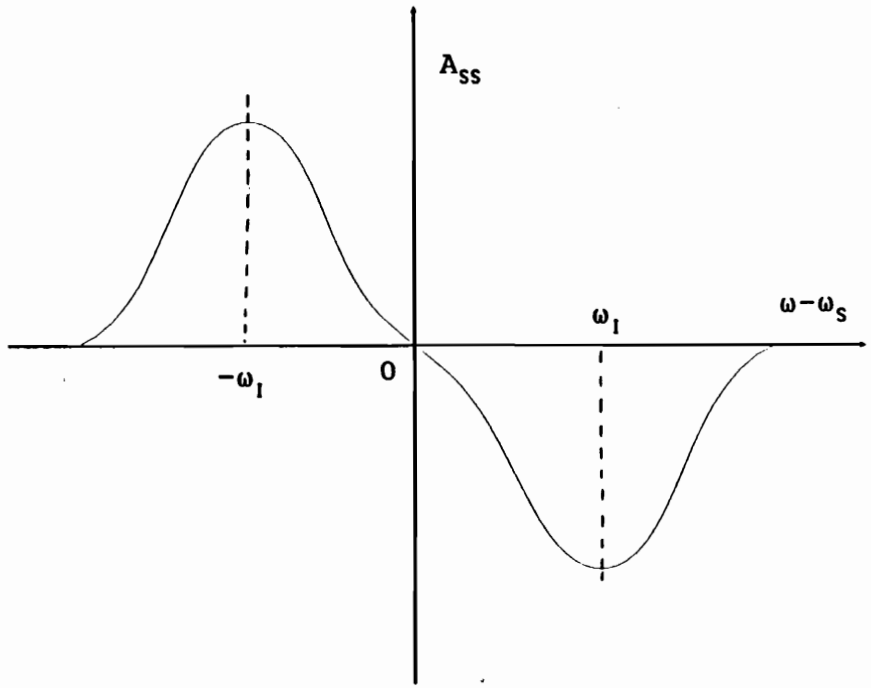

Fig. 6.2 The Solid State Enhancement as a Function of Microwave Frequency.

In addition to the liquid/liquid intermolecular transfer (LLIT) DNP experiment, Dorn et al.[12] have demonstrated solid-liquid intermolecular transfer (SLIT) of the polarization from an immobilized spin label to a flowing fluid bolus. In this experiment, spin labels were immobilized on silica gel surfaces. When the flowing bolus (e.g. benzene) entered the low magnetic field, the microwave field irradiated the electron transitions for the immobilized radical. The polarization builds up for the flowing bolus in the low field and is transferred to a high magnetic field where the ^{1}H NMR signal of this bolus was monitored. The flow SLIT ^{1}H DNP results obtained were similar to those obtained in previous solid state ^{1}H DNP studies[59,68]. Thus the flowing liquid bolus represents a messenger spatially removed from the immobilized reporter group. Since the reporter group reflects properties of the surface, the flow SLIT NMR experiment could provide a new method for monitoring solid/liquid surface intermolecular interaction.

In these studies the liquid/liquid and solid/liquid interfaces for C_{60} (buckminsterfullerene) with free radical TEMPO were investigated by LLIT and SLIT ^{13}C DNP experiments. In addition the solid/liquid interfaces for activated carbon with free radicals were characterized by EPR and by flow ^{1}H and ^{13}C SLIT DNP techniques utilizing flowing benzene. The

dynamic information about the electron nuclear interactions on these carbon samples have been obtained.

6.2 ^{1}H and ^{13}C SLIT DNP in Activated Carbon Samples

6.2.1 Introduction

The carbonaceous chars are the end product of the pyrolysis of organic materials such as wood and cellulose. These chars are very porous and contain high levels of unpaired free electrons. The composition and structure of the chars have been investigated by several other techniques like FT-IR[69,70], CP/MAS ^{13}C NMR[69,70] and EPR experiments[71-75].

Both IR and ^{13}C NMR techniques[69,70] show that the formation and the structure of chars depend on the heating temperature. The intermediate chars produced in the temperature range of 325-350^{0}C contain 8-10% carboxyl and carbonyl groups which are drastically reduced on further heating, presumably through homolytic cleavage of CO and CO_2 creating free radicals involved in the cyclization and condensation of the remaining carbon skeleton to polycyclic aromatic structures. The methyl and other paraffinic carbons are formed largely at 350^{0}C and reach a maximum at 400^{0}c. The formation of aromatic rings starts with decomposition of the glycosyl units and proceeds rapidly as the heat temperature is increased. On further

heating from 400^{0}C to 500^{0}C the concentration of aromatic carbon increases dramatically. The increased aromaticity of the char is due to the preferential loss of the less stable paraffinic groups. Homolytic cleavage of these groups and other substitutes of the aromatic rings create free radicals, promoting further cyclization and cross-linking. The application of higher temperatures such as 950^{0}C leads to annealing, (i.e., the removal of functional groups) and formation of relatively inert, aromatic type structures that show little tendency towards chemisorption.

Among those techniques used to study activated carbon samples, EPR studies are more extensive because the high sensitivity of the technique and the high concentration of unpaired electrons make the EPR signal easy to detect. A number of groups have used EPR to study charred and carbonized organic materials over a very large temperature range of 200^{0}C - 3000^{0}C[71-75]. Unfortunately, the EPR spectrum for a variety of carbon samples yields only one featureless signal. The only difference observed in the EPR spectra is the line width and spin concentration. At low heat treatment temperatures (HTT)(<500^{0}C) chars exhibit a linewidth of 5-7 G with lineshape between Gaussian and Lorentzian. In the heating range of 500-750^{0}C, the EPR signals narrow and become completely Lorentzian, resulting in electron-electron spin-

exchange processes. This occurs when the concentration of radicals is high and when the unpaired electrons are delocalized over a network of bonds in the aromatic rings. A maximum spin concentration and minimum linewidth were observed for a heating temperature of 550-600^{0}C. The HTT > 750^{0}C charred materials become electrically conducting and exhibit broad, weak EPR signals.

In solids containing both magnetic nuclei and unpaired electrons, the dynamic nuclear polarization has been combined with NMR of abundant and rare spins in a variety of materials such as coal[10,76], organic conductors[77], semiconductors[78], and doped polymers[10,79] to increase NMR sensitivity, to study electron mobility, and the chemical environment of the unpaired electrons. Therefore, the use of DNP in pyrolysis experiments can serve as a bridge between NMR and EPR via which more detailed information can be obtained than is possible by either NMR or EPR separately.

6.2.2 Experimental

6.2.2.1 Preparation of Cellulose Chars

A set of activated carbon samples were prepared by heating powdered cellulose in a stream of dry nitrogen. Two grams of cellulose were placed in a quartz heating tube and

flushed with nitrogen gas. The gas was delivered to within 1-2 cm of the bottom of the heating tube via a concentric quartz tube so that the gas flowed over the top of the sample. The samples were brought up to maximum temperature over a period of 1 hr. and heated at that temperature for six hours under nitrogen gas flow. The samples were then cooled under nitrogen. Then the heating tube was evacuated slightly, closed off, and transferred to the sample tube in a glove box so that the activated chars were never exposed to air.

6.2.2.2 EPR Measurements

EPR spectra were recorded using a Varian E-3 EPR spectrometer with 4 mm sample tubes and 100 KHz modulation. Microwave frequencies were 9.3 GHz and the magnetic field was near 3400 G. All spectra were recorded at room temperature. The linewidths were measured as the peak to peak distance of the first derivative of the EPR signal. The spin concentration of the free radicals were measured by comparison with a standard sample of α, α-diphenyl-B-picryl-hydrazyl (DPPH).

6.2.2.3 ^{1}H and ^{13}C SLIT DNP Measurements

The apparatus used in the flow DNP experiment was the same as that in the LLIT DNP experiment as shown in Fig 5.2. The samples of ca. 20-30 mg of activated carbon were removed

from the glove box and placed inside the ceramic tube which was then placed in the microwave cavity of the EPR spectrometer and connected to the benzene reservoir and the high magnetic field detector. The benzene was degassed by bubbling dry nitrogen gas prior to and during experiment. While benzene flowed through the carbon sample, the microwave power was turned on and the polarization was built up at low field. Subsequently the benzene was transferred to the high magnetic field (4.7 T) where the ^{1}H or ^{13}C NMR signal of benzene was detected.

6.2.3 Results and Discussions

6.2.3.1 EPR Characterization of the Cellulose Chars

The EPR spectra obtained for the carbon samples in the HTT range of 350^{0}C - 750^0 C are single featureless lines (Fig. 6.3) with a large variation in the linewidth and spin concentration (Table 6.1). The number of unpaired electron spins increases and the linewidth of EPR signal decreases as the HTT increases. A maximum spin concentration and a minimum of the EPR linewidth were obtained at HTT = 600^{0}C. When HTT > 600^{0}C, the linewidth broadens and the spin count decreases again. The results are consistent with the earlier works[72].

The EPR signals of the cellulose chars are extremely sensitive to air. On exposure to oxygen the EPR spectra of the high temperature chars exhibit broadening to the point of broad lines which are difficult to detect. The characteristic shape EPR linewidth can be restored by re-exposure to nitrogen, which is attributed primarily to physisorption of the oxygen on the carbon surface.

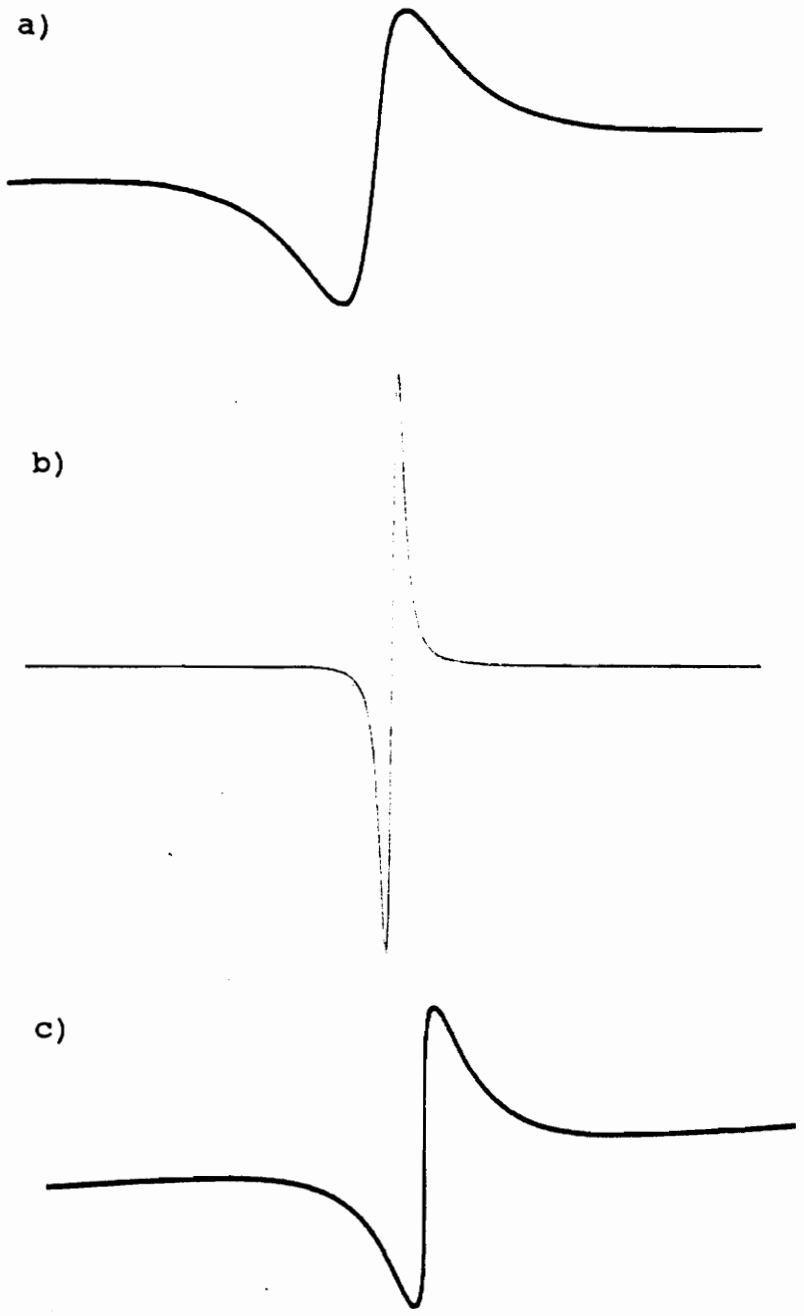

Fig. 6.3 EPR Spectra for Cellulose Chars Prepared at Different Heat Temperatures. a) 450 ^{0}C, b) 550 ^{0}C, and c) 650 ^{0}C.

Table 6.1: The EPR linewidth and Spin Concentration for Cellulose Chars Prepared at Different Heat Treatment Temperatures

Temp. (^{0}C)	LineWidth (G)	Spin Count (10^{20}/g)
350	11.3	.13
400	10.4	.22
450	8.7	.84
500	4.7	1.6
550	1.0	18
600	0.9	25
650	2.3	4.2
700	4.7	2.9

6.2.3.2 ^1H Flow SLIT DNP Experiment for Cellulose Chars

6.2.3.2.1 Characterization of Cellulose Chars Prepared at Different Heat Treatment Temperatures (HTT)

The ^1H DNP enhancement as a function of the microwave frequency for the pyrolyzed samples are shown in Fig. 6.4 to Fig 6.8. The ^1H DNP enhancement curves for the samples heated at 450^0C and 500^0C are anti-symmetrical about the zero microwave offset and become a maximum at the microwave frequency $(\omega - \omega_s)/2\pi \approx \pm$ 14 MHz. Since $\omega_1/2\pi$ is equal to 14 MHz over experimental conditions, it is tempting to conclude that a solid state effect is dominant in these samples. On the other hand, a thermal mixing effect possibly exists since the linewidth $\omega_{1/2}$ of the EPR line is also in this range. Therefore, the results suggest that a static interaction between the electrons and hydrogen occur in these samples and that the unpaired electron spins in these chars move slowly on a scale comparable to ω_s^{-1} in these lower temperature chars.

For the char prepared at HTT 525^0C the ^1H DNP enhancement curve is not completely symmetrical or anti-symmetrical about the electron frequency ω_s. The time-dependent interaction, Overhauser effect, resulting from electrons undergoing spin-exchange interactions yields a symmetric curve while the static interaction, solid state effect, resulting from the fixed electron on the chars yields an anti-symmetric curve.

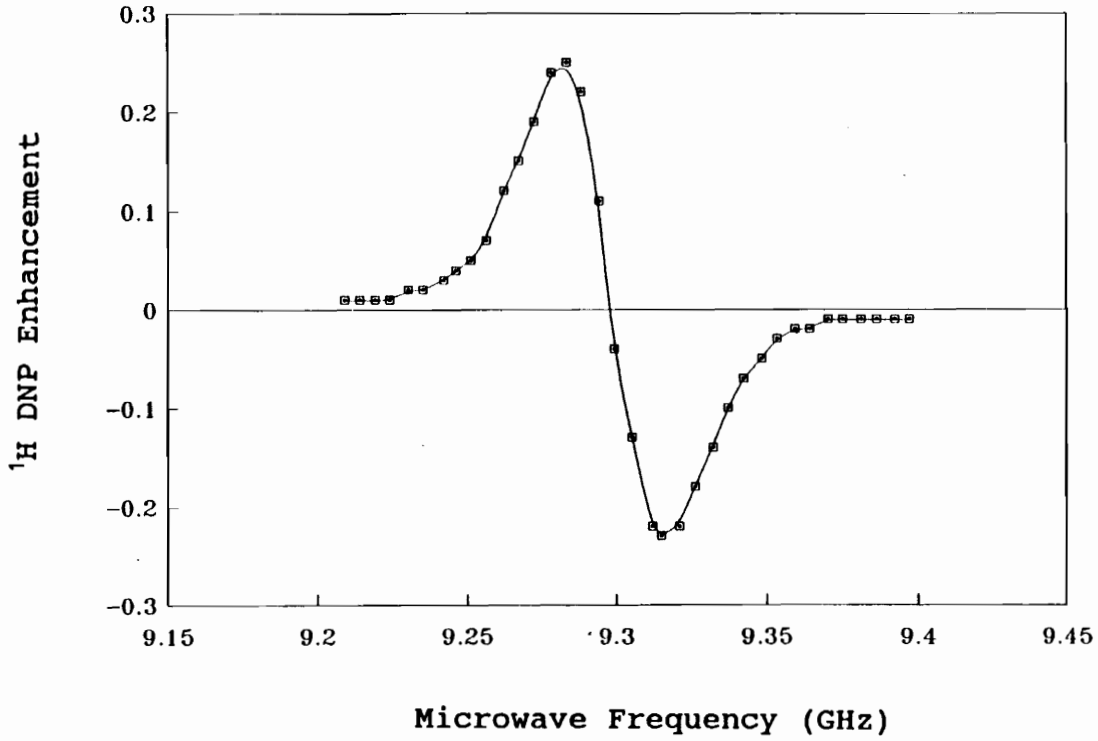

Fig. 6.4 ^{1}H SLIT DNP Enhancement Curve as a Function of Microwave Frequency for the 450^{0}C Cellulose Char.

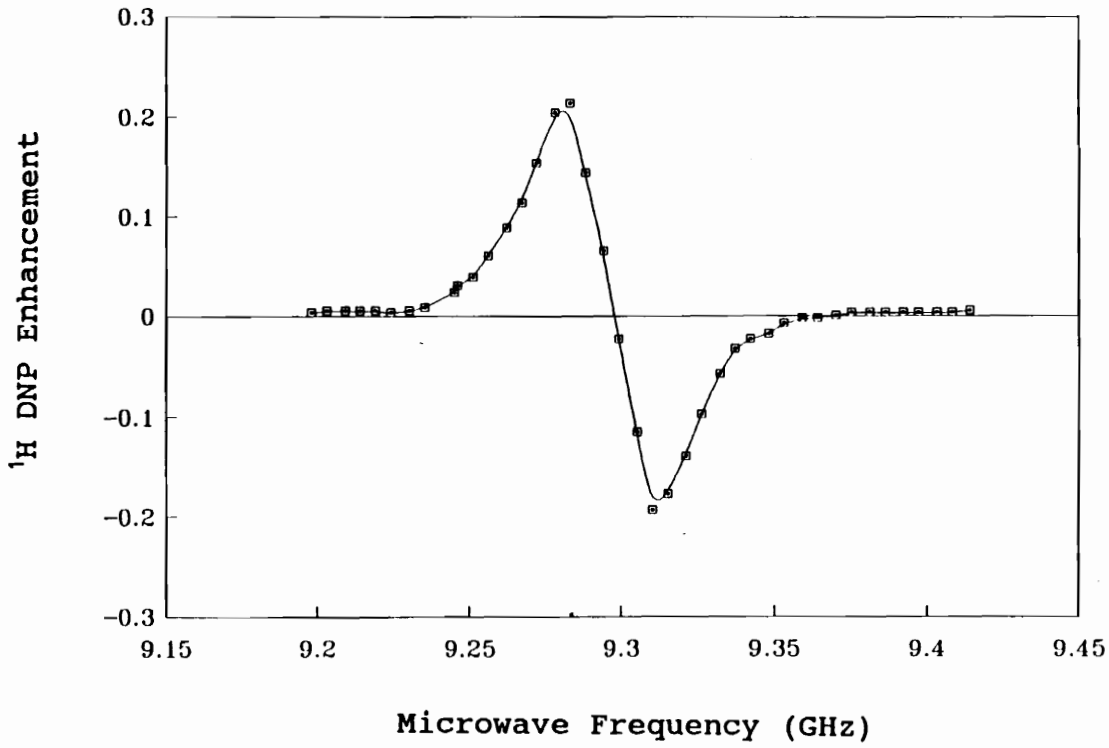

Fig. 6.5 ^{1}H SLIT DNP Enhancement Curve as a Function of Microwave Frequency for the 500^{0}C Cellulose Char.

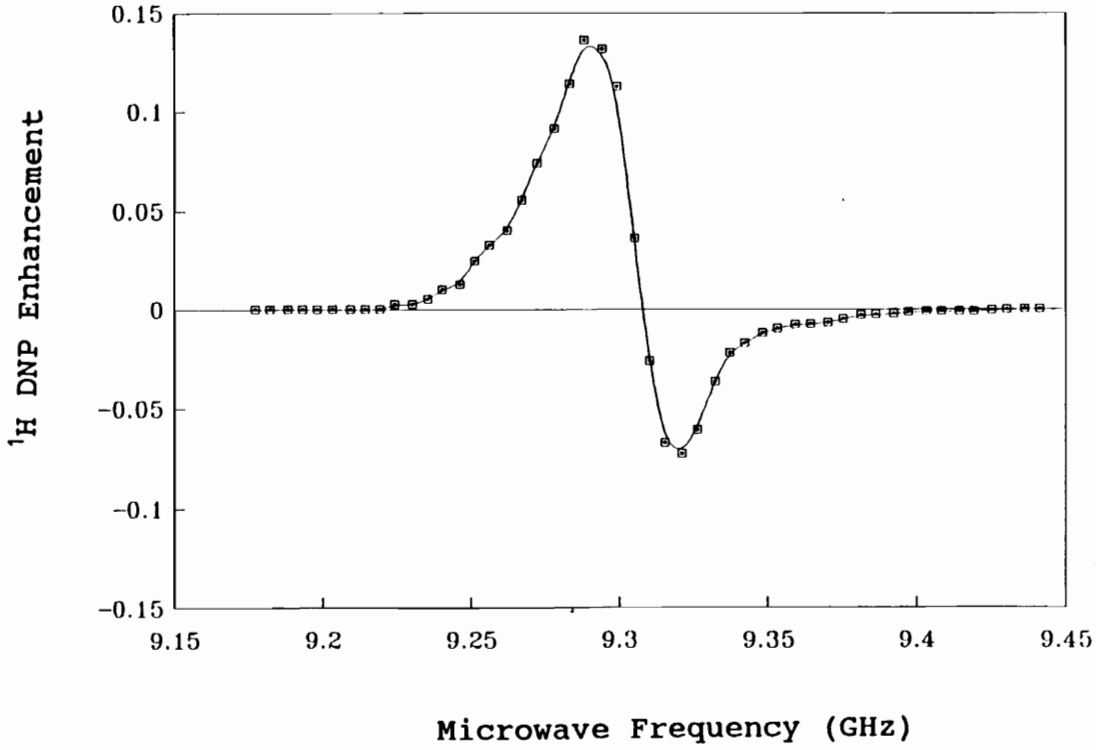

Fig. 6.6 ^{1}H SLIT DNP Enhancement Curve as a Function of Microwave Frequency for the 525^{0}C Cellulose Char.

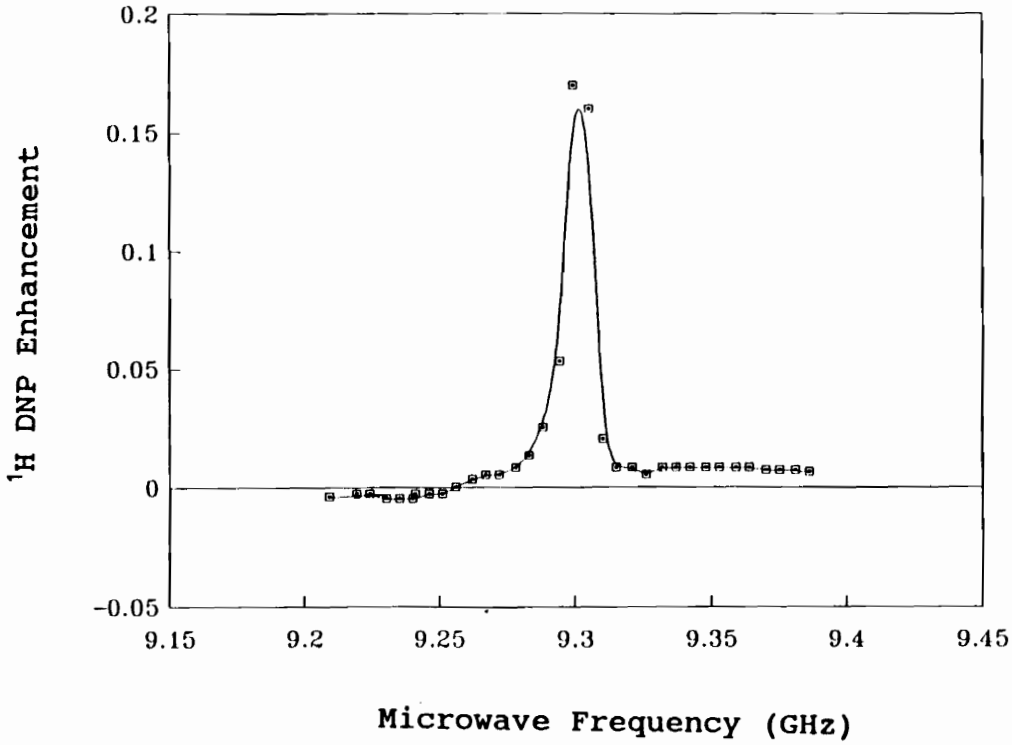

Fig. 6.7 ^{1}H SLIT DNP Enhancement Curve as a Function of Microwave Frequency for the 550^{0}C Cellulose Char.

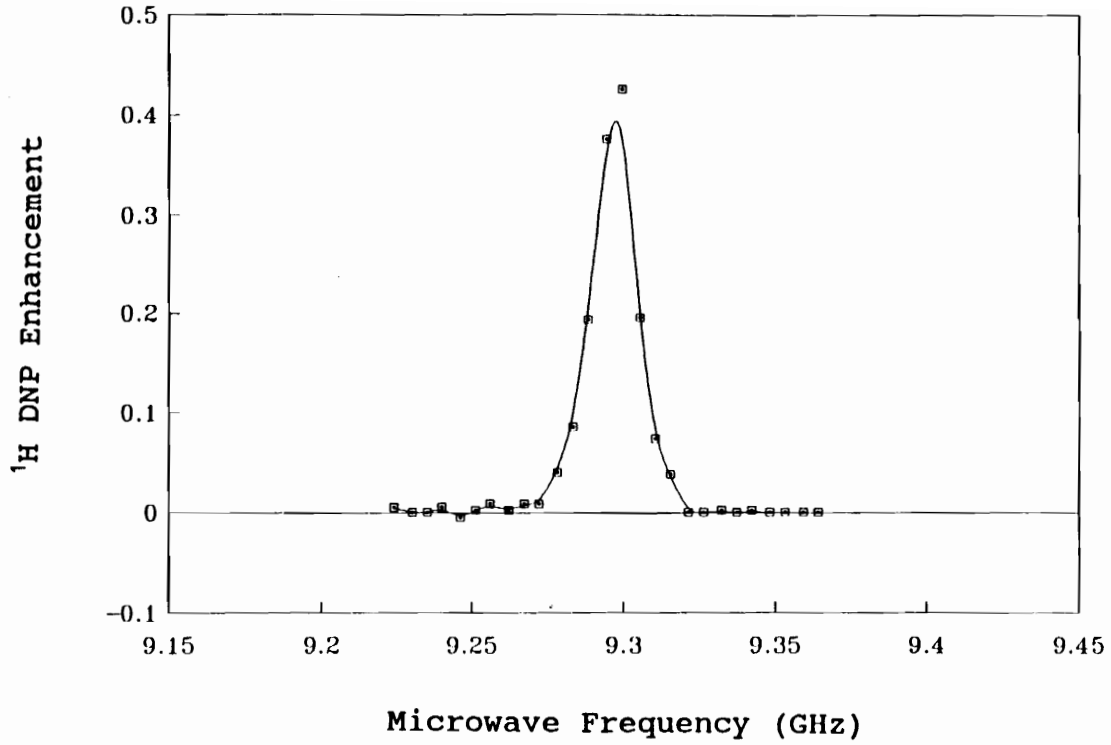

Fig. 6.8 ^{1}H SLIT DNP Enhancement Curve as a Function of Microwave Frequency for the 600^{0}C Cellulose Char.

Therefore, the result suggests that both the time-dependent and the static interactions between electrons and nuclei occur in the 525 ^{0}C char sample. The shape of the ^{1}H DNP enhancement curve shows a positive Overhauser effect, meaning that the nuclear-electron interaction is dominated by the scalar interaction which is consistent with the results observed in related systems[10,77]. The observation of the time-dependent electron-nuclear interaction indicates the presence of delocalized electrons undergoing a rapid spin-exchange interaction in the 525^{0}C char.

Unlike the chars pyrolyzed at lower temperatures, the carbon samples pyrolyzed at 550^{0}C and 600^{0}C exhibit only the positive Overhauser effect, since the ^{1}H DNP enhancement curves are symmetric about the electron frequency ω_s. The results indicate that the electron-electron exchange interaction has become so strong that the static electron-nuclear interaction is completely averaged out in these samples.

In conclusion, the ^{1}H DNP results show that the electron nuclear interactions for lower temperature chars are dominated by the solid state and mixing thermal effects while the positive Overhauser effect is observed in higher temperature chars. Therefore, the results suggest that the properties of

free radicals in the cellulose chars are related to the pyrolysis conditions, particularly to the heating temperature. As HTT increases the electrons in chars become more mobile, presumably due to a corresponding increase in aromaticity (Fig. 6.9).

6.2.3.2.2 Characterization of Adsorption of Oxygen on the Cellulose Chars

Activated carbons are characterized by a high surface area[69]. Due to its high surface area, physical and chemical adsorptions easily take place on the surface. Physisorption is caused by the forces of molecular interaction which are called Van der Waals adsorption. Chemisorption, on the other hand, involves the rearrangement of the electrons of the interacting gas and solid with consequential formation of chemical bonds. The chemisorption of oxygen on carbonized cellulose is a significant factor in controlling the solid phase combustion of cellulosic materials. It is the first step leading to formation of the ultimate gaseous combustion products and provides a mechanism for low temperature ignition of these materials[80]. Therefore, the oxygen chemisorption on carbonaceous materials has received considerable attention[80-82]. Results[80] show that the chemisorption rate is a function of pyrolysis time and temperature. The chars in the temperature range of 400^{0}C - 800 ^{0}C show a high chemisorptive affinity for

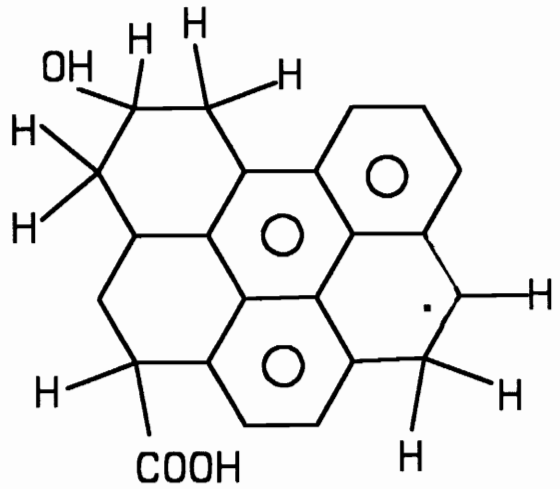

a)

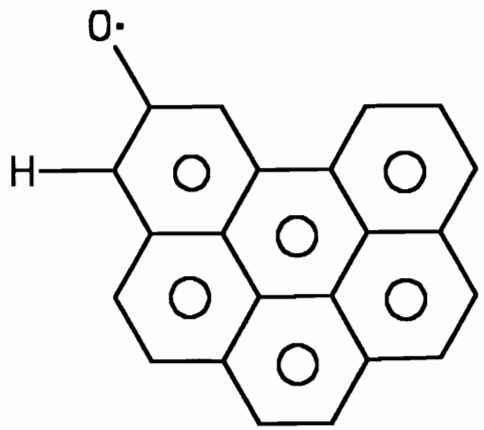

b)

Figure 6.9 The Proposed Structures of Activated Carbon. a) the 450^{0}C cellulose char, and b) the 600^{0}C cellulose char.

oxygen. Maximum chemisorption occurred on chars prepared at the HTT of 550^{0}C. However, the chemisorption of oxygen was insignificant and only the physical adsorption was observed at room temperature.

In this study, the adsorption of oxygen on cellulose chars was characterized by the ^{1}H SLIT DNP experiment. The experiment was similar to the normal DNP measurement except that air was bubbled through benzene instead of nitrogen. Both physical and chemical adsorption were observed at room temperature. The effect of oxygen on the relative ^{1}H DNP enhancement for the 600^{0}C char is shown in Fig. 6.10. The ^{1}H DNP enhancement decreased when dry air was bubbled through benzene and was restored after purging with nitrogen for 30 min. The shape of the DNP enhancement curve remained unchanged before and after exposure to air, indicating that the adsorption of Oxygen on the 600 ^{0}C char is reversible. The result can be mainly explained by physical adsorption. However, the oxygen treated 525 ^{0}C char exhibits a different pattern of enhancement from that observed prior to oxygen treatment (Fig 6.11). The untreated 525 ^{0}C char exhibits a complex enhancement curve which is a composite of the contributions from the Overhauser, the solid state, and the thermal mixing effects. However, the oxygen treated 525 ^{0}C char exhibits an almost anti-symmetric DNP curve around the

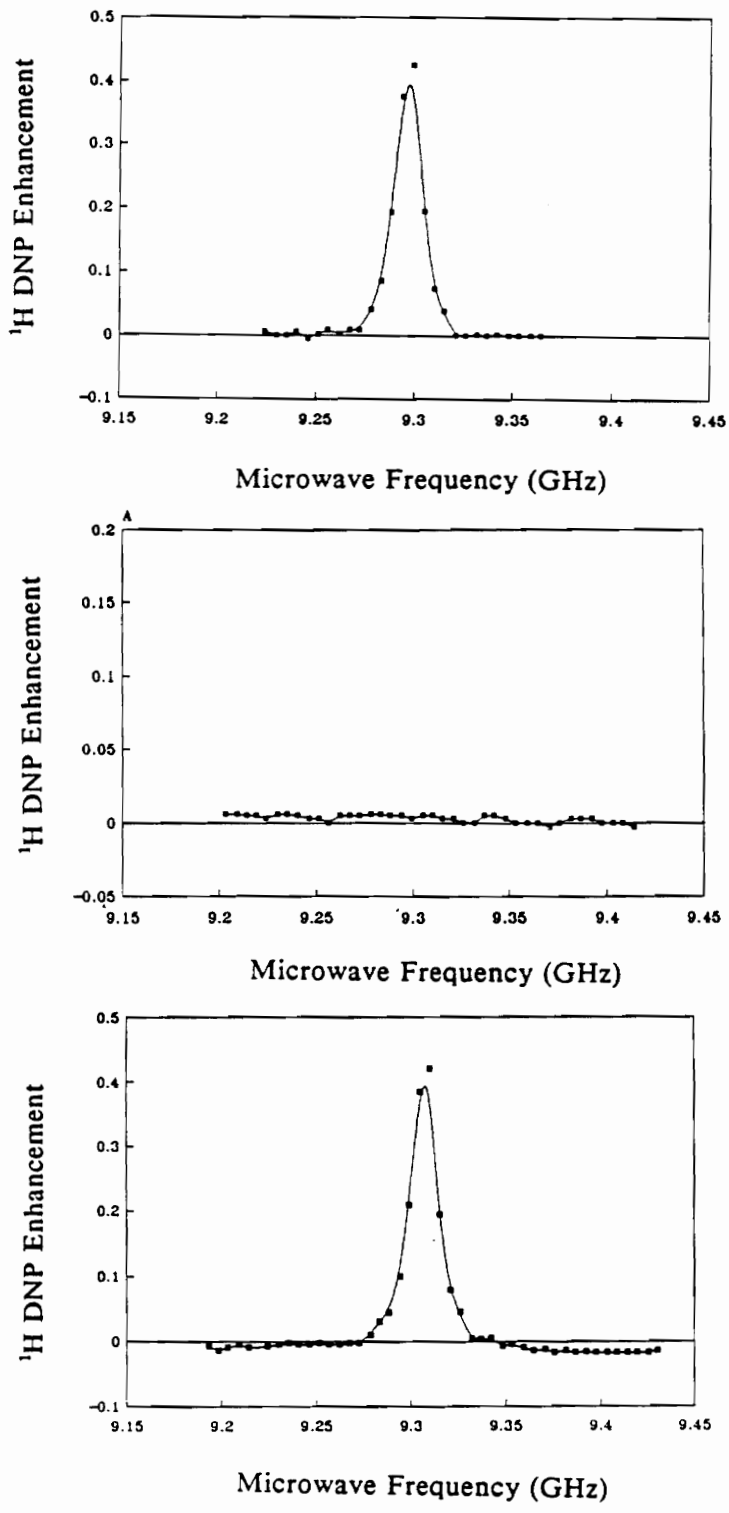

Fig. 6.10 DNP Characterization of Adsorption of Oxygen on the Cellulose Char. 1) ^{1}H DNP enhancement curve as a function of microwave frequency for the 600^{0}C cellulose char. 2) After purging with air for 30 min. 3) After purging with nitrogen for 30 min.

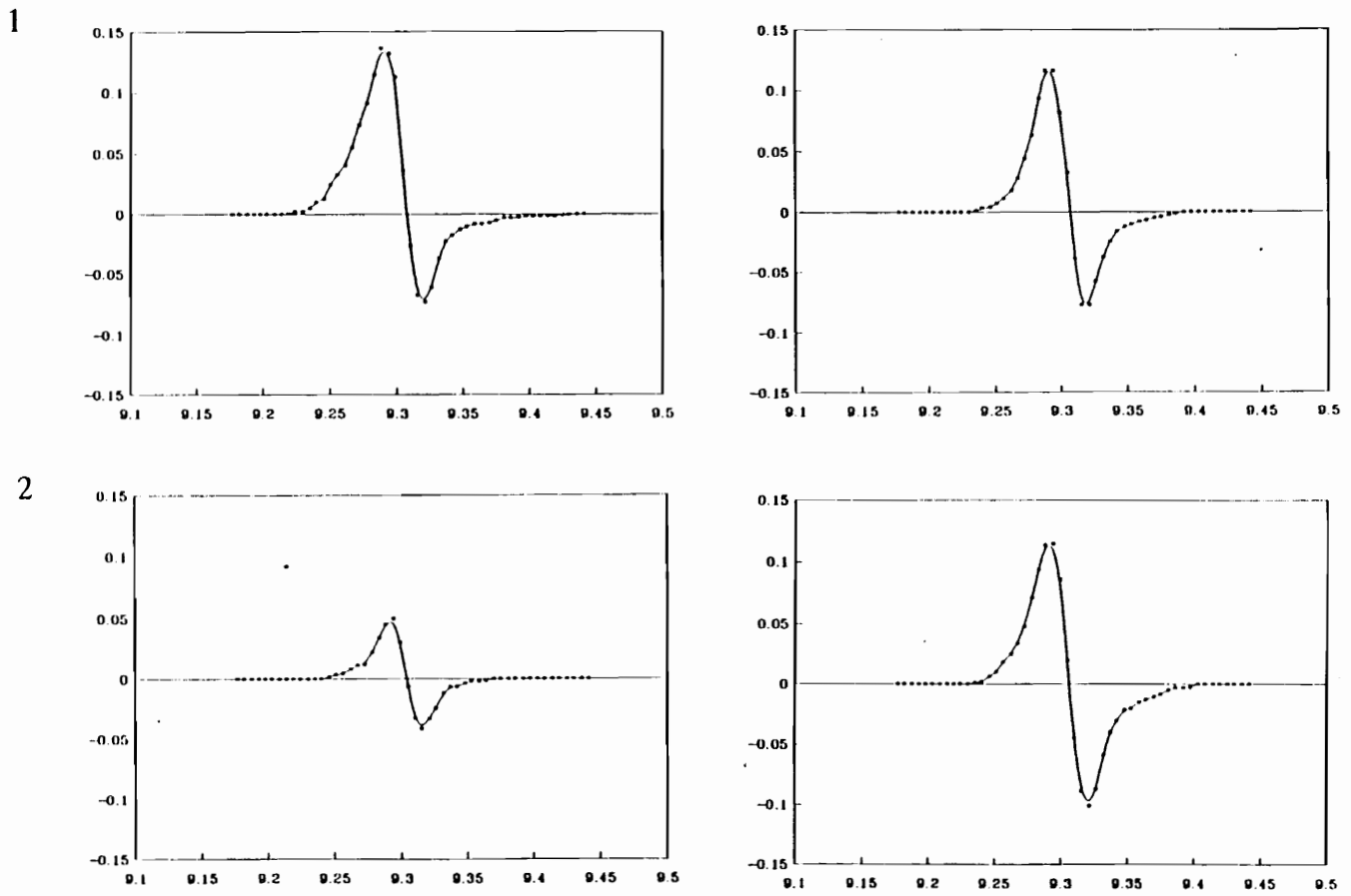

Fig. 6.11 DNP Characterization of Adsorption of Oxygen on the Cellulose Char. 1) Initial ^{1}H DNP enhancement curve as a function of microwave frequency for the $525^{0}C$ cellulose char. 2) After purging with air for 30 min. 3) After purging nitrogen for 30 min. 4) After 3 days (measured under N_2).

zero microwave offset, meaning only the static nuclear-electron interaction is observed. Therefore, oxygen treatment of the char has clearly generated localized unpaired electron centers in the char as indicated by the solid state and thermal mixing effects. Presumably, the fixed unpaired electron centers are formed from surface radicals where the polynuclear aromatic rings have been modified by combination with oxygen. The formation of surface oxygen complexes would locally reduce the size of the aromatic clusters and decrease the extent of electron delocalization, resulting in completely a static interaction.

6.2.3.2.3 Characterization of the Influence of an Inorganic Additive on Cellulose Char.

A variety of inorganic materials are used for suppression of flaming and smoldering combustion of cellulosic materials. For example, $(NH_4)_2HPO_4$ is a well known flame retardant and smolding inhibitor which lowers the pyrolysis temperature, increases the char yield and enhances the aromaticity of char[83]. The mechanisms of pyrolysis and the combustion kinetics of carbonaceous materials have been extensively investigated in the presence of inorganic additives[70,84]. Flame retardants lower the decomposition temperature by catalyzing the dehydration of the glucose units in the cellulose molecule. The increased char formation is due to the increased

condensation and cross-linking of the carbon skeleton. In addition, the inorganic additives affect the composition of the intermediate chars, which have been studied by the CP/MAS ^{13}C NMR technique[70]. In this study, the effectiveness of flame retardants in the aromatic structure of activated carbon was studied by the flow DNP experiment.

Cellulose powders were treated with H_3PO_4 by soaking in aqueous solutions of suitable strength. After soaking, samples were rolled thoroughly to remove excess water and washed with deionized water twice. The treated cellulose samples were then dried and charred at 500 ^0C as described previously. The ^1H DNP enhancements as a function of the microwave frequency for H_3PO_4 treated 500 ^0C char as well as untreated 500 ^0C char are shown in Fig. 6.12. The H_3PO_4 treated 500 ^0C cellulose char exhibits a positive Overhauser effect while the untreated 500 ^0C shows a solid state effect. As previously discussed, the Overhauser effect indicates a time-dependent electron-nuclear interaction whereas the solid effect means a time-independent interaction. Therefore, the Overhauser effect observed suggests that the unpaired electrons in the H_3PO_4 treated 500 ^0C char are more delocalized on the carbon skeleton. The increased aromaticity of the char due to inorganic additives at lower temperatures is confirmed by the ^1H SLIT DNP experiment.

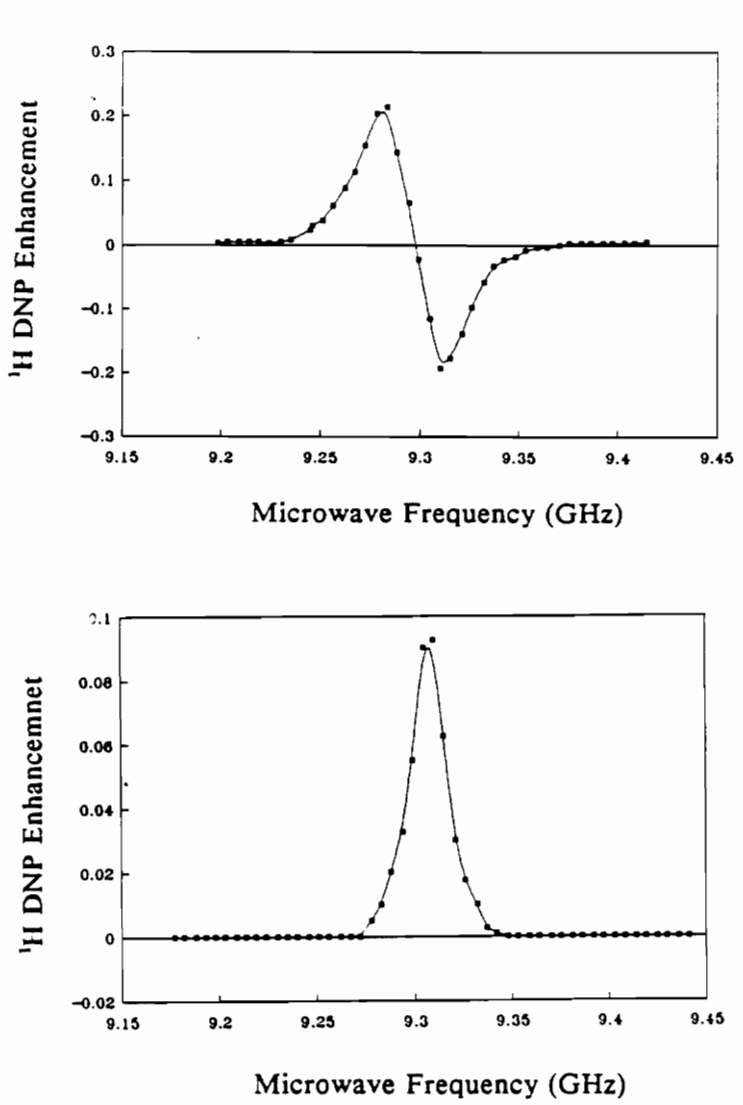

Fig. 6.12 DNP Characterization of Influence of the Organic Additive on the Cellulose Char. 1) ^{1}H DNP enhancement curve as a function of microwave frequency for the 500^{0}C cellulose char. 2) ^{1}H DNP enhancement curve as a function of microwave frequency for the 500^{0}C cellulose char treated by phosphoric acid.

6.2.3.3 ^{13}C Flow SLIT DNP Experiment of Cellulose Char

In contrast with the ^{1}H DNP enhancement, a negative ^{13}C DNP enhancement for benzene was observed for the 600 ^{0}C cellulose char (Fig. 6.13). The ^{13}C DNP enhancement as a function of the microwave frequency for the 600^{0}C char is shown in Fig. 6.14 together with the corresponding ^{1}H DNP enhancement curve. Both enhancement curves are symmetric around the electron frequency, meaning that the electron nuclear interaction is time-dependent and that only the Overhauser effect is observed. The negative DNP enhancement usually indicates a dipolar-dipolar dominated interaction between the electrons and carbon nuclei. However, a three spin effect is also a possible mechanism[85]. The possibility arises that the carbon nuclei are influenced by the proton polarization as well as by the direct coupling to the electron spins. Qualitatively, the three spin effect in this sample arises from the following sequence of spin dynamic processes: the protons in benzene are positively enhanced by the Overhauser effect due to a fluctuating scalar coupling with the unpaired electron spins and then motional modulation of the dipolar coupling between the positively polarized protons and the rare ^{13}C nuclei in benzene generates the negative enhancement of the ^{13}C spins. If this is the case, the three spin effect should be minimized by using deuterated benzene instead of regular benzene. The three spin effect should

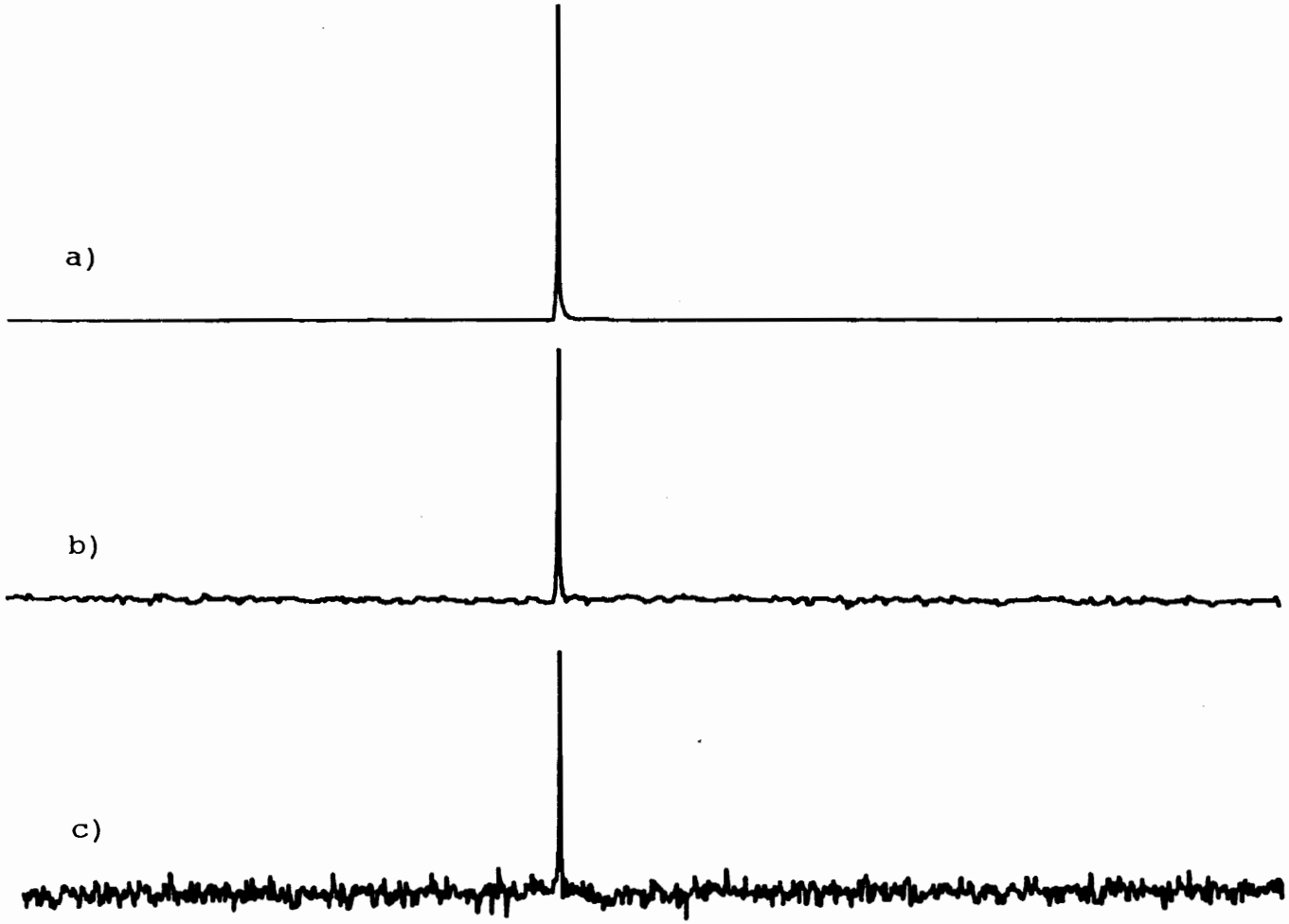

Figure 6.13 ^{13}C SLIT DNP Spectrum (50.1 MH_z) for C_6H_6/600^{0}C Cellulose Char: a) static NMR spectrum M_0^H, b) flow NMR spectrum M_z^{HL} at 2 ml/min.), c) flow DNP spectrum M_z^* at 2 ml/min.

1

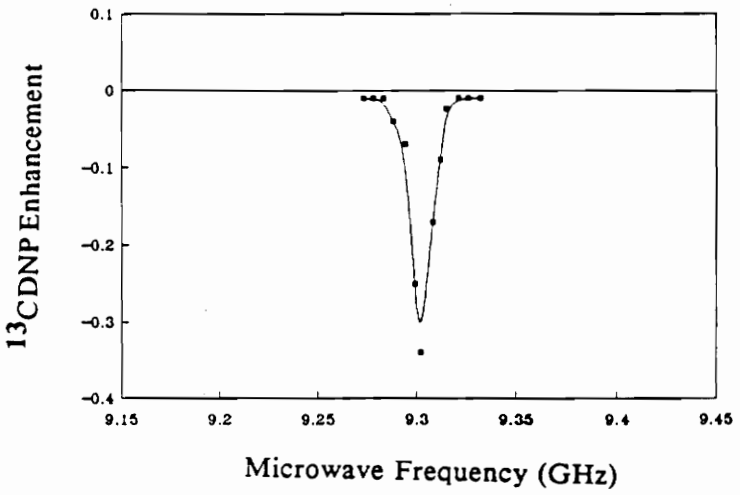

2

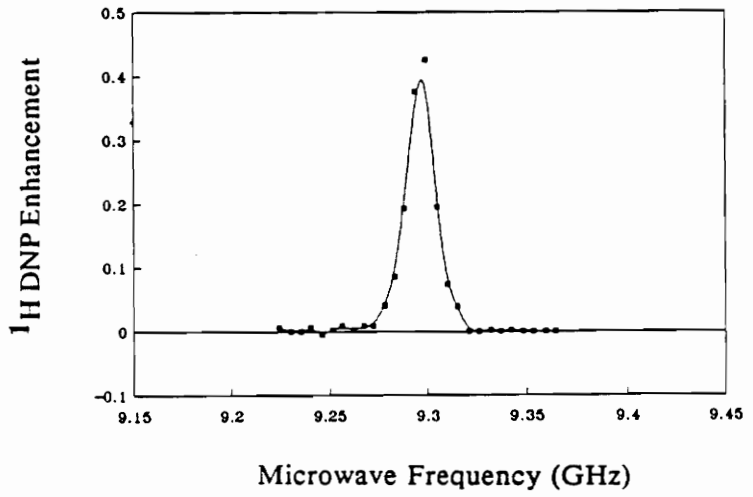

Figure 6.14 1. The ^{13}C DNP Enhancement as a Function of Microwave Frequency for the 600^{0}C Cellulose Char. 2. The ^{1}H DNP Enhancement as a Function of Microwave Frequency for the 600^{0}C Cellulose Char.

be dramatically reduced for the deuterated analog. In the absence of the three spin effect, the ^{13}C DNP enhancement for deuterated benzene is expected to be close to zero because of a mixed dipolar and scalar interactions between the carbon nuclei and the unpaired electrons (Fig. 6.15).

6.2.3.4 ^{1}H and ^{13}C SLIT DNP Experiments of Commercial Carbon Samples

The primary goal of this study was to employ the flow SLIT DNP technique to actual commercially prepared carbon samples. Initially, DNP enhancements were not observed for several commercial activated carbon samples in spite of the fact that EPR signals were observed. The failure to observe DNP enhancements was explainable due to the low spin concentration of paramagnetic species present in these commercial samples. However, numerous commercial samples exhibit both ^{1}H and ^{13}C DNP enhancements. The results are given in the next section.

6.2.3.4.1 ^{1}H SLIT DNP Result for Commercial WestVaco Carbon CHR 149 Sample

The ^{1}H DNP enhancement of benzene as a function of the microwave frequency for activated carbon WestVaco CHR 149 sample is shown in Fig. 6.16. Analogous to the 600 ^{0}C cellulose char, the ^{1}H DNP enhancement curve is symmetric

Figure 6.15 ^{13}C SLIT DNP Spectrum (50.1 MH_z) for C_6D_6/600^{0}C Cellulose Char: a) static NMR spectrum M_0^H, b) flow NMR spectrum M_z^{HL} at 2 ml/min.), c) flow DNP spectrum M_z^* flow rate 2 ml/min.

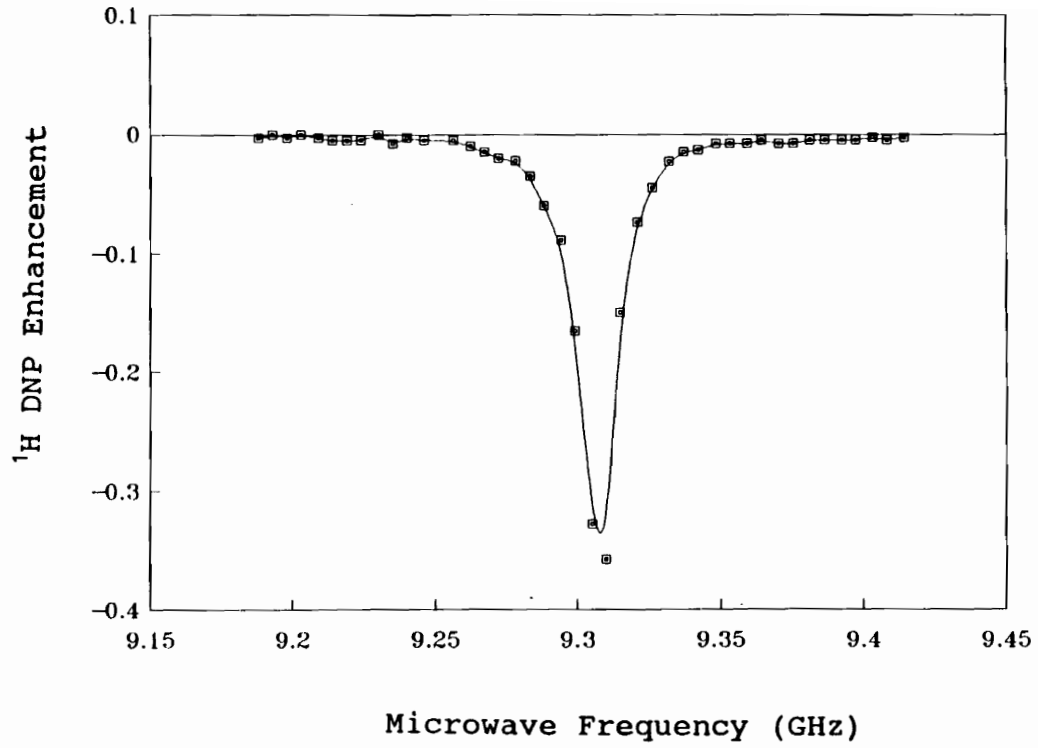

Figure 6.16 ^{1}H DNP Enhancement as a Function of Microwave Frequency for WESTVACO CHR 149 Char.

about the electron Lamor frequency, which means that the electron nuclear interaction is time dependent and an Overhauser effect is observed. In contrast with the 600 ^{0}C cellulose char, however, a negative ^{1}H DNP enhancement has been observed for the commercial Westvaco sample CHR 149. To our knowledge a positive Overhauser effect has always been reported in solids contained mobile electrons[10,76,77]. The negative DNP enhancement suggests that a dipolar dominated electron-nuclear interaction is present between hydrogen and surface free radicals. An actual explanation for the negative Overhauser effect on this carbon sample has not been advanced at this dissertation.

6.2.3.4.2 ^{13}C DNP Results for WestVaco Sample CHR 149

The ^{13}C DNP spectra for benzene and d_6-benzene are shown in Fig. 6.17 and 6.18, respectively. The ^{13}C DNP signal of d_6-benzene exhibits a negative peak while that of benzene exhibits a weak positive peak. The difference may be explained by the three spin effect. The ^{13}C nuclei in d_6-benzene are directly coupled to the electron spins in activated carbon by a dipolar dominated electron nuclear interaction. The ^{13}C nuclei in benzene, however, are influenced by the proton polarization as well as by the direct coupling to the unpaired electron. The dipolar coupling between the negatively polarized proton and carbon nuclei

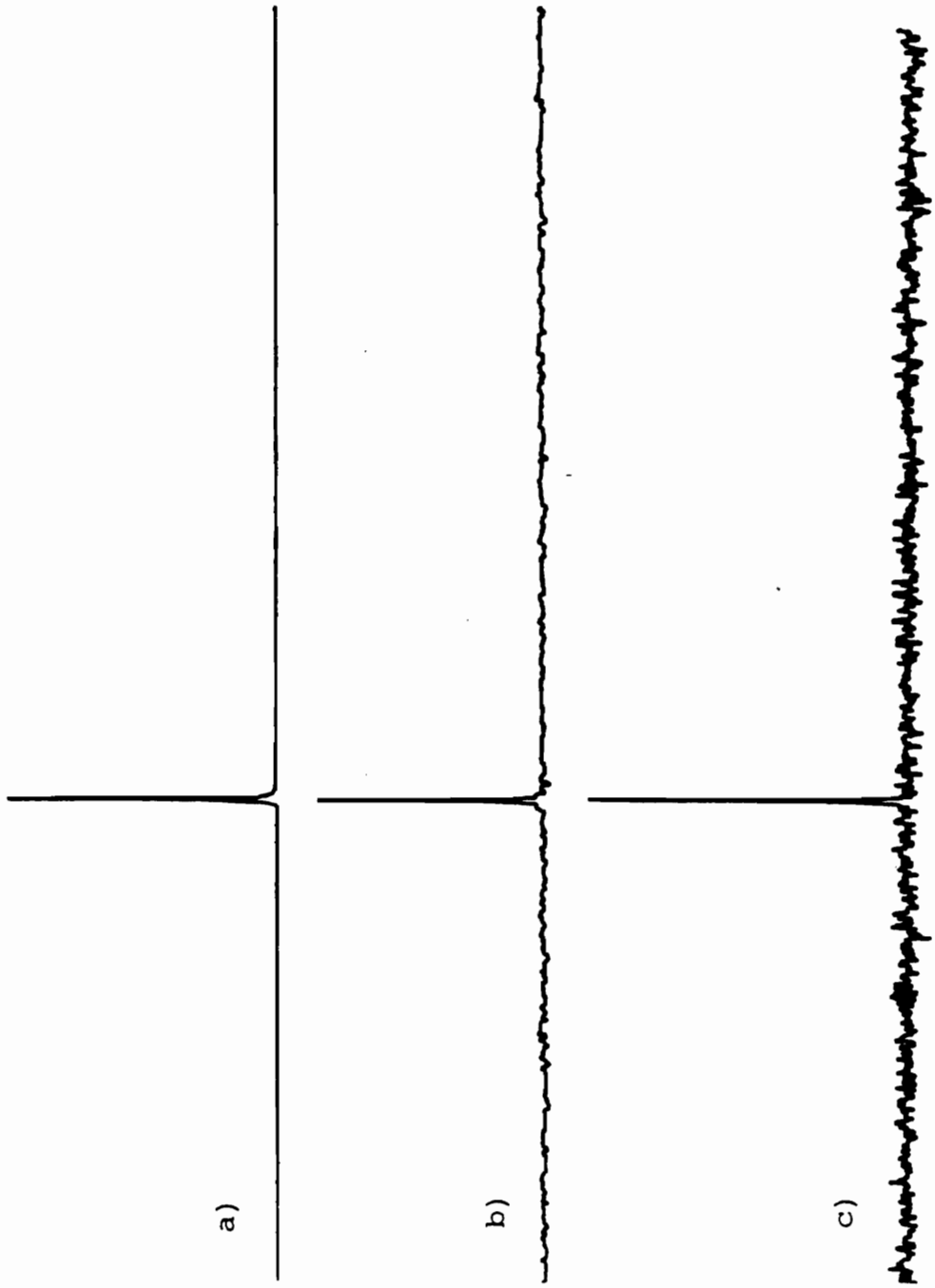

Figure 6.17 ^{13}C SLIT DNP Spectrum (50.1 MH_z) for C_6H_6/WESTVACO char # 149: a) static NMR spectrum M_0^H b) flow NMR spectrum M_z^{HL} at 2 ml/min.), c) flow DNP spectrum M_z at 2 ml/min.

Figure 6.18 ^{13}C SLIT DNP Spectrum (50.1 MH_z) for C_6D_6/WESTVACO char # 149: a) static NMR spectrum M_0^H, b) flow NMR spectrum M_z^{HL} at 2 ml/min.), c) flow DNP spectrum M_z^* at 2 ml/min.

generates a positive enhancement for ^{13}C spins which partially cancels the negative ^{13}C DNP enhancement from the direct coupling of ^{13}C nuclei to the surface free radical spins, resulting in a small negative ^{13}C DNP enhancement for benzene. The ^{13}C DNP enhancements were measured as a function of microwave frequency. The enhancement curve (Fig 6.19) is symmetric about the electron frequency, indicating the electron nuclear interaction between ^{13}C and free spins is time dependent.

6.2.3.4.3 Characterization of Adsorption of Oxygen on Commercial WestVaco Carbon Samples CHR 146 and CHR 147

Two commercial WestVaco carbon samples CHR 146 and CHR 147 were prepared under identical conditions except that CHR 146 char had never been exposed to air while sample CHR 147 had previously been exposed to air. The adsorption of oxygen on both samples was characterized by the flow ^{1}H DNP experiment, and both physical and chemical adsorption were observed. The ^{1}H DNP results for both WestVaco carbon samples CHR 147 and CHR 146 are shown in Fig. 6.20 and Fig. 6.21, respectively. The CHR 146 char exhibits only a symmetric enhancement curve due to the Overhauser effect, whereas the CHR 147 char gives a complex enhancement curve which is a composite of the contributions from the Overhauser, the solid

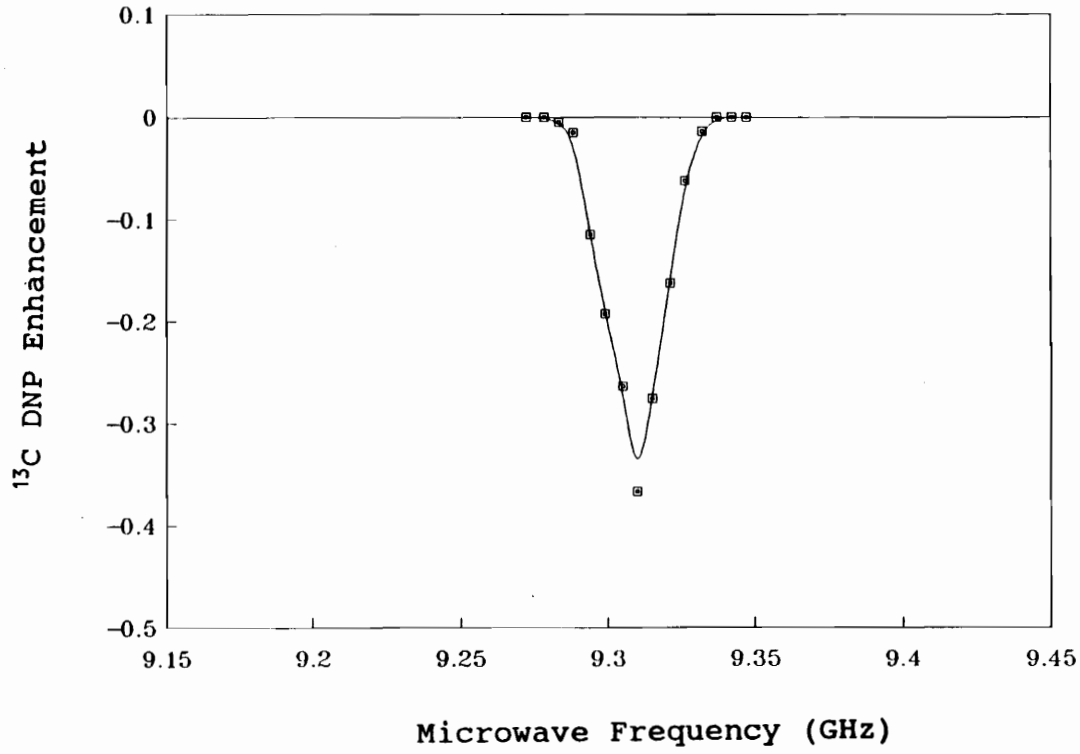

Figure 6.19 ^{13}C DNP Enhancement of Benzene-d_6 as a Function of Microwave Frequency for WESTVACO CHR 149 Char.

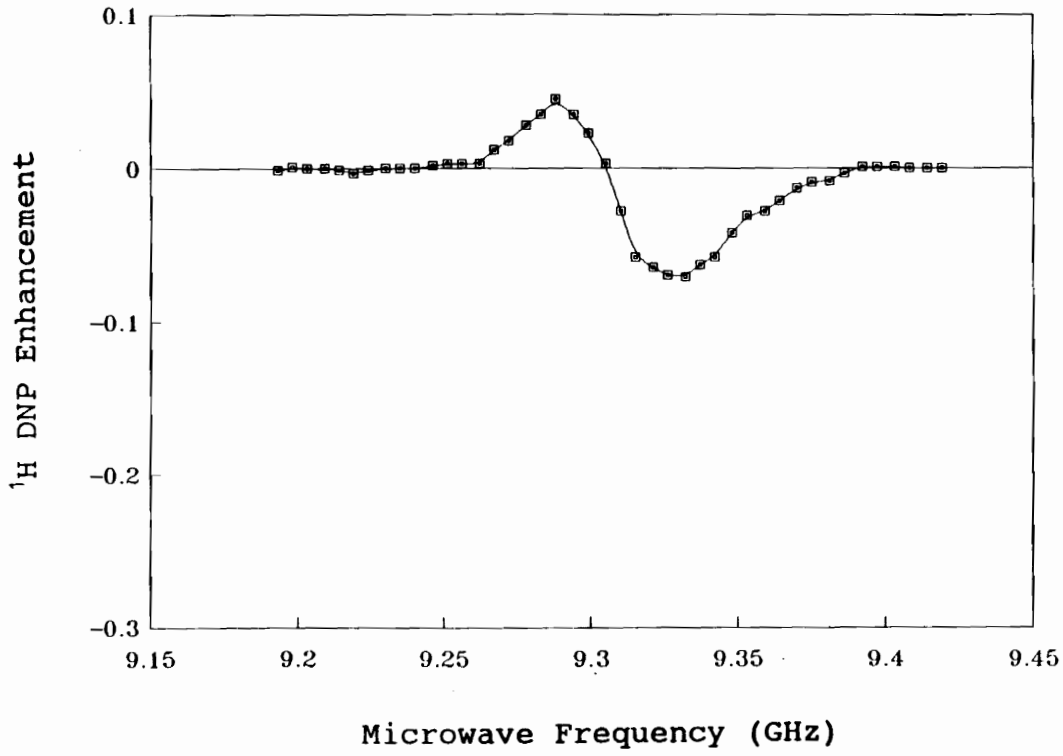

Figure 6.20 ^{1}H DNP Enhancement as a Function of Microwave Frequency for Commercial CHR 147 Char.

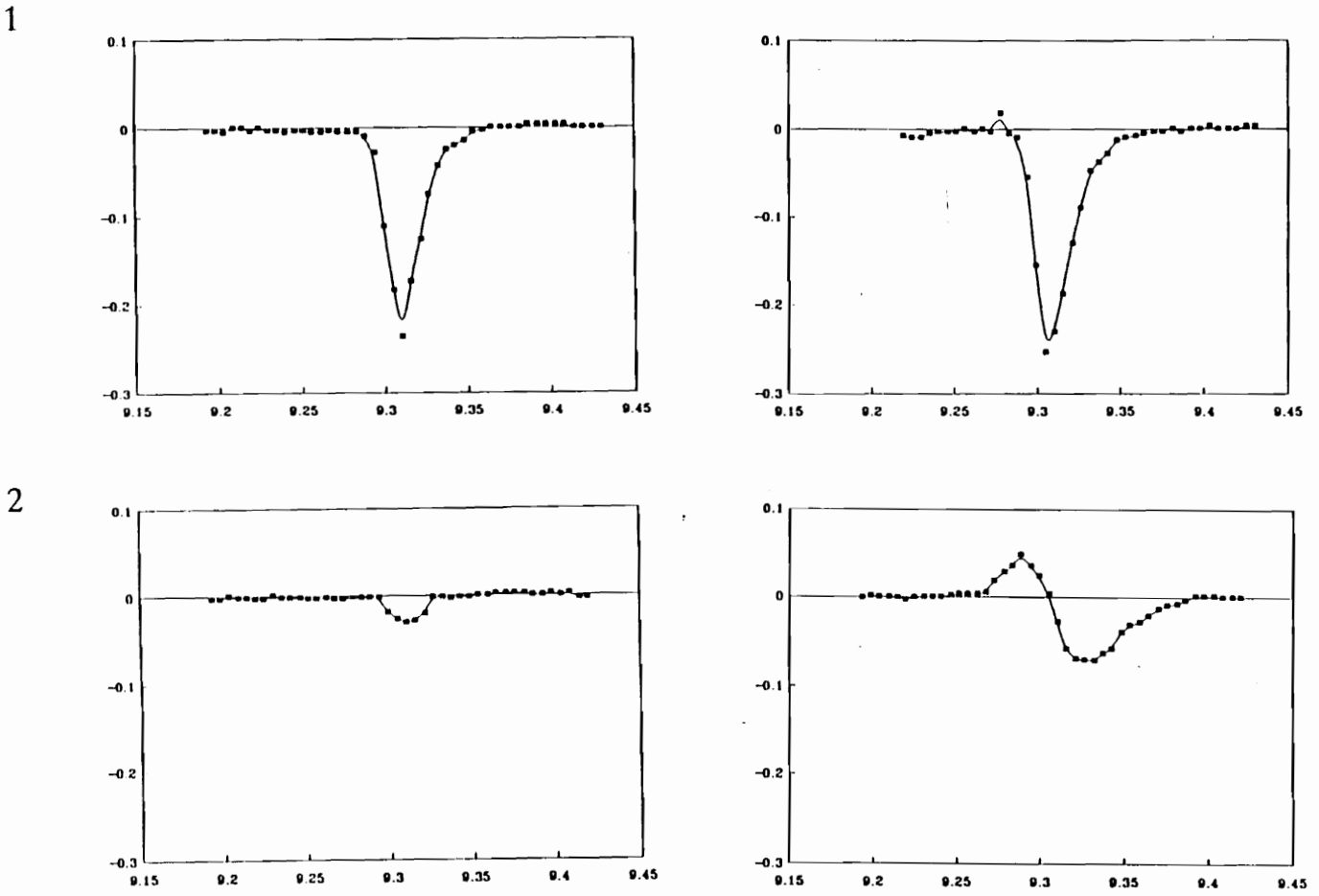

Figure 6.21 ^{1}H SLIT DNP Characterization of Adsorption of Oxygen on WESTVACO CHR 146 Char. 1. ^{1}H DNP enhancement as a function of microwave frequency. 2. After bubbling air for 30 min. 3. After purging with N_2 for 30 min. 4. After 1 day (measured under N_2).

state, and the thermal mixing effects.

The adsorption of oxygen on both the WestVaco CHR 146 and CHR 147 chars was performed by bubbling air before and during the DNP measurement. The shape of the DNP enhancement curve for CHR 147 char remained unchanged before and after oxygen treatment, meaning only the physisorption of oxygen took place. After exposure to air for 30 minutes, however, CHR 146 char began to show an unsymmetric pattern of DNP enhancement. Furthermore, after exposure to air for one day the WestWeco CHR 146 char showed the same pattern of enhancement as that of the WestVaco CHR 147 char. The observation of only the Overhauser effect for the untreated WestVaco CHR 146 char indicated the presence of delocalized electrons undergoing rapid exchange electron-electron interactions. The solid state and the thermal mixing effects observed for the oxygen treated WestVaco CHR 146 char indicated that localized spin center were created. Presumably, the aromatic carbon layers were modified by combination with oxygen, and the extent of electron delocalization is reduced by the formation of the surface oxygen complex. The fact that CHR 146 and CHR 147 show the same patten of DNP enhancements after exposure to air for one day indicates the chemisorption of oxygen on these activated carbon samples is also a significant effect even at room temperature over an extended period of time.

6.3 ^{13}C LLIT and SLIT DNP Experiments for C_{60}

6.3.1 Introduction

As a new isolated form of elemental carbon, the structure and properties of C_{60} is of considerable current interest and has been studied by a variety of techniques and groups[86-93]. Its existence and its structure, a spherical, aromatic molecule with the geometry of a truncated icosahedron, was first suggested by R. E. Smalley, of Rice University, and by H. W. Kroto, of the University of Sussex, England[86]. After that a systematic study of fullerene chemistry is beginning to emerge and this structure has been confirmed by several techniques, including Raman, NMR, STM, IR spectroscopy and X-ray diffraction[87-93]. The results by the groups at Rice, UCLA, IBM and others have shown that the C_{60} molecule has a D_{5h} symmetry with a ball diameter of 7.1 Å. There are two different kinds of carbon-carbon bonds in C_{60} molecule with bond lengths of 1.45 Å and 1.40 Å, respectively. A single NMR line has been observed due to rapid reorientation in the solid state. Chemists have recently discovered that C_{60} is a ready participant in a number of classes of chemical reactions such as its reaction with photochemically generated benzyl radicals[94] and nucleophilic addition reactions.

In this study, the liquid-liquid intermolecular interaction between C_{60} and the free radical TEMPO was studied by the flow liquid-liquid intermolecular transfer dynamic nuclear polarization (LLIT ^{13}C DNP) technique[11]. The solid-liquid intermolecular interaction between C_{60} and immobilized free radical TEMPO which was prepared by chemically bonded on the surface of silica gel was studied by the flow Solid-Liquid intermolecular transfer dynamic nuclear polarization (SLIT DNP) technique[12] (Fig. 6.22). Thus the dynamic information of the electron-nuclear interaction between C_{60} and free radical TEMPO has been obtained for both liquid/liquid and surface/liquid interactions.

6.3.2 ^{13}C LLIT DNP Results

A 20% ^{13}C enriched C_{60} sample was provided by the IBM Research Center. Vaporizing ^{13}C rich graphite by resistive heating under a helium atmosphere produced soot. A mixture of C_{60} and C_{70} was obtained by extracting the soot with boiling toluene and by evaporation of toluene[95]. Column chromatography on neutral alumina with hexane gave excellent separation of these two fullerenes.

The ^{13}C LLIT DNP results for C_{60} in C_6D_6 with 0.1 M TEMPO solution is shown in Figure 6.23. The ^{13}C DNP spectrum exhibits a negative DNP enhancements for both the C_{60} and the

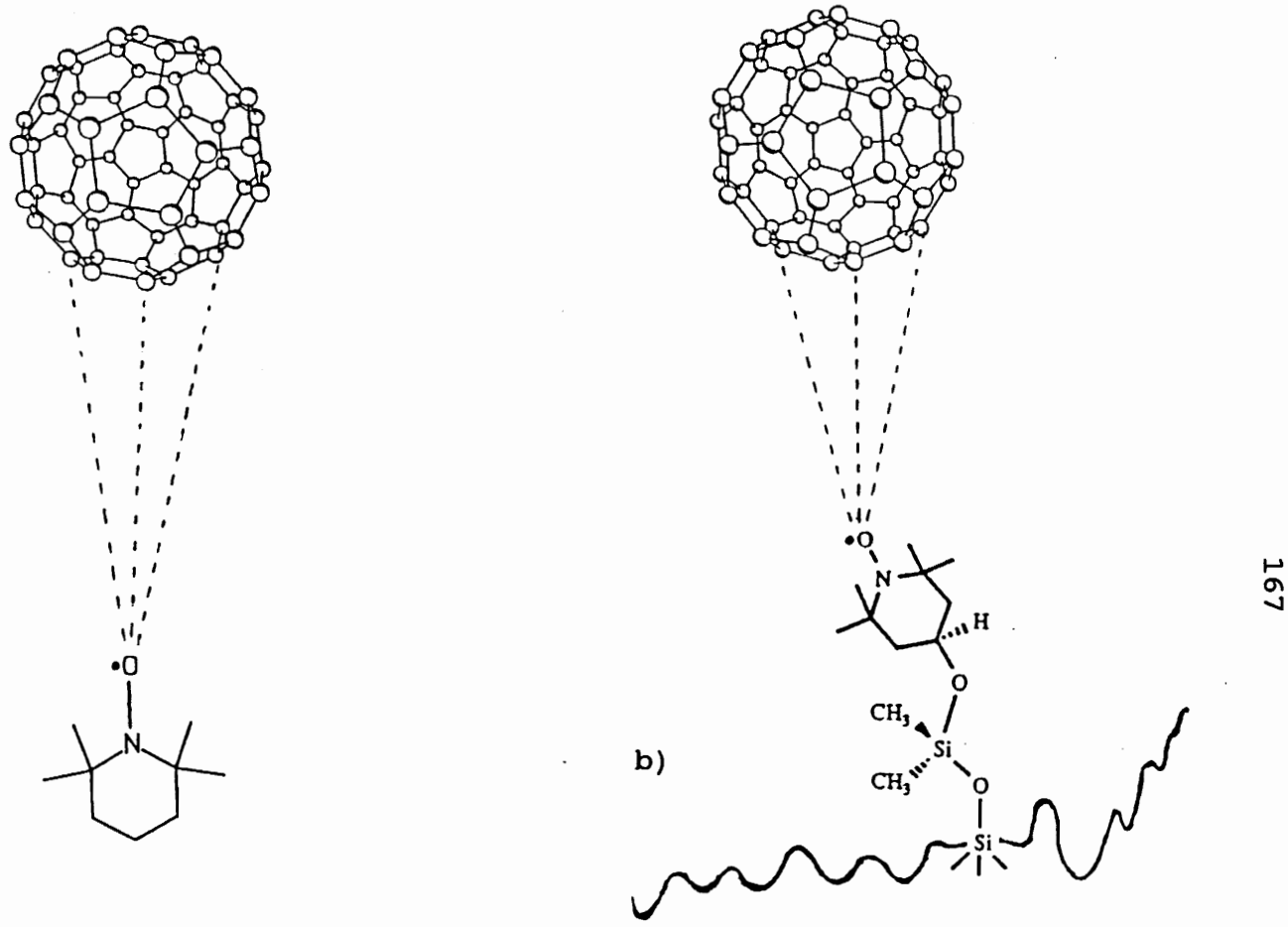

Figure 6.22 The Liquid/Liquid and Solid/Liquid Intermolecular Interactions for C_{60}/C_6D_6/TEMPO System. a) the liquid/liquid intermolecular interaction, b) the solid/liquid intermolecular interaction.

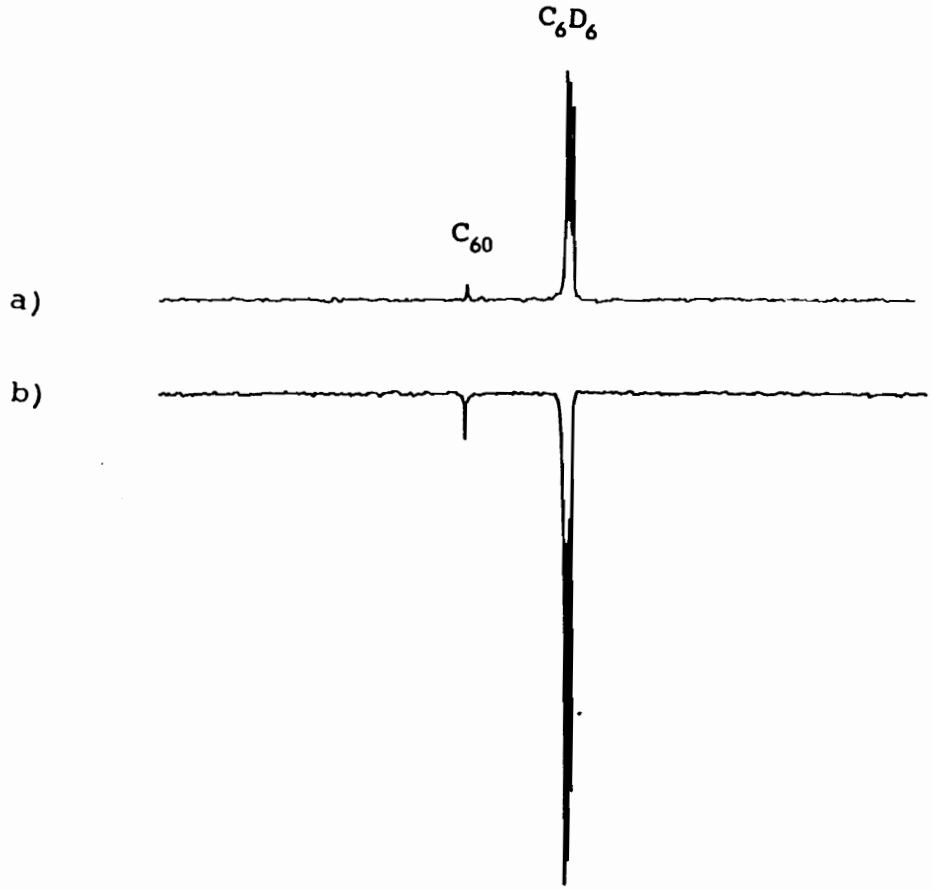

Figure 6.23 LLIT ^{13}C DNP Spectra (50.1 MHz) for C_{60}/C_6D_6/TEMPO solution: a) static ^{13}C NMR spectrum, b) flow LLIT ^{13}C DNP spectrum.

solvent C_6D_6, indicating the electron nuclear interaction between the C_{60} and the solvent C_6D_6 with the free radical TEMPO are dipolar dominated.

The observed DNP enhancements were measured at different flow rates. The plot of the log (base e) of observed DNP enhancement versus inverse flow rate yields a straight line (Figure 6.24). The ^{13}C DNP enhancement factor A was then obtained from the intercept. The leakage factor f for the both the C_{60} and the solvent C_6D_6 was determined by high magnetic field ^{13}C spin-lattice relaxation time measurements. The saturation factor s was determined from a plot of the inverse of the observed ^{13}C DNP enhancement versus inverse microwave power. The ultimate DNP enhancement A_∞, leakage factor f, and saturation factor s for C_{60}/C_6D_6/TEMPO system are presented in Table 6.2. The ultimate DNP enhancement for the C_{60} and the solvent C_6D_6 are -250 and -200, respectively. Both C_{60} and C_6D_6 exhibit negative DNP enhancements, indicating the dipolar dominated electron-nuclear interaction. Although the C_{60} molecule has ten times more carbon atoms and is a considerably larger molecule, it is still remarkable that a large negative ^{13}C DNP enhancement is observed for C_{60} in comparison with the solvent C_6D_6. This indicates that the electron-nuclear interaction between the C_{60} and the free radical TEMPO is dipolar dominated with little tendency to

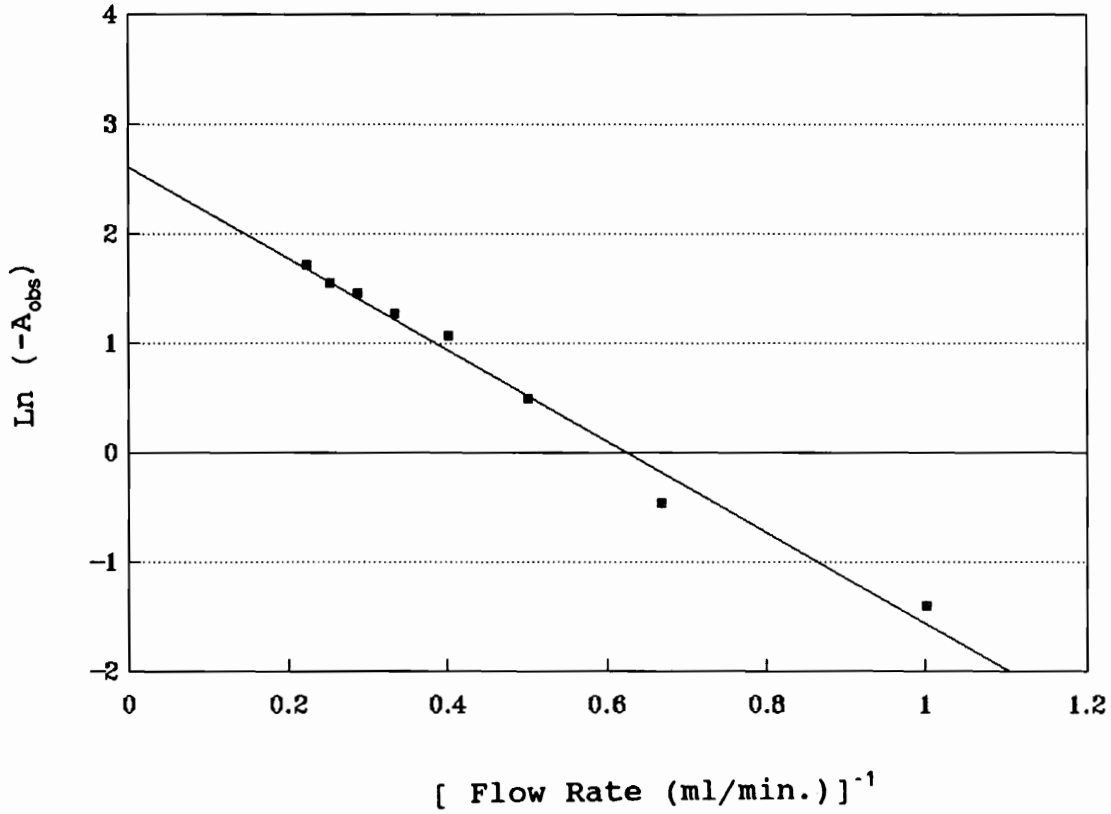

Figure 6.24 Plot of Ln ($-A_{obs}$) Versus Inverse Flow Rate for ^{13}C LLIT DNP of C_{60}/C_6D_6/TEMPO System.

Table 6.2: ^{13}C LLIT DNP Data[a] for C_{60}/C_6D_6/0.1 M TEMPO System

Sample	$\frac{M_0^L A}{M_0^H}$ [b]	f[c]	s	A_∞[d]
C_{60}	-13.6	0.96	0.8	-250 ± 20
C_6D_6	-10.9	0.97	0.8	-200 ± 20

a) All data were obtained at room temperature.
b) The ratio M_0^L/M_0^H under this experiment condition is 0.007 (see Eq. 5.19).
c) The leakage factors were determined from high field (4.7 T) spin lattice relaxation time measurements (see Eq. 5.14).
d) The relative standard deviations were estimated from regression analysis.

form a scalar interaction.

6.3.3 ^{13}C Contact Shift Measurements

In order to further examine whether a significant scalar interaction is present between the C_{60} and the free radical TEMPO, ^{13}C contact shift measurements were explored. In a solution containing a free radical R and a substrate S the interaction can be expressed as previously shown by the equation 3.9

$$R+S \rightleftharpoons R\cdot\cdot S$$

The observed contact shift Δ which is the average of the chemical shifts of the complexed Δ_0 and uncomplexed species (RS and S, respectively) is dependent on the concentration of the free radical C_R, the concentration of the substrate C_0, and on the complex formation constant K_C as in equation 3.17

$$\frac{C_R}{\Delta} = \frac{1}{K_C \Delta_0} + \frac{C_0}{\Delta_0}$$

However, if intermolecular interactions involve only weak Van der Waal forces, then to a good approximation, ideal solution behavior will be obtained and the various equilibrium constants will be small. Therefore, as pointed out by Draney and Kingsbury[24]

$$\Delta = K_C C_R \Delta_0 \qquad (6.5)$$

The chemical shift appears functionally independent of the substrate concentration and is linearly proportional to the free radical concentration.

C_{60}/C_6D_6/TEMPO solutions with different concentrations of C_{60} were prepared and no difference in chemical shift of the C_{60} was observed. On the other hand, a set of C_{60} solutions were prepared with different concentration of TEMPO and the contact shifts observed for the C_{60} and the solvent C_6D_6 were linearly proportional to the free radical concentration (Figure 6.25). Upon correcting the value of the apparent paramagnetic shifts, (4.06 ppm/M for internal reference cyclohexane)[19] the ^{13}C molar contact shifts for C_{60} and the solvent C_6D_6 are 2.45 ppm/M and 5.20 ppm/M, respectively. Therefore, the ^{13}C contact shift results suggest that there is little if any specific complexation between the C_{60} and the free radical TEMPO, and that a momentary contact interaction is merely governed by diffusional constraints with ideal solution behavior obtained (vide supra).

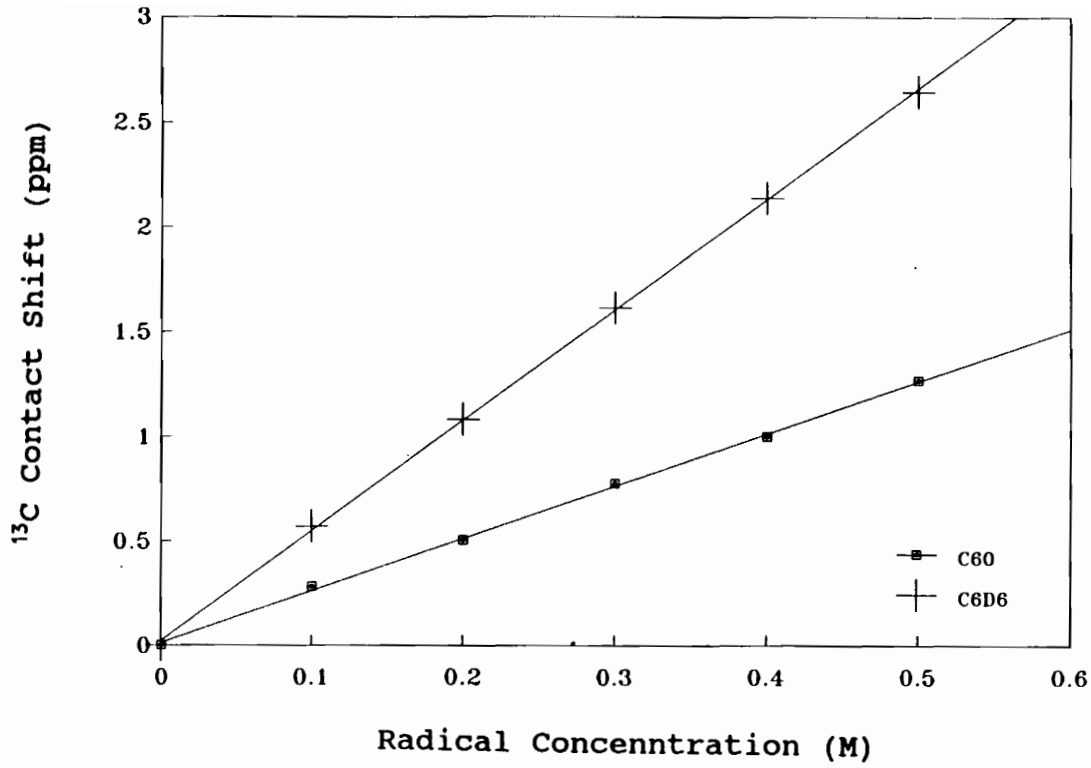

Figure 6.25 Plot of ^{13}C Contact Shift Versus Concentration of the Free Radical for C_{60}/C_6D_6/TEMPO System.

6.3.4 ^{13}C SLIT DNP Experiment

In the LLIT ^{13}C DNP experiment, both the C_{60} and the free radical TEMPO are dissolved in the solvent C_6D_6. Therefore, molecules move very rapidly in solution and only a time-dependent electron-nuclear interaction is observed. In the SLIT ^{13}C DNP experiment, however, the free radical is chemically bonded on the surface of the silica gel which restricts the motion of surface molecules. In this case, both the time-dependent and time-independent interactions are possible[10]. As to which interaction will dominate a particular case will depend both on the materials being studied and on the experimental conditions. The correlation time describing the time dependence of the electron nuclear interactions must be on the scalar comparable to ω_s^{-1} if the time-dependent interaction, that is, the Overhauser effect is observed. Therefore, the sign, the magnitude, and the shape of the enhanced NMR signals provide dynamic information regarding the molecular motion and electron-nuclear interaction.

The EPR spectrum for the silica phase immobilized nitroxide (SPIN) free radical #511[96] is shown in Figure 6.26. The three EPR signals result from ^{14}N nitrogen atom splitting, (I = 1). The ^{13}C SLIT DNP results for the C_{60}, which is a plot of the observed ^{13}C DNP enhancement versus irradiation magnetic field, is shown in Figure 6.27. The results show an

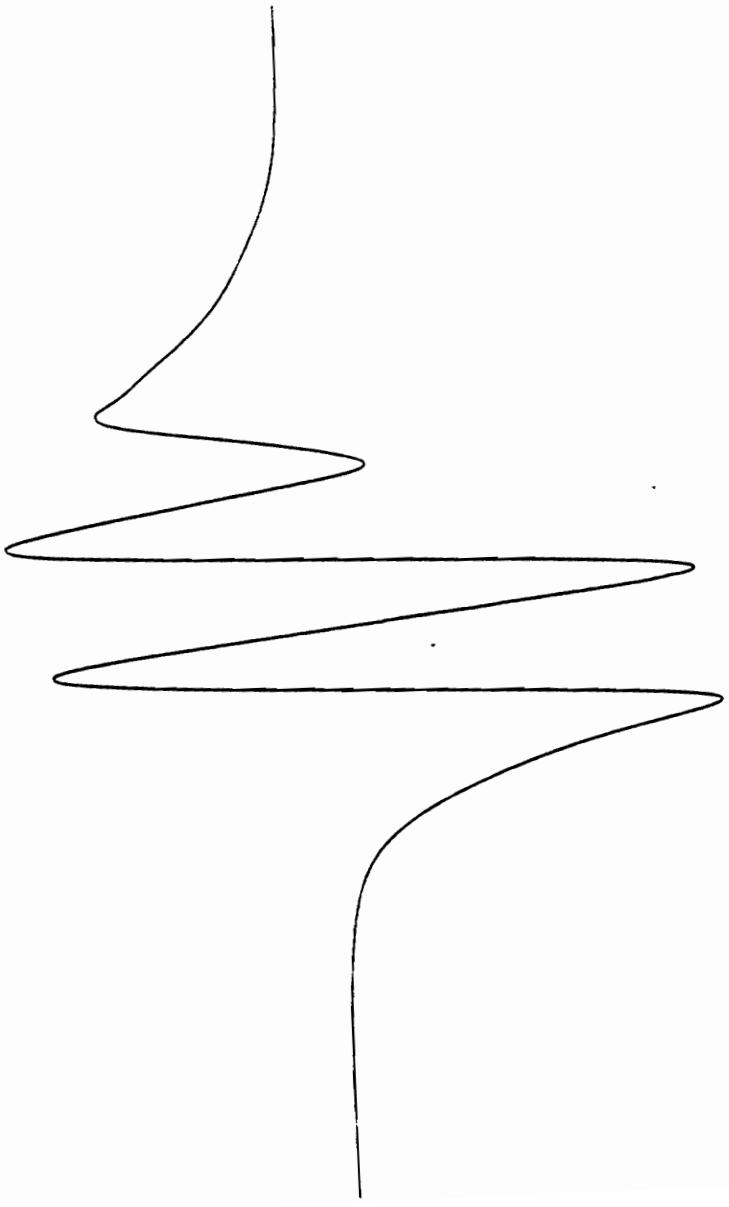

Figure 6.26 The EPR Spectrum for SPIN #511 in C_6D_6.

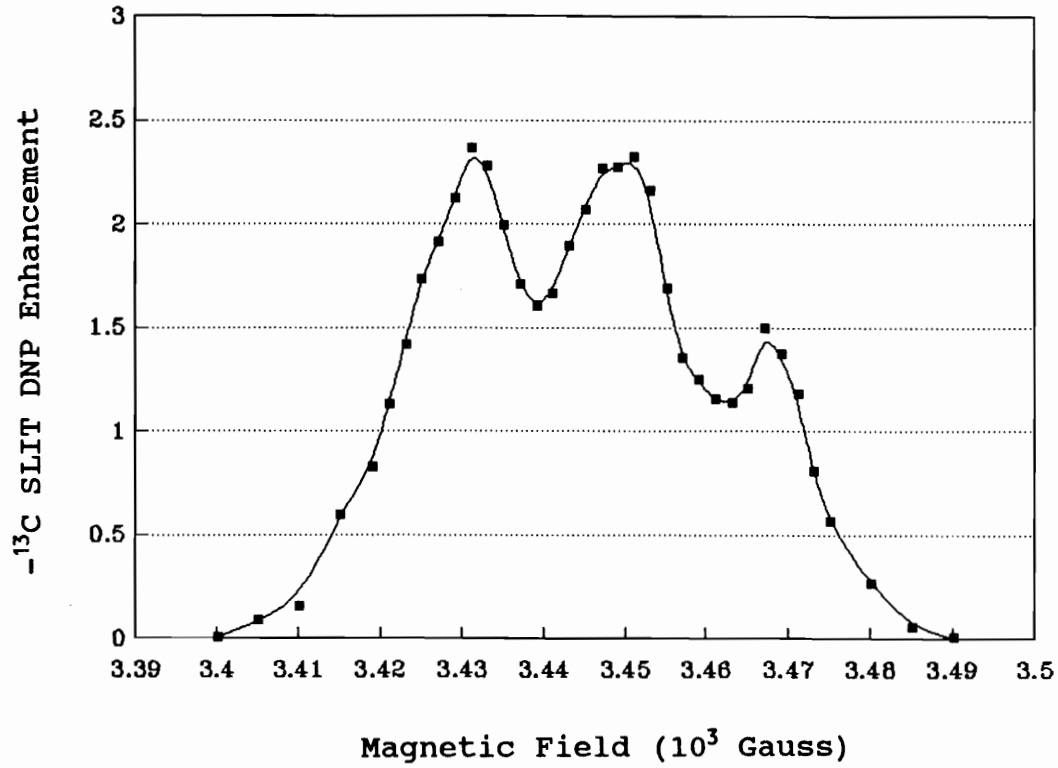

Figure 6.27 Flow ^{13}C SLIT DNP Enhancement as a Function of the Low Magnetic Field for C_{60} in C_6D_6 with SPIN #511.

Overhauser effect, indicating that the electron nuclear interaction is time-dependent. As discussed earlier, the correlation time must be on the scale comparable to ω_s^{-1} if the Overhauser effect is to be observed. At the magnetic field of 0.33 T used in this study ($\omega_s = 5.8 \times 10^{10}$rad.s), the correlation time must be smaller than 2×10^{-11}s if the Overhauser effect is to be important.

In summary, both LLIT and SLIT DNP results show that C_{60} has a relatively short correlation time in solution (~ 10^{-11}s) and very little tendency to form scalar contact interaction. The results are consistent with a model of C_{60}/TEMPO interaction involving weak and nonspecific complex formation.

CHAPTER 7

CONCLUSION

The complementary information provided by liquid/liquid and liquid/solid intermolecular interactions have been studied by the combination of NMR and DNP techniques. Both weak hydrogen bond formation and non-specific complex formation have been observed in this study.

The weak hydrogen bond formation in CH_3CN/TEMPO and CH_3CONH_2/TEMPO systems has been extensively investigated. The parameters such as complex formation K_c and the hyperfine coupling constant A have been derived from the radical induced paramagnetic shifts results, and the dynamic parameters for intermolecular interaction such as correlation times and radical nuclear distances have been resolved from relaxation times studies. The results show that methyl hydrogens in the CH_3CN molecule tend to form hydrogen bonds with the N-O linkage of the free radical TEMPO, and the nitrogen atom in CH_3CN tends to orient away from the N-O group in TEMPO radical solution. In contrast to the CH_3CN/TEMPO system, the N-H bond in the acetamide molecule exhibits a large contact shift and

consequently a larger coupling constant, indicating that the N-H bond is the site of complexation. The scalar and dipolar contributions derived from the NMR studies show that the scalar contribution is critically dependent on the site of hydrogen bonding (i.e., methyl group in the acetonitrile molecule and amino group in the acetamide molecule).

The ^{1}H, ^{13}C, and ^{15}N DNP enhancements at low magnetic field (0.33 T) have been predicted for the first time using the parameters obtained from the NMR studies. The results have been obtained based on the rotational diffusion model for the dipolar interaction and the sticking model for the scalar interaction. Good agreement between the NMR predicted and the experimental measured DNP enhancements have been obtained for the CH_3CN/TEMPO system. The small disagreement in the CH_3CONH_2/TEMPO system can be explained by the possible anisotropic motion, multiple sites of complexation, and inaccuracies in the measured correlation times.

In contrast with the CH_3CN/TEMPO and CH_3CONH_2/TEMPO system, both paramagnetic contact shift and DNP results for the C_{60}/TEMPO system exhibit very little tendency to form a scalar contact interaction with the free radical TEMPO. The flow LLIT and SLIT ^{13}C DNP studies of the C_{60}/TEMPO system show that the C_{60} molecule has a short correlation time in solution

and does not have a specific interaction site with TEMPO radical.

The ^{1}H and ^{13}C DNP results for the activated carbon samples show that the structure of the activated carbon is critically dependent on the heat treatment temperatures. As the temperature increases the unpaired electrons become more delocalized on the carbon skeleton due to an increased aromaticity. Three-spin effects for ^{13}C DNP results have been observed. Both physisorption and the chemisorption of oxygen on the activated carbon have been observed, and the influence of an inorganic additive has been noted.

Therefore, both NMR and DNP are powerful techniques which provide a very detailed picture of the dynamic electron-nuclear interaction for various liquid/liquid and surface/liquid interfaces.

REFERENCES

1. K. Bundfuss, K. Meisr-Gresch, and W. Müller-Warmuth, J. Magn. Reson. 55, 408 (1983), and references cited therein.

2. N. A. Sysoeva, A. Yn. Karnilov, and A. L. Buchachennko, Chem. Phys. 15, 321 (1976); 15, 313 (1976).

3. K. Endo, I. Motishima, and T. Morishima, and T. Yonezawa, J. Chem. Phys. 67, 4760 (1977).

4. W. Kolodziejski and Z. Kecki, Ber. Bunsenges. Phys. Chem. 82, 1314 (1978).

5. E. Dally and W. Müller-Warmuth, Ber. Bunsenges. Phys. Chem. 81, 1133 (1977); 82, 792 (1978); 84, 260 (1980).

6. H. W. Nientiedt, K. Bundfuss, and W. Müller-Warmuth, J. Magn. Reson. 43, 154 (1981).

7. G. C. Levy, R. A. Komoroski, J. Am. Chem. Soc. 96, 678 (1974).

8. K. H. Hausser and D. Stehlik, Adv. Magn. Reson., 3, 79 (1969).

9. J. A. Potenza, Adv. Mol. Relaxation Processes, 4, 229 (1972).

10. R. A. Wind, M. J. Duijvestijn, C. Van Der Lugt, A. Manenschijn and J. Vriend Prog. in NMR Spec. 17, 33 (1985).

11. K. H. Tsai and H. C. Dorn, Appl. Magn. Reson., 1, 231 (1990).

12. H. C. Dorn, T. E. Glass, R. Gitti and K. H. Tsai, Appl. Mang. Reson., 2, 9 (1991).

13. A. Carrington and A. D. Mclachlan "Introduction to Magnetic Resonance"; Harper & Row, New York, Evanston, and London. (1967).

14. E. Fermi, Z. Physik, 60, 320 (1930).

15. C. C.Hinckley, J. Am. Chem. Soc., 91, 5160 (1969).

16. Reuben, J. Prog. Nucl. Magn. Reson. Spectrosc. 9, 1 (1975).

17. I. Morishima, K. Kawakami, T. Yonezawa, K. Goto, M. Imanari, J. Am. Chem. Soc. 94, 6555 (1972); I. Morishima, K. Toyoda, K. Yoshikawa, T. Yonezawa, Ibit. 95, 8627 (1973); I. Morishima, K. Ishihara, T. Tomishima, T. Inubushi, T. Yonezawa, Ibit. 97, 2749 (1975).

18. Y. Deguchi, Bull. Chem. Soc. Jap. 35, 260 (1962); T. Kawamura, S. Matsunami and T. Yonezawa, Bull. Chem. Soc. Jap. 40, 1111 (1967).

19. Z. W. Qiu, D. M. Grant, and P. J. Pugmire, J. Am. Chem. Soc., 104, 2747 (1982).

20. G. N. LaMar, W. D. Horrocks, R. H. Holm, Jr. "NMR of Paramagnetic Molecules"; Academic Press: New York, (1973).

21. R. K. Harris "Nuclear Magnetic Resonance Spectroscopy"; Pitman Books Limited: London, 207 (1983).

22. M. Hirayama, Y. Honyu, Bull. Chem. Soc. Jpn. 46, 2687 (1973).

23. D. R. Morgan, and H. C. Dorn, J. of Labeled Compounds and Radiopharmaceuticals, in press.

24. D. Draney, C. A. Kingsbury, J. Am. Chem. Soc. 103, 1041 (1981).

25. J. R. Stewart, E. H. Poindexter, J. A. potenza, J. Am. Chem. Soc. 89, 6017 (1967).

26. Z. W. Qiu, D. M. Grant, and P. J. Pugmire, J. Am. Chem. Soc., 106, 557 (1984).

27. U. Stark and W. Müller-Warmuth, Ber. Bunsenges. Phys. Chem. 94, 168 (1990).

28. H. S. Gutowsky and J. C. Tai, J. Chem. Phys. 39, 208 (1963)

29. E. H. poindexter, P. J. Caplan, B. E. Wagner, and R. D. Bates, Jr., J. Chem. Phys. 61, 3821 (1974).

30. K. Endo, B. Knuettel, I. Morishima, T. Inubushi, and T. Yonezawa, Chem. Phys. Lett. 31, 387 (1975).

31. I. Solomon, Phys. Rev., 99, 559 (1955)

32. I. Solomon, and N. Bloembergen, J. Chem. Phys. 25, 261 (1956).

33. P. S. Hubbard, Proc. Roy. Soc., A 291, 537 (1966) (1956).

34. B. Borah, and R. D. Bates Jr., Chem. Phys. Lett. 76, 101 (1980). J. Chem. Phys. 74, 1538 (1981).

35. J. A. Potenza, Advances in Molecular Relaxation Processes, **4**, 229 (1972).

36. E. H. Poindexter, P. H. Caplan, B. E. Wagner, and R. D. Bates, Jr., Chem. Phys. 61, 3821 (1974).

37. N. Bloembergen, E. M. Purcell, and R. W. Pound, Phys. Rev. 73, 6 (1948).

38. K. D. Kramer, and W. Müller-Warmuth, Z. Naturforsch. A 19, 375 (1964).

39. H. Pfeifer, Ann. Phys. (Leipzig) 8, 1 (1961).

40. K. Meise, W. Müller-Warmuth, and H. W. Nientiedt, Ber. Bunsenges. Phys. Chem. 80, 584 (1976).

41. A. Abragam, The Principles of Nuclear Magnetism (Clarendon, Oxford, England, 1961).

42. N.Bloembergen, and L. O. Morgan, J. Chem. Phys. 34, 842 (1961).

43. J. W. H. Schreurs, and G. K. Fraenkel, J. Chem. Phys. 34, 757, (1961).

44. D. J. E. Ingram, Free Radicals as Studied By ESR (Butter-Worths, London, 1958).

45. T. R. Krugh, "Molecular Biology" Academic Press. New York, San Francisco, Landon, 1976.

46. J. Kowalewski, G. C. Levy, L. F. Johnson, and L. Palmer, J. Magn. Reson., 26, 533 (1977).

47. J. L. Hintze, Number Cruncher Statistical System, Version 5.3 Kaysville, Utah (1989).

48. D. F. S. Natusch and R. E. Richards, Chem. Comm. 579 (1966).

49. A. W. Overhauser, Phys. Rev., 92, 411, 1953.

50. T. R. Carver and C. P. Slichter, Phys. Rev., 92, 212, 1953.

51. A. Abragam, A. Landesman and J. M. Winter, C. R. Acad. Sci., 247, 1852, 1958.

52. E. H. Poindexter, Nature, 182, 1087, 1958; J. Chem. Phys., 31, 1477, 1959; J. Chem. Phys., 36, 507, 1962; .J Chem. Phys., 43, 3857, 1965.

53. T. R. Carver and C. P. Slichter, Phys. Rev., 102, 975, 1956.

54. R. S. Codrington and M. Bloembergen, J. Chem. Phys., 29, 600, 1958.

55. H. G. Beljers, L. Van Der Kint and J. S. Van Wieringen, Phys. Rev., 95, 1683, 1954.

56. R. E. Richards and J. W. White, Disscuss. Faraday Soc., 34, 96, 1962.

57. R. E. Richards and J. W. White, Proc. Roy. Soc., Ser. A, 283, 459, 1965.

58. R. A. Dwek, R. E. Richards and D. Taylor, Annu. Rev. NMR Spectrosc. 2, 293 (1969).

59. R. D. Bates and W. S. Drozdoski, J. Chem. Phys., 67, 4038 (1977).

60. K. H. Tsai, Ph.D. Thesis, Blacksburg, VA (1990).

61. D. W. Woessner, J. Chem. Phys., 67, 4769 (1977).

62. A. Abragam, Phys. Rev. 98, 1729 (1955).

63. E. Erb, J. L. Motchane and J. Unebersfeld, C. R. Acad. Sci. 246, 2121 (1958).

64. J. F. Jacquinot, W. Th. Wenckebach, M. Goldman and A. Abragam, Phys. Rev. Lett. 32, 1096 (1974).

65. R. A. Wind, J. Trommel and J. Smidt, Fuel 58, 900 (1979). 61, 398 (1982).

66. R. A. Wind, J. Trommel and J. Smidt, Bull. Magn. Res. 2, 438 (1981).

67. R. A. Wind, M. J. Duijvestijn and J. Smidt, Bull. Magn. Res. 5, 114 (1983).

68. R. D. Bates, J. Magn. Reson., 42, 111 (1982).

69. Y. Sekiguchi, J. S. Frye, and F. Shafizadeh, J. Appl. Polym. Sci. 28, 3513 (1983).

70. Y. Sekiguchi and F. Shafizadeh, J. Appl. Polym. Sci. 29, 1267 (1984).

71. S. Mrozowski and A. Gutsze, Carbon 15, 335 (1977).

72. J. G. Castle, Phys. Rev. 92, 1063 (1953).

73. L. S. Singer, Proc. Fifth Carbon Conf., Vol. II, Pergamon Press, N. Y., 1963.

74. W. F. Degroot and F. Shafizadeh, Carbon 21, 61 (1983).

75. B. Milsch, W. Windsch, and H. Heinzelmann, Carbon 6, 807 (1968).

76. R. A. Wind, M. J. Duijvestijn, C. Van Der Lugt, and J. Smidt, Fuel 66, 876 (1987).

77. R. A. Wind, H. Lock, and M. Mehring, Chem. Phys. Lett. 141, 283 (1987).

78. H. Lock, R. A. Wind, G. E. Maciel and N. Zumbulyadis, Solid State Comm. 64, 41 (1987).

79. M. J. Duijvestijn, R. A. Wind and J. Smidt, Physica 138b, 147 (1986).

80. A. G. W. Bradbury and F. Shafizadeh, Carbon 18, 109 (1980).

81. R. C. Bansal, F. J. Vastola and P. L. Walker Jr., J. Coll. Interface Sci. 32, 187 (1970).

82. R. C. Bansal, F. J. Vastola and P. L. Walker Jr., Carbon 10, 443 (1972).

83. W. F. DeGroot and F. Shafizadeh, Carbon 21, 61 (1983).

84. F. Shafizadeh and Y. Sekiguchi, Carbon 21, 511 (1983).

85. G. G. Maresch, R. D. Kendrick, C. S. Yannon and M. E. Galvin, J. Magn. Reson., 82, 41 (1989).

86. H. W. Kroto, J. R. Heath, S. C. O'Brien, R. F. Curl, and R. E. Smalley, Nature, 318, 162 (1985).

87. W. Krätschmer, L. D. Lamb, K. Fostiropoulos, and D. R. Huffman, Nature, 347, 354 (1990).

88. D. S. Bethune, G. Meijer, and H. J. Rosen, Chem. Phys. Lett., 174, 219 (1990).

89. D. S. Bethune, G. Meijei, W. C. Tang, H. J. Resen. W. G. Golden, H. Seki, C. A. Brown, and M. S. DeVries, Chem. Phys. Lett., 179, 181 (1991).

90. R. D. Johnson, G. Meijei, and D. S. Bethune, J. Am. Chem. Soc., 112, 8983 (1990).

91. J. L. Wragg, J. E. Chamberlain, H. W. White, W. Krätschmer, and D. R. Huffman, Nature, 348, 623 (1990).

92. R. Taylor, J. P. Hare, A. K. Abdul-Sada, and H. W. Kroto, J. Chem. Soc., Chem. Comm., 20, 1423 (1990).

93. H. Ajie, M. M. Alvarez, S. J. Anz, R. D. Beck, F. Diederich, K. Fostiropoulos, D. R. Huffman, W. Krätschmer, Y. Rubin, K. E. Schriver, D. Sensharma, and R. L. Whetten, J. Phys. Chem. 94, 8630 (1990).

94. R. M. Baum, C&EN, Oct. 29 (1990).

95. R. D. Johnson, K. S. Yannoni, H. C. Dorn, J. R. Salem, and D. S. Bethune, Science, 255, 1235 (1992).

96. R. Gitti, Ph.D. Thesis, VPI&SU (1991).

VITA

Juan Gu was born on January 4. 1945 in Shanghai, China. She graduated with a B.S. degree in Chemistry from China Pharmaceutical University, Najing, China in June 1966. Since then, she had been working in the area of chemistry for the period 1966-1986. In the Fall of 1986, she was a visiting scholar working under direction of Dr. Harry C. Dorn at Department of Chemistry, Virginia Polytechnic Institute and State University (VPI & SU). In the Spring of 1987, she began her Ph.D. graduate studies in chemistry at VPI & SU. Her work there under Dr. Dorn has involved molecular motion and dynamic nuclear-electron interaction studies using nuclear magnetic resonance which leads to completion of her Ph.D. work in April, 1992.

Juan Gu